Synthesis of linear and star miktoarm ABC terpolymers and their self-assembly in thin films

Ségolène Antoine

Thèse présentée

pour obtenir le grade de

DOCTEUR DE

L'UNIVERSITE DE BORDEAUX

Ecole doctorale des sciences chimiques

Spécialité : Polymères

Par Ségolène ANTOINE

Synthesis of linear and star miktoarm ABC terpolymers and their self-assembly in thin films

Synthèse de terpolymères ABC linéaires et en étoile et étude de leur auto-organisation en films minces

Directeur de Thèse: Georges Hadziioannou

=

Soutenue le 22 décembre 2017

Devant la commission d'examen formée de:

M. Sinturel Christophe	Professeur, Université d'Orléans	Rapporteur
M. Gigmes Didier	Directeur de recherche, CNRS, ICR Marseille	Rapporteur
M. Chapel Jean-Paul	Directeur de recherche, CNRS, CRPP Bordeaux	Examinateur
M. Iliopoulos Ilias	Directeur de recherche, CNRS, PIMM Paris	Examinateur
M. Lecommandoux Sébastien	Professeur, Bordeaux INP	Examinateur
M. Hadziioannou Georges	Professeur, Université de Bordeaux	Examinateur
M. Aissou Karim	Chargé de recherche, CNRS, LCPO Bordeaux	Invité

Remerciements

Les résultats obtenus lors de cette thèse sont le fruit d'un travail collaboratif, je souhaite remercier l'ensemble des personnes qui ont contribué à ce projet.

Je remercie le Pr. Georges Hadziioannou, mon directeur de thèse, qui m'a accueilli dans son équipe au sein du Laboratoire de Chimie des Polymères Organiques (LCPO). J'ai été très heureuse de faire partie du B8. Les équipements, instruments, produits chimiques et les locaux mis à notre disposition permettent de travailler dans des conditions des plus agréables. Monsieur Hadziioannou, je vous remercie d'avoir été particulièrement présent lors de la fin de ma thèse, de m'avoir donné l'opportunité de présenter mes travaux à vos étudiants de master 2, et de votre confiance tout au long de la thèse. Vous m'avez beaucoup apporté, et notamment votre vision très large sur mon sujet et ses applications. Vous m'avez appris à communiquer plus efficacement et à valoriser intelligemment mes résultats.

Je tiens également à remercier le Dr Karim Aissou, mon tuteur de thèse. Karim merci pour ton accompagnement, ton soutien, ta disponibilité et ton dynamisme. Merci d'avoir toujours pris le temps de parler avec moi de mes résultats (bons ou mauvais) et pour ton écoute. Tu m'as formée à la démarche scientifique, tu m'as permis de structurer mes idées, remettre en question des points clefs et tu m'as transmis ta passion pour la science. J'ai énormément apprécié travailler et échanger avec toi. Merci de m'avoir soutenue sur la partie chimie et éclairer sur la partie physique de ma thèse. J'ai énormément appris grâce à toi lors de ces 3 années de thèse, aussi bien sur le plan professionnel que personnel.

Je tiens à remercier le Dr Guillaume Fleury pour ses conseils lors de ma thèse. Guillaume, tu as suivi mon projet d'un peu plus loin que Karim, mais toujours avec attention. Je te remercie pour tes conseils et ton écoute. Comme Karim, tu as toujours laissé la porte ouverte, et tu as été une oreille attentive lors de ces 3 années.

Je tiens à remercier l'ensemble des personnes présentes dans le jury pour avoir accepté de juger ce travail :

- Monsieur Gigmes et Monsieur Sinturel, en qualité de rapporteur pour avoir apporté des remarques pertinentes sur mon manuscrit.

- Monsieur Lecommandoux pour avoir accepté la responsabilité d'être président du jury, mais aussi de m'avoir accueilli au sein du LCPO.
- Monsieur Chapel et Monsieur Iliopoulos pour l'intérêt porté à mon travail et la discussion que vous avez animée lors de ma soutenance.

Je tiens à remercier toutes les personnes du LCPO, et tout particulièrement mon bureau, Dimitrios, Alberto, Sylvain, Muriel, Damien, Paul et bien sûr Florian pour avoir corriger ma thèse en anglais. La bonne entente entre les membres du Bu5 a été une vraie bouffée de bonne humeur tous les jours. Merci pour votre soutien. Je remercie aussi tout particulièrement mes collègues et amies les plus proches : Anna, Camille, et Cindy. Vous avez été de vrais piliers pendant ma thèse. Toujours partantes pour prendre un verre après le boulot, et parler de tout et de rien. Merci pour les bons moments passés ensembles.

Je remercie mes amis d'enfance de Paris, et en particulier Maud, Priscille, Karen, Anne-Lise, Hugues, et Nicolas. Merci pour d'avoir toujours été là pour moi dans les bons et les moins bons moments. Je remercie aussi mes amis de Bordeaux qui m'ont accueilli comme une vraie famille. Bené, Améline, Alexis, Thomas et Antho un grand merci, grâce à vous, je me suis toujours sentie comme chez moi à Bordeaux. Je remercie également mon colocataire et ami François pour la super année passée au 26 rue Louis Liard.

Enfin, je remercie ma famille, qui m'a toujours soutenue afin que je puisse donner le meilleur. Merci pour votre confiance lorsque je vous ai dit que je voulais faire une thèse, et merci d'avoir essayé de comprendre mon sujet. Grace à votre soutien, j'ai pu confirmer ma passion pour les sciences et la recherche. Merci à mes sœurs. Klervie et Daphné, vous avez toujours été des sœurs en or, et vous l'avez encore été tout au long de cette thèse, merci pour tout (« toi-même tu sais » comme on dit).

Titre et résumé en français :

Synthèse de terpolymères ABC linéaires et en étoile et étude de leur auto-organisation en film minces.

La miniaturisation des composants électroniques devient de plus en plus difficile avec les méthodes classiques. C'est pourquoi, l'industrie de la microélectronique envisage aujourd'hui de nouvelles façons de fabriquer des objets discrets, à l'échelle nanométrique, parfaitement organisés dans un réseau dense. Par exemple, la course à la miniaturisation des cellules DRAM prévoit une demi-distance de 5 nm entre deux plots constituant les éléments de stockage de charge dans les mémoires non-volatiles pour 2020.

Actuellement, des techniques de nano-fabrications très coûteuses permettent déjà de produire des objets à une si petite échelle. Afin de réduire le coût de fabrication, l'utilisation copolymères à blocs (CPBs) en tant que masques pour la nanolithographie pourrait représenter une alternative industrielle. En effet, les CPBs sont compatibles avec les technologies au silicium déjà utilisées par l'industrie de la microéléctronique, et ils ont la capacité de s'auto-assembler en réseaux denses et réguliers possédant de petite période.

Aujourd'hui, la communauté scientifique a déjà largement étudié l'auto-assemblage de copolymères diblocs, qui permettent la formation de sphères, de cylindres, de gyroides ou de lamelles. L'auto-assemblage des copolymères diblocs est assez bien compris. Ajouter un bras supplémentaire de nature chimique différente au copolymère dibloc donne lieu à la formation d'un terpolymère ABC. Ce terpolymère peut adopter une architecture linéaire lorsque le bloc C est attaché à la fin du bloc B, ou une architecture en étoile lorsque les trois bras sont reliés en un point au cœur de la molécule. Les terpolymères ABC linéaires ou en étoile donnent accès à des structures qui ne sont pas accessibles avec les copolymères diblocs telles que des structures hiérarchiques cœur-écorce ou alternées, ou encore à des pavages d'Archimède.[1] Les paramètres gouvernant l'auto-assemblage de terpolymères ABC linéaires ou en étoile en films minces sont plus nombreux et donc plus complexes à appréhender que ceux gouvernant l'auto-assemblage des copolymères diblocs. Une des limitations liées à l'utilisation de terpolymère ABC linéaires ou en étoile provient du fait que la synthèse de ce type de CPBs se révèle plus complexe que la synthèse de copolymères diblocs.

[1] Hadjichristidis, N., Iatrou, H., Pitsikalis, M., Pispas, S. & Avgeropoulos, A. Linear and non-linear triblock terpolymers. Synthesis, self-assembly in selective solvents and in bulk. *Prog. Polym. Sci.* **30,** 725–782 (2005).

Dans cette thèse, nous nous sommes tout d'abord concentrés sur la synthèse de terpolymères ABC linéaires et en étoile puis sur l'étude de l'auto-assemblage de ces terpolymères en film minces.

Dans la première partie de cette thèse, nous avons mis en place une méthode de synthèse efficace pour la synthèse de terpolymères ABC linéaires et en étoile. L'un des paramètres clés est le degré d'incompatibilité entre les blocs, représenté par le paramètre d'interaction de Flory-Huggins. La conception de terpolymères dont les blocs sont hautement incompatibles permet de promouvoir la micro-séparation de phase. Ici, nous avons choisi de travailler avec du polystyrène (PS), poly(2-vinylpyiridine) (P2VP), et du polyisoprène (PI) dont les paramètres de Flory-Huggins, χ, entre les blocs sont élevés ($\chi_{PS\text{-}PI}$[2] $\approx \chi_{PS\text{-}P2VP}$[3] $\approx 0{,}1$ et $\chi_{PI\text{-}P2VP}$[4] $\approx 0{,}8$).

Notre but a été de trouver une méthode de synthèse efficace permettant de garder la masse moléculaire de PS et de P2VP constante tout en variant la masse moléculaire de PI. Nous avons choisi de travailler avec des méthodes de couplage qui permettent d'attacher un dibloc PS-*b*-P2VP de masse moléculaire constante à des blocs PI de masses moléculaires différentes afin de moduler facilement la masse moléculaire de PI.

Dans un premier temps, nous avons synthétisé des terpolymères ABC linéaires. La polymérisation anionique a été choisie comme voie de synthèse car elle permet un bon contrôle de la croissance des chaînes polymères lors de la synthèse ce qui permet d'obtenir des terpolymères bien définis. Dans la littérature, la méthode la plus reportée pour la synthèse de terpolymères ABC linéaires est la polymérisation anionique séquentielle. Cette méthode consiste en la polymérisation anionique du monomère A qui, après avoir été consommé, initie la polymérisation anionique du monomère B et ainsi de suite. Dans notre étude, nous avons choisi de travailler avec un PS-*b*-P2VP-*b*-PI. La polymérisation anionique séquentielle des deux premiers blocs (PS et P2VP) est possible, tandis que le centre actif porté par la P2VP vivante ne pourra pas initier la polymérisation du PI. C'est pourquoi, la polymérisation anionique séquentielle n'a pas pu être envisagée dans cette étude.

---

[2] Ren, Y., Lodge, T. P. & Hillmyer, M. A. Synthesis, characterization, and interaction strengths of difluorocarbene-modified polystyrene-polyisoprene block copolymers. *Macromolecules* **33,** 866–876 (2000).

[3] Hammond, M. R., Cochran, E., Fredrickson, G. H. & Kramer, E. J. Temperature dependence of order, disorder, and defects in laterally confined diblock copolymer cylinder monolayers. *Macromolecules* **38,** 6575–6585 (2005).

[4] Funaki, Y. *et al.* Influence of casting solvents on microphase-separated structures of poly(2-vinylpyridine)-block-polyisoprene. *Polymer (Guildf).* **40,** 7147–7156 (1999).

Ainsi, les terpolymères ABC linéaires ont été obtenus par synthèse de PS-*b*-P2VP et de PI tous deux fonctionnalisés en bout de chaîne puis couplage.

La synthèse de PI fonctionnalisé en bout de chaîne a été réalisée par polymérisation anionique sans étape de protection ou de deprotection. La fonctionnalisation en bout de chaine a été réalisée par carboxylation du PI en croissance. Un schéma général de la synthèse est montré ci-dessous (Fig. 1).

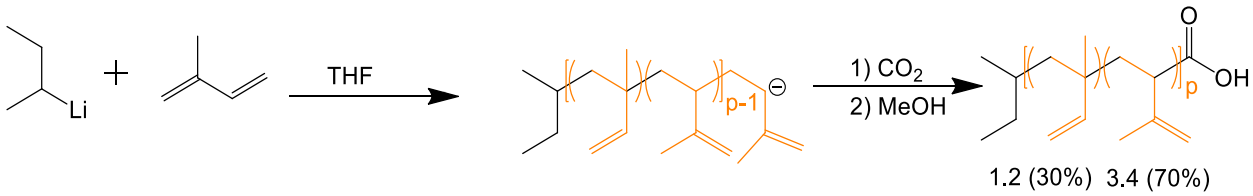

Figure 1: Schéma réactionnel de la synthèse du polyisoprène fonctionnalisé en bout de chaîne avec une fonction acide carboxylique.

La polymérisation anionique de l'isoprène a été réalisée dans le THF à -30°C en utilisant le *sec*-Butyllithium (*sec*-BuLi) comme amorceur. Une fois tout le monomère consommé, du dioxyde de carbone a été bullé dans la solution puis la réaction a été stoppée par ajout de méthanol. Les différentes masses moléculaires de PI ont été obtenues en faisant varier la quantité d'amorceur lors de la polymérisation.

Les PI synthétisés ont été caractérisés par résonnance magnétique nucléaire (RMN) du proton et par chromatographie d'exclusion stérique (SEC). Le nombre d'unités 1.2 (δ = 5,5 – 6 ppm) et 3.4 (δ = 4,4 – 5 ppm) a été déterminé par RMN du proton et est respectivement de 30 et 70% dans le PI. Les masses moléculaires du PI ont été déterminées par SEC dans le THF de 9, 13, 16 et 28 $kg.mol^{-1}$. La fonctionnalisation quantitative du PI a été vérifiée par un titrage à la phénoltphtaléine.

La synthèse du dibloc de PS-*b*-P2VP a été réalisée par polymérisation anionique séquentielle. La fonctionnalisation en bout de chaîne a été effectuée par ajout d'oxyde d'éthylène sur les chaines vivantes de PS-*b*-P2VP. Un schéma général de la réaction est présenté ci-dessous (Fig. 2).

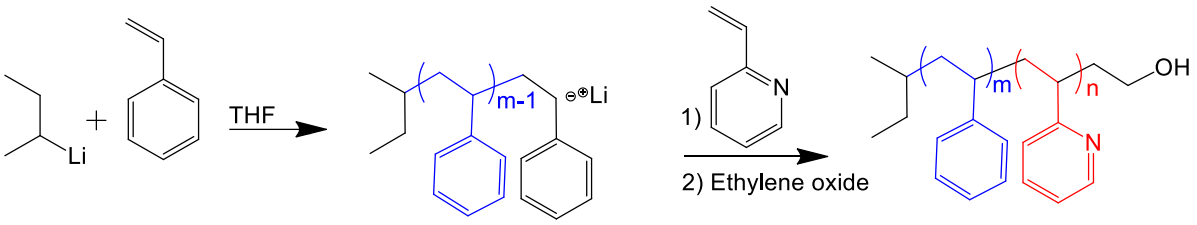

Figure 2: Schéma réactionnel de la polymérisation anionique séquentielle du PS-b-P2VP fonctionnalisé en bout de chaîne avec une fonction alcool.

La polymérisation anionique du styrène est amorcée par le *sec*-BuLi dans le THF à -78°C. Lorsque tout le monomère est consommé, la 2VP est ajoutée. Le polystyrillithium amorce alors la polymérisation anionique de la 2VP. Lorsque toute la 2VP est consommée, de l'oxyde d'éthylène est ajouté afin d'apporter la fonction alcool en bout de chaîne. Enfin, la réaction est stoppée par ajout de méthanol.

Le dibloc ainsi synthétisé est caractérisé par SEC et par RMN du proton. Les masses moléculaires du PS et du P2VP ont été déterminées par SEC de 21 et 24 kg.mol^{-1} respectivement. La fraction obtenue entre les blocs de PS et de P2VP a été confirmée par RMN du proton (PS : P2VP = 1 : 1.1).

Les terpolymères ABC linéaires de PS-*b*-P2VP-*b*-PI ont été synthétisé par couplage entre le dibloc PS-*b*-P2VP et les PI de différentes masses moléculaires. La méthode la plus reportée dans la littérature pour la synthèse de CPBs est la chimie « click » d'Huisgen. Cette méthode de couplage permet d'obtenir un rendement proche de 1. Néanmoins, elle met en jeu l'intervention de métaux (souvent du cuivre) en tant que catalyseur. Ces métaux peuvent être chélatés par la 2VP ce qui augmentent le nombre d'étapes de purification. De plus, cette méthode nécessite de nombreuses étapes de fonctionnalisation. Nous avons donc décidé d'utiliser l'estérification de Steglich qui a un rendement proche de 1 et nécessite peu d'étapes de fonctionnalisation et de purification. Le dibloc PS-*b*-P2VP fonctionnalisé par une fonction alcool en bout de chaîne a alors été couplé au PI possédant une fonction acide carboxylique terminale. Un schéma général de la synthèse est présenté ci-dessous (Fig. 3).

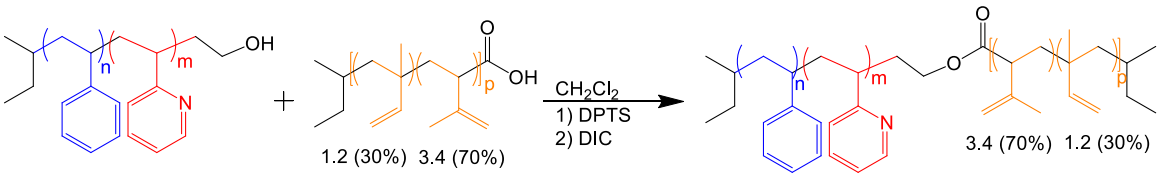

Figure 3: Schéma réactionnel du couplage entre PS-b-P2VP et PI par estérification de Steglich.

Les chaînes de PS-*b*-P2VP et de PI sont solubilisées dans du dichlorométhane et la réaction de Steglich est catalysée par du 1,4-diméthylpyridinium *p*-toluènesulfonate (DPTS) et du *N,N'*-diisopropylcarbodiimide (DIC). Le terpolymère ainsi obtenu est alors caractérisé par RMN et par SEC. La présence des signaux caractéristiques du PS (δ = 6 – 7,5 ppm), du P2VP (δ = 6 - 7,5 ppm et δ =8 – 8,5 ppm) et du PI (δ = 5,5 – 6 ppm et δ = 4,4 – 5 ppm) sur le spectre RMN après purification confirme le couplage entre le dibloc et l'homopolymère. Une preuve supplémentaire est apportée par le déplacement des courbes obtenues par SEC des plus petites masses molaires vers les plus hautes masses molaires. Enfin, une analyse DOSY a été effectuée. La présence d'un unique coefficient de diffusion sur le spectre RMN DOSY atteste de la pureté du terpolymère synthétisé.

Tableau 1: Tableau récapitulant les terpolymères ABC linéaires synthétisés par la combinaison de polymérisations anioniques avec un couplage par estérification de Steglich.

	PS		P2VP		PI		volume fraction/PS		
sample	M_n (kg/mol)	vol. frac.	M_n (kg/mol)	vol. frac.	M_n (kg/mol)	vol. frac.	S	P	I
$S_{21}P_{24}I_9$	21	0.39	24	0.41	9	0.20	1	1.1	0.5
$S_{21}P_{24}I_{13}$	21	0.36	24	0.38	13	0.26	1	1.1	0.7
$S_{21}P_{24}I_{16}$	21	0.34	24	0.36	16	0.30	1	1.1	0.9

Trois terpolymères ABC linéaires ont été synthétisés avec cette méthode en gardant la masse moléculaire de PS et de P2VP constante, mais en faisant varier uniquement la masse moléculaire de PI. Un tableau récapitulatif est présenté ci-dessus (Tableau 1).

Nous avons ensuite synthétisé des terpolymères ABC en étoile. Dans la littérature, trois méthodes principales ont été reportées pour la synthèse de terpolymères ABC en étoile. La première, développée par Hadjichristidis[5] consiste en la synthèse de trois bras par polymérisation vivante ou contrôlée, les trois étant ensuite liés à une molécule cœur de chlorosilane. Cette méthode appelée « arm-first » nécessite l'utilisation d'une verrerie spécifique. Elle n'a donc pas été envisagée dans cette thèse. La seconde méthode met en jeu

[5] Iatrou, H. & Hadjichristidis, N. Synthesis of a Model 3-Miktoarm Star Terpolymer. *Macromolecules* **25,** 4649–4651 (1992).

l'utilisation d'une molécule cœur multifonctionnelle.[6] Des polymérisations vivantes ou contrôlées sont alors réalisées à partir de cette molécule cœur. Cette méthode appelée « grafting from » est limitée dès lors que les monomères doivent être sélectifs. La dernière méthode appelée « hybrid approach » est une combinaison de la première et de la deuxième méthode.[7] Ainsi, la molécule cœur est un mélange de sites de terminaison et d'amorçage. Nous avons choisi de travailler avec cette méthode dans le cadre de cette thèse.

La première étape de la synthèse d'un terpolymère ABC en étoile avec la méthode « hybrid approach » consiste en la synthèse d'une molécule cœur comportant des sites de terminaison et d'amorçage. Ainsi, nous avons synthétisé un dérivé de la diphényléthylène portant une fonction alcool protégée.

A partir d'une 4-bromobenzophenone, nous avons réduit la fonction cétone par une réaction de Wittig afin d'obtenir une diphényléthylène substituée par une fonction bromure. Nous avons ensuite réalisé un réactif de Grignard à partir de la fonction bromure capable d'ouvrir l'oxyde d'éthylène et ainsi obtenir une diphényléthylène substituée par une fonction alcool. La dernière étape de la synthèse consiste en la protection par un composé silylé de la fonction alcool. Le schéma réactionnel est montré ci-dessous (Fig. 4).

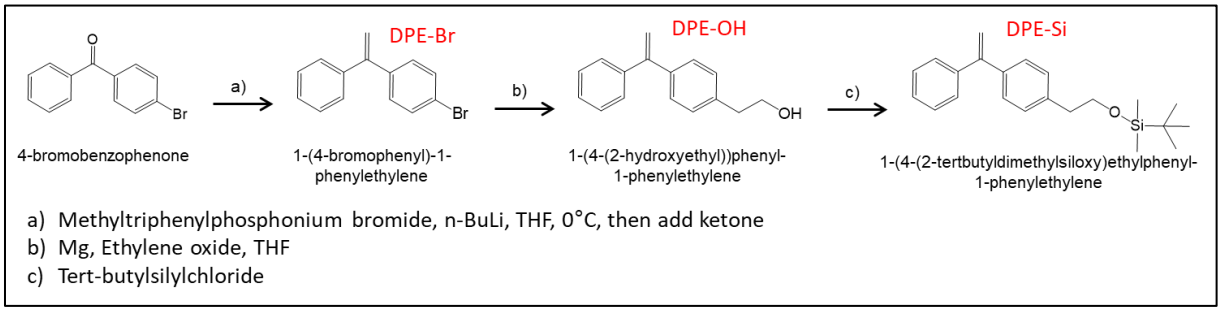

Figure 4: Schéma réactionnel de la synthèse de la molécule cœur (1-(4-(2-tertbutyldiméthylsiloxy)éthyl)phényl-1-phényléthylène) à partir du 4-bromobenzophénone

A chaque étape de la synthèse, les produits ont été purifiés par chromatographie flash et caractérisés par RMN du proton. L'intégration des pics a confirmé la synthèse d'une 1-(4-(2-tertbutyldiméthylsiloxy)éthyl)phényl-1-phenylethylène.

---

[6] He, T., Li, D., Sheng, X. & Zhao, B. Synthesis of ABC 3-miktoarm star terpolymers from a trifunctional initiator by combining ring-opening polymerization, atom transfer radical polymerization, and nitroxide-mediated radical polymerization. *Macromolecules* **37,** 3128–3135 (2004).

[7] Fujimoto, T. *et al.* Preparation and characterization of novel star-shaped copolymers having three different branches. *Polymer (Guildf).* **33,** 2208–2213 (1992).

Une fois la molécule cœur synthétisée, la synthèse d'un PS-*b*-P2VP fonctionnalisé en son cœur a été réalisée. Ainsi, le styrène a été polymérisé par polymérisation anionique dans le THF à -78°C amorcée par du *sec*-BuLi. Après consommation complète du monomère, la molécule cœur est ajoutée. Le polystyryllithium réagit alors sur la double liaison de la diphényléthylène substituée pour former un macroamorceur. La 2VP est ensuite ajoutée dans le milieu. Le macroamorceur vivant amorce alors la polymérisation anionique de la 2VP. Une fois le monomère consommé, du méthanol est ajouté afin de stopper la réaction. La fonction alcool portée par la molécule cœur est alors déprotégée par hydrolyse. Un schéma de la réaction est montré ci-dessous (Fig. 5).

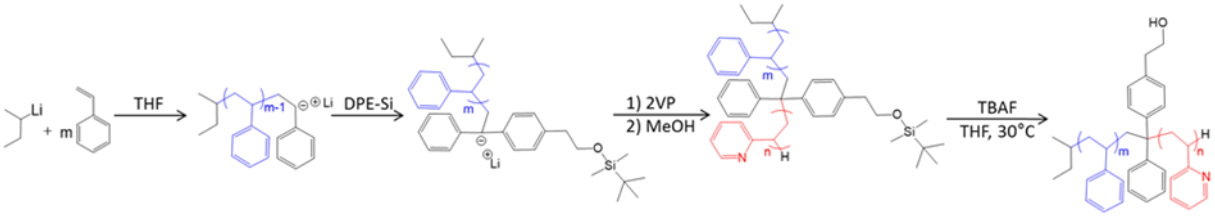

Figure 5: Schéma réactionnel de la synthèse d'un dibloc (PS-b-P2VP) fonctionnalisé en son cœur.

Le dibloc fonctionnalisé en son cœur a été caractérisé par RMN du proton et par SEC. Le spectre RMN présente des signaux caractéristiques des protons portés par la 2VP et le styrène confirmant ainsi la synthèse du dibloc. La courbe obtenue par SEC du dibloc ne présente un seul pic fin et monomodal confirmant ainsi la pureté du dibloc. Les masses moléculaires ont été déterminées par SEC de 19 et 24 kg.mol^{-1}, respectivement pour le PS et la P2VP. Les masses moléculaires obtenues par SEC sont en accord avec la fraction de PS et de P2VP obtenue par RMN.

Afin d'obtenir des terpolymères ABC en étoile, le PS-*b*-P2VP fonctionnalisé en son cœur a été couplé aux différents PI synthétisés précédemment par une estérification de Steglich. Le schéma de la réaction est présenté ci-dessous (Fig. 6).

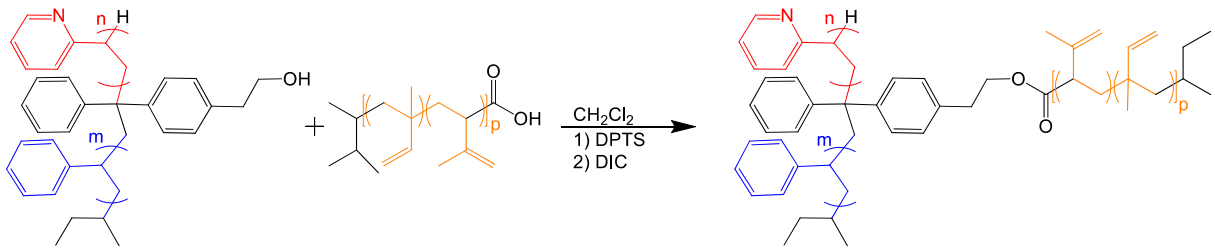

Figure 6: Schéma réactionnel présentant le couplage par estérification de Steglich de PS-b-P2VP et PI afin d'obtenir un terpolymère ABC en étoile.

Les terpolymères ABC en étoile ainsi synthétisés ont été caractérisés par RMN, SEC et RMN DOSY confirmant ainsi la synthèse de quatre terpolymères ABC en étoile. Un tableau récapitulatif est présenté ci-dessous (Tableau 2).

	PS		P2VP		PI		volume fraction/PS		
sample	M_n (kg/mol)	vol. frac.	M_n (kg/mol)	vol. frac.	M_n (kg/mol)	vol. frac.	S	P	I
3 μ-$S_{19}P_{24}I_9$	19	0.37	24	0.43	9	0.20	1	1.2	0.6
3 μ-$S_{19}P_{24}I_{13}$	19	0.34	24	0.39	13	0.27	1	1.2	0.8
3 μ-$S_{19}P_{24}I_{16}$	19	0.32	24	0.37	16	0.31	1	1.2	1.0
3 μ-$S_{19}P_{24}I_{28}$	19	0.26	24	0.30	28	0.44	1	1.2	1.7

Tableau 2: Tableau récapitulant les terpolymères ABC en étoile synthétisés par couplage d'un PS-b-P2VP fonctionnalisé en son cœur avec un polyisoprène fonctionnalisé en bout de chaîne.

Pour conclure sur cette première partie de cette thèse, nous avons mis au point une méthode de synthèse permettant d'obtenir des terpolymères ABC linéaires et en étoile ayant deux blocs (PS et P2VP) de taille identique, tandis que la taille du dernier bloc (PI) varie (composition symétrique par rapport aux autres blocs ou asymétriques).

Nous avons ensuite étudié les morphologies accessibles par l'auto-assemblage d'un terpolymère ABC linéaire frustré de type II dans une configuration de film mince. L'auto-assemblage de ce type de terpolymère (frustré de type II) n'a jamais été décrit en film mince mais uniquement en masse dans la littérature. Ainsi, des études théoriques et expérimentales (uniquement en masse) ont montré que des sphères dans des sphères, des sphères sur des cylindres, des anneaux sur des cylindres, des cylindres dans des lamelles, des gyroïdes alternées, des lamelles alternées, ou encore des hélices sur des cylindres sont autant de morphologies accessibles avec des terpolymères ABC linéaires de type II.[8]

Le comportement en film mince du PS_{21}-*b*-$P2VP_{24}$-*b*-PI_9 (les chiffres en indice correspondent aux masses moléculaires des blocs en $kg.mol^{-1}$) a été étudié. Pour cela, une solution de polymère à 2% en masse dans du toluène a été déposée à la tournette sur un substrat en silicium. L'épaisseur du film est contrôlée par la vitesse de rotation du substrat (1,5 krpm). La mobilité des chaînes polymères a été apportée par un recuit des films dans une vapeur de chloroforme. Afin d'augmenter le contraste lors des analyses microscopiques, les films ont été traités par un plasma CF_4/O_2 et le bloc de P2VP a été marqué par des sels de platine. Des images

[8] Li, S., Jiang, Y. & Chen, J. Z. Y. Morphologies and phase diagrams of ABC star triblock copolymers confined in a spherical cavity. *Soft Matter* **9,** 4843 (2013).

de microscopie à force atomique (AFM) et microscopie électronique à balayage (MEB) ont alors été réalisées. Les images MEB de la morphologie obtenue sont montrées ci-dessous (Fig. 7).

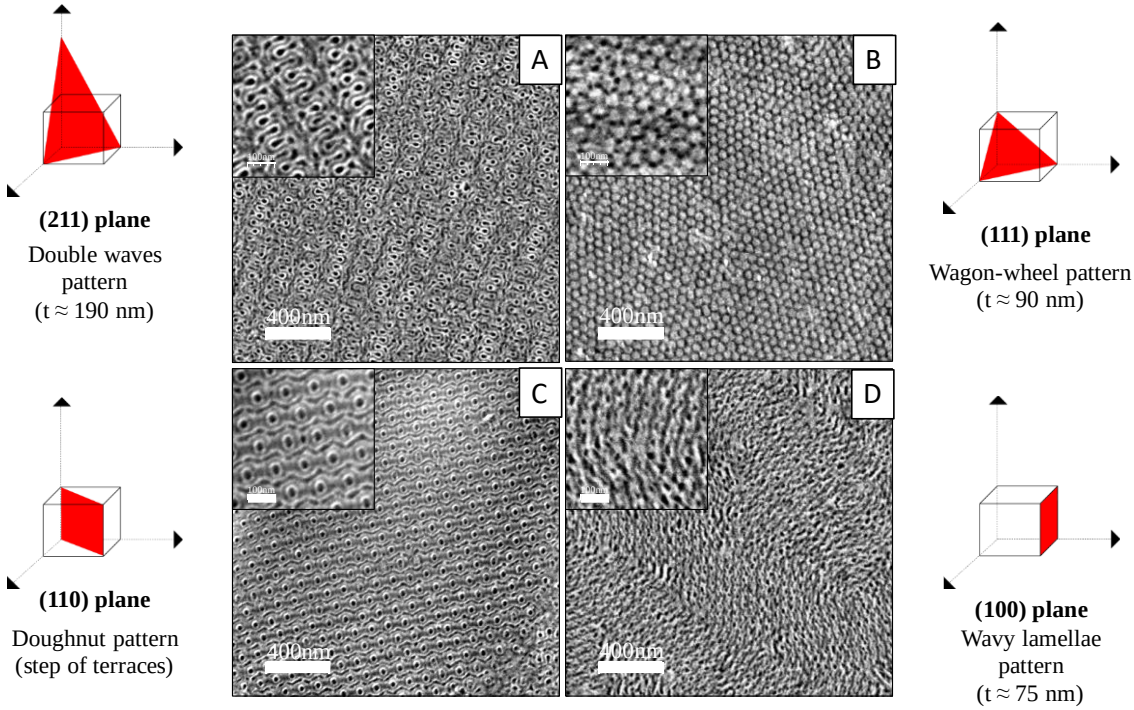

Figure 7: Images MEB (2 x 2 μm^2; encart: 0,5 x 0,5 μm^2) d'un film mince de PS_{21}-b-$P2VP_{24}$-b-PI_9 recuit deux heures dans des vapeurs de chloroforme, traité avec un plasma $CF_4/0_2$ qui révèle quatre plans de la structure Q^{230} (A : (211) ; B : (111) ; C : (110) ; D : (100))

Sur les images MEB, le PI apparait en noir (car le PI est le polymère le plus gravé), le P2VP apparait en blanc (du fait de son marquage au platine) et le PS en gris. Lorsque le film présente une épaisseur de 190 nm, on observe un motif présentant deux vagues ayant des amplitudes différentes (Fig 7. A). Les vagues de grandes amplitudes sont séparées par des vagues de petites amplitudes avec une période de l'ordre de 120 nm. Ce motif correspond au plan (211) d'une structure double gyroïde cœur-écorce aussi appelée structure Q^{230}. La période du motif correspond alors environ à la dimension de la cellule unité de la structure Q^{230}. Le PS occupe la matrice, le PI le cœur et le P2VP l'écorce de la structure.

Lorsque l'on diminue l'épaisseur du film au-dessous de la dimension de la cellule unité (Fig. 7 B, C et D), le motif obtenu diffère du plan (211) de la structure Q^{230}. En effet, lorsque l'épaisseur du film est de l'ordre de 90 nm, un motif en roue de charrette caractéristique du plan (111) de la structure Q^{230} apparaît. Si l'épaisseur du film est réduite jusqu'à 75 nm, on obtient le plan (100) de la structure Q^{230} et entre les terrasses formées par le film, on observe le plan (110) de la structure Q^{230} présentant un motif de donuts.

Ces observations ont permis de conclure que l'orientation des plans de la structure double gyroïde cœur-écorce est contrôlée par l'épaisseur du film. Afin d'en savoir plus sur cette relation entre épaisseur du film et orientation des plans de la structure, nous nous sommes intéressés à une étude réalisée par Hashimoto et son équipe.[9] Dans cette étude, ces auteurs montrent qu'il existe un lien direct entre l'aire occupée par la matrice à la surface du film et les différents plans de la gyroïde. Ils ont mis en relief le fait que le plan (211) minimise l'aire de la matrice (PS) à la surface du film. Ceci permet ainsi d'optimiser la présence de PI à la surface du film. Contenu de la faible énergie de surface du PI, celui-ci minimise l'énergie libre du système en déplétant à la surface du film. On peut noter que ceci est rendu possible uniquement car l'épaisseur du film laissant apparaître le plan (211) de la structure Q^{230} est supérieure à la dimension de la cellule unité. En effet, pour des raisons de commensurabilité, lorsque l'on diminue l'épaisseur du film, on va vers des périodicités de plus en plus petite en passant par des plans où la fraction volumique occupée par le PI en surface décroit de plus en plus. L'ordre des plans observés par Hashimoto *et al.* est en accord avec les résultats obtenus expérimentalement dans notre étude.

Pour conclure, quatre plans différents de la structure Q^{230} ont été démontrés. Si l'épaisseur du film est supérieure à la dimension de la cellule unité, le plan (211) est le plan thermodynamiquement le plus stable dès lors que l'aire de PI (bloc ayant l'énergie de surface la plus faible) à la surface du film est maximisé.
Si l'épaisseur du film est inférieure à la dimension de la cellule unité, l'orientation du plan est dirigée par la commensurabilité entre l'épaisseur di film et la période du motif.

Dans un dernier temps, nous nous sommes intéressé à l'auto-assemblage en film mince de deux terpolymères ABC en étoile. Dans la littérature, peu d'études reportent l'auto-assemblage en film mince de terpolymères ABC en étoile. Les pavages d'Archimède (4.8.8), (6.6.6) ainsi que des morphologies hiérarchiques sont les seules morphologies démontrées en film mince.

Dans cette thèse, nous avons étudié l'auto-assemblage de deux terpolymères ABC en étoile (3 μ-$S_{19}P_{24}I_9$ et 3 μ-$S_{19}P_{24}I_{16}$) dans une configuration de type film mince. Pour cela, les terpolymères ont été solubilisés à 2% en masse dans le toluène et déposés à la tournette (1,5

[9] Hashimoto, T., Nishikawa, Y. & Tsutsumi, K. Identification of the 'voided double-gyroid-channel': A new morphology in block copolymers. *Macromolecules* **40,** 1066–1072 (2007).

krpm) sur un substrat en silicium. Le film obtenu a ensuite été recuit dans différentes vapeurs de solvant puis traité par un procédé plasma.

L'image AFM d'un film mince de 3 μ-$S_{19}P_{24}I_9$ recuit dans une vapeur de THF est reportée ci-dessous (Fig. 8A). Pour un film de 80 nm, une morphologie hexagonale où le PS (en jaune) est entouré par 6 colonnes de PI (en noir) et 6 colonnes de P2VP (en marron) apparaît. Les domaines de PS ont une période de 46 nm tandis que ceux de PI et de P2VP ont une période de 23 nm. Cette structure correspond au pavage d'Archimède (4.6.12). C'est la première fois que ce type de pavage est obtenu en film mince.

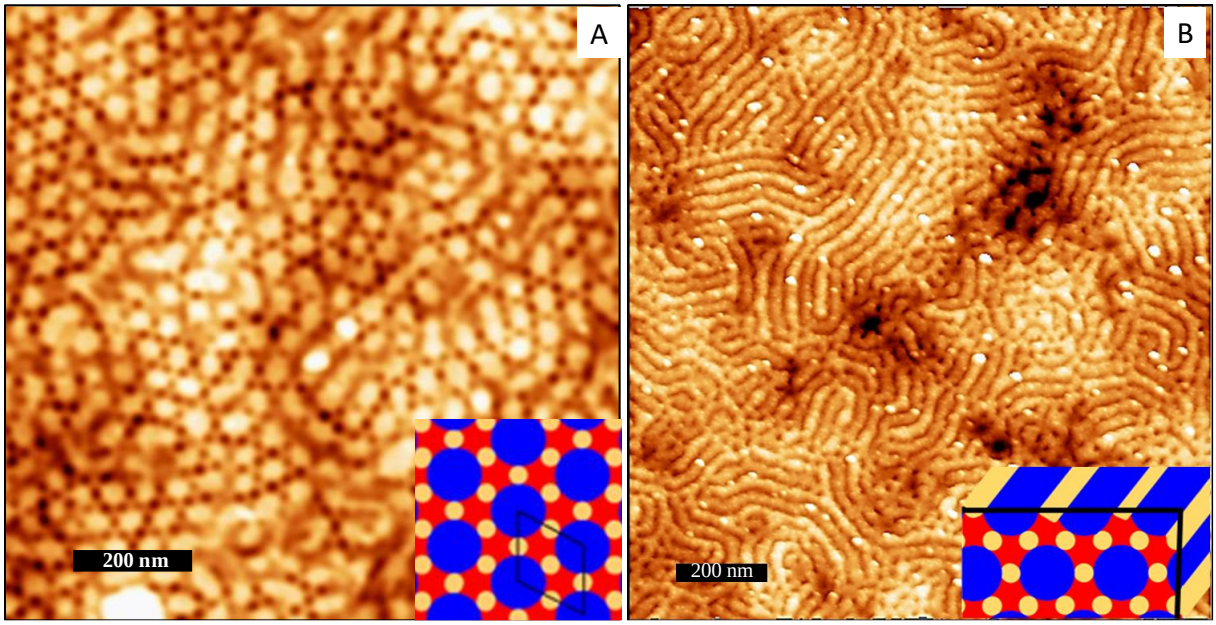

Figure 8: Images AFM (1 x 1 μm^2) d'un film mince de 3 µ-$S_{19}P_{24}I_9$ *recuit deux heures dans une vapeur de THF et traité par un plasma CF_4/O_2. A : pavage d'Archimède (4.6.12) orienté perpendiculairement à la surface libre du film (épaisseur du film : 80nm) et B : pavage d'Archimède (4.6.12) orienté parallèlement à la surface libre du film (épaisseur du film : 100nm)*

Si on augmente l'épaisseur du film (Fig. 8B), on obtient une orientation parallèle à la surface libre du film de la structure (4.6.12) selon le plan coupant les domaines de PI et de PS au centre des colonnes. L'orientation parallèle à la surface libre du film est favorisée en film épais car le THF gonfle plus le bloc PS que les autres blocs (celui-ci va donc remonter à la surface libre du film) et le PI, qui a une faible énergie de surface, va donc lui aussi se positionné à l'interface film-air. On remarque ici une forte dépendance entre l'orientation de la structure et l'épaisseur du film.

Un terpolymère ABC en étoile ayant une composition symétrique (3 μ-$S_{19}P_{24}I_{16}$) entre les trois blocs a lui aussi été auto-assemblé dans une configuration de film mince. Le film a été recuit par vapeur de chloroforme. L'image AFM ainsi obtenue est présentée sur la figure 9.

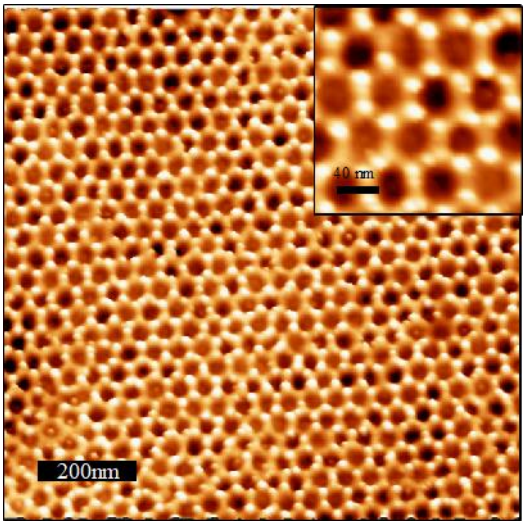

Figure 9: Image AFM (1 x 1 μm^2) d'un film de 3 μ-$S_{19}P_{24}I_{16}$ *(épaisseur = 80 nm) recuit deux heures dans une vapeur de* $CHCl_3$ *et traité par un plasma* CF_4/O_2 *faisant apparaître un pavage d'Archimède (4.6.12) où le PI (en noir) est entouré par 6 colonnes de PS (jaune clair) et 6 colonnes de P2VP (marron).*

Le film montre une morphologie colonnaire hors du plan où les colonnes de PI (noir) sont entourées par 6 colonnes de PS et 6 colonnes de P2VP. La période des domaines de PI est de 41 nm tandis que celle des domaines de PS et de P2VP est de 24 nm. Cette structure correspond elle aussi au pavage (4.6.12) précédemment décrit. On notera que les blocs occupent des places différentes dans la structure par rapport au pavage (4 .6.12) obtenu pour une composition en PI plus asymétrique.

Le bloc de PI occupant le cœur de la structure présente un ordre à plus longue distance que les domaines de PS et de P2VP. En effet, ces derniers ne forment pas toujours 6 colonnes autour du bloc PI. Les domaines de PI étant le plus organisés, on peut supposer que la séparation de phase se produit selon un mécanisme en deux étapes où l'auto-organisation du bloc PI est plus avancée que celle des blocs de PS et de P2VP.

Lorsque l'on augmente l'épaisseur du film, on obtient une maille carrée (Fig. 10). Les domaines de PI sont alors entourés par 4 colonnes de PS et 4 colonnes de P2VP. Cette structure correspond à un pavage d'Archimède (4.8.8). Les pavages (4.8.8) et (4.6.12) présentent des minima énergétiques proche l'un de l'autre ce qui semblerait faciliter le passage d'un pavage à l'autre en changeant l'épaisseur.

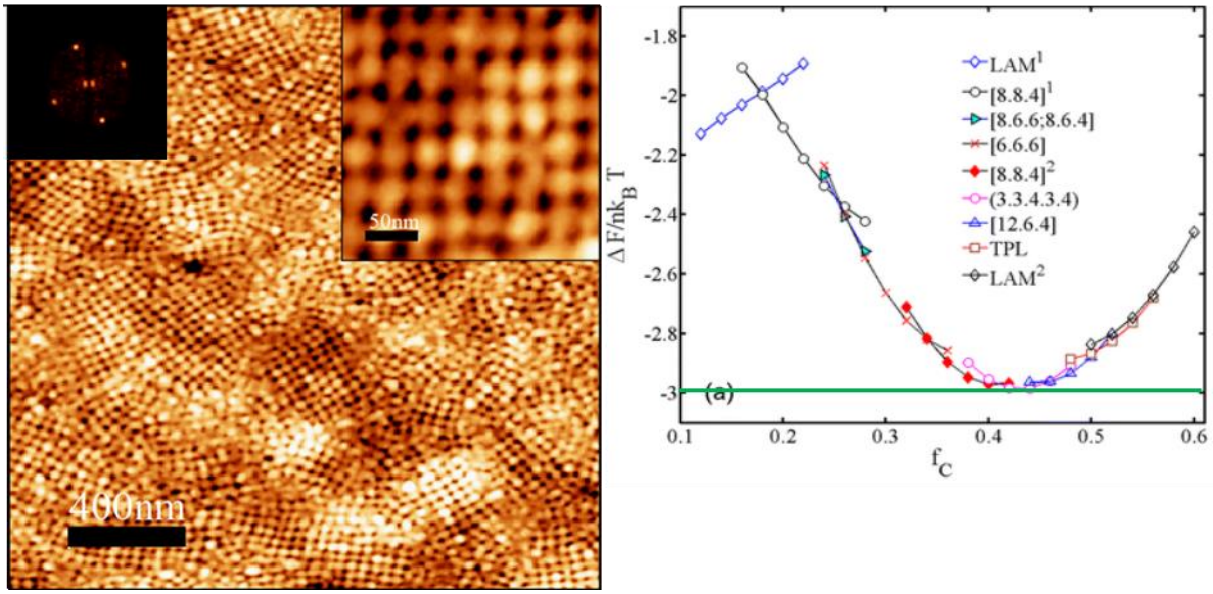

Figure 10: Image AFM (2 x 2 μm^2) d'un film de 3 μ-$S_{19}P_{24}I_{16}$ *(épaisseur = 110nm) recuit deux heures dans une vapeur de $CHCl_3$ et traité par un plasma CF_4/O_2 faisant apparaître un pavage d'Archimède (4.8.8) où PI (en noir) est entouré par 4 colonnes de PS (jaune clair) et 4 colonnes de P2VP (marron).*

Dans cette étude, nous avons obtenus des pavages d'Archimède (4.6.12) en film mince. Nous avons montré qu'un mécanisme en deux étapes régissait la micro-séparation de phase. Les deux pavages (4.6.12) ont été obtenus pour des compositions en PI et des solvants de recuit différents. Nous avons ainsi montré que la position occupée par le centre de la structure était occupée par le polymère ayant la plus grande affinité avec le solvant de recuit.

En augmentant l'épaisseur des films, nous avons montré que nous pouvions passer d'un pavage (4.6.12) à un pavage (4.8.8), ou encore d'une structure colonnaire perpendiculaire à l'interface air/film à une structure parallèle à l'interface air/film.

Pour conclure, dans cette thèse, nous avons développé une méthode efficace pour la synthèse de terpolymères ABC linéaires et en étoile composés de PS, P2VP et PI. Une bibliothèque de terpolymères ABC linéaires et en étoile a été synthétisé en gardant la fraction volumique des blocs de PS et de P2VP constante mais en faisant varier la fraction volumique du bloc PI. La méthode de synthèse développée dans cette thèse s'est révélée intéressante car les étapes de fonctionnalisations sont simples et quantitatives. De plus, peu d'étapes de purifications sont nécessaires à l'obtention de terpolymères purs et la méthode de couplage utilisée ne met pas en jeu l'utilisation de métaux en tant que catalyseur.

L'auto-assemblage en film mince de terpolymères ABC linéaires et en étoile a été démontré. Pour cela, un procédé de recuit par vapeur de solvant a été utilisé pour promouvoir

la mobilité des chaines polymères. Un plasma et parfois un marquage aux atomes lourds ont ensuite été réalisés afin d'obtenir du contraste entre les blocs lors des analyses microscopiques.

Nous avons démontré que l'auto-assemblage d'un terpolymère ABC linéaire frustré de type II permettait d'obtenir une structure double gyroïde cœur-écorce en film mince. Différents plans cristallographiques de la structure Q^{230} ont ensuite pu être observés suivant l'épaisseur du film.

Un pavage d'Archimède (4.6.12) a été obtenus par auto-assemblage de deux terpolymères ABC en étoile ayant des fractions volumiques pour le bloc C (PI) différentes. Nous avons mis en évidence la dépendance entre l'affinité du solvant de recuit avec les blocs et la nature du domaine occupant le centre de la structure du pavage d'Archimède (4.6.12). Augmenter l'épaisseur du film nous a, par la suite, permis d'obtenir un pavage d'Archimède (4.8.8).

General introduction

The microelectronic miniaturization becomes more and more difficult with classical technologies such as optical lithography coupled with etching processes. Therefore, the electronic industry is investigating alternative methodologies to fabricate discrete objects with nanoscale dimensions perfectly-ordered into dense arrays. For instance, the DRAM cell miniaturization race foresees a mid-distance of 5 nm between two memory points in 2020. Currently, nanofabrication techniques able to produce devices of this scale are based on serial processes (e-beam, Dip Pen Lithography,…), but those techniques are too many time-consuming for the industry. Block copolymers (BCPs) could be a great industrial alternative. Indeed they are compatible with the silicon technology already used on microelectronic tracks and BCPs have the ability to self-assemble into dense and regular arrays with small periods.

Nowadays, the scientific community has widely studied the self-assembly of diblock copolymers (AB-type BCP), which allows the formation of spheres, cylinders, gyroid, and lamellae. The self-assembly of AB-type BCP thin films is quiet well-understood. Adding another chemically different block leads to the formation of an ABC triblock terpolymer with a star- or linear-architecture. Unlike AB-type BCPs, ABC triblock terpolymers give access to hierarchical, core-shell and alternating morphologies as well as Archimedean tiling patterns. The parameters governing the self-assembly of ABC triblock terpolymer thin films are more numerous than those driving the AB-type BCP self-assembly leading to a more complex phase behavior. Another challenge to the use of ABC triblock terpolymers can be the difficulty of their synthesis as multistep reactions are needed for their formation.

In this PhD thesis, we will focus on the synthesis of linear and star ABC terpolymers and their self-assembly in thin films. This work will first be devoted to the synthesis and the macromolecular characterizations of ABC triblock terpolymers. The synthesis route should allow the formation of well-defined terpolymers with few purification steps. Then, we will focus our study on the self-assembly of linear and star ABC terpolymer thin films in order to better apprehend the structural diversity offered by these complex architectures.

Chapter I of this manuscript will describe the general context of this study. Afterwards, we will study the phenomenon leading to the phase-separation of the BCP chains, the existing synthetic methodologies for the production of complex BCP architectures, as well as the state of the art regarding the self-assembly of linear and star ABC terpolymers.

In **chapter II** we will describe the synthesis of linear and star terpolymers used in this PhD thesis, which consist of polystyrene, poly(2-vinylpyridine) and polyisoprene. Those ABC triblock terpolymers will also be characterized using analytical methods, such as nuclear magnetic resonance (NMR) and size-exclusion chromatography (SEC) characterizations in order to correlate their macromolecular characteristics with the observed self-assembly behavior.

Chapter III will describe the self-assembly of linear ABC terpolymer thin films. We will mainly focus on the self-assembly behavior of a double-core shell gyroid structure with a special attention on the different crystallographic planes oriented parallel to the air surface depending on the film thickness.

In **chapter IV**, we will finally, present the morphologies obtained from the self-assembly of star miktoarm ABC terpolymers (3 μ-ABCs). Two 3 μ-ABCs with different molecular weights and compositions will be presented. We will demonstrate for the first time thin film (4.6.12) Archimedean tiling patterns.

LIST OF ABBREVIATIONS

AFM: Atomic Force Microscope

a_G: Unit cell dimension of the gyroid structure

ATRP: Atom Transfer Radical Polymerization

BCP: Block Copolymer

C_3: Triple cylinders-*on*-cylinders

C_4: Quadruple cylinders-*on*-cylinders

CaH_2: Calcium hydride

CED: Cohesive Energy Density

CF_4: Tetrafluoromethane

CH_2Cl_2: Dichloromethane

$CHCl_3$: Chloroform

CO_2: Carbon dioxide

CSC: Core–shell cylinders

D: Diffusion coefficient

DIC: *N*,*N*'-diisopropylcarbodiimide

DMA: 2-(dimethylamino)ethyl methacrylate

DOSY: Diffusion-Ordered Spectroscopy

DPE : Diphenylethylene

DPE-Si: 1-(4-(2-tert-Butyldimethylsiloxy)ethyl)phenyl-1-phenylethylene

DPTS: 4-(Dimethylamino)pyridinium-4-toluene

FFT: Fast Fourier Transform

FTIR: Fourier Transform InfraRed spectroscopy

H_2C: Double helices-*on*-cylinders

H_3C: Triple helices-*on*-cylinders

hP2VP: P2VP homopolymer

hPI: PI homopolymer

hPS: PS homopolymer

IS: International System

Ka: Acid dissociation constant

χ: Flory-Huggins interaction parameter

KP: Knitting pattern

L_3: Three-color lamellae

LC: Cylinders-*within*-lamellae

MEK: Methyl ethyl ketone

$MgSO_4$: Magnesium sulfate

M_n: Number average molecular weight

M_w: Mass average molar mass

N: Polymerization degree

Na_2SO_4: Sodium sulfate

n-BuLi: *n*-butyllithium

NMR: Nuclear Magnetic Resonance

O_2: Dioxygen

OTDD: Ordered Tricontinuous Double-Diamond

P2VP: Poly(2-vinylpyridine)

P4VP: Poly(4-vinylpyridine)

PAA: Polyacrylic acid

PAN: Polyacrylonitrile

PB: Polybutadiene

PC: Perforated Circular lamella-*on*-cylinders

PCEMA: Poly(2-cinnamoylethyl methacrylate)

PCL: Poly(ε-caprolactone)

PDMA: Poly(*N*,*N*-dimethylacrylamide)

PDMS: Polydimethylsiloxane

PDMSB: Poly(1,1-dimethylsilacyclobutane)

PEA: Poly(ethyl acrylate)

PEM : PhotoElastic Modulator

PEO: Poly(ethylene oxide)

PFS: Polyferrocenylsilane

PFT: PeakForce Tapping

PI: Polyisoprene

PI-COOH: Carboxyl-end-functionalized polyisoprene

PL: Perforated Lamellae

PLA: Pol(D,L-lactide acid)

PLL: Poly-L-lysine

PM-IRRAS : Phase-Modulation InfraRed Reflection Absorption Spectroscopy

PMMA: Poly(methyl methacrylate)

PnBMA: Poly(*n*-butyl methacrylate)

ppm: Parts-per-million

PS: Polystyrene

PS-*b*-P2VP-OH: Hydroxyl-end-functionalized PS-*b*-P2VP

PtBA: Poly(tert-butyl acrylate)

PtBMA: Poly(tert-butyl methacrylate)

RIE: Reactive-Ion Etching

ROP: Ring Opening Polymerization

rpm: Round per minute

SAXS: Small-Angle X-Ray Scattering

SEC: Size exclusion chromatography

sec-BuLi : *sec*-butyllithium

SPM: Scanning probe microscopy

SVA: Solvent-Vapor Annealing

TBAF: Tetra-*n*-butylammonium fluoride

TEM: Transmission Electronic Microscope

TEMPO: 2,2,6,6-tetramethylpiperidinyloxyl

Tg: Glass transition temperature

THF: Tetrahydrofuran

TM: Tappingmode

SOMMAIRE

CHAPTER 1. BIBLIOGRAPHIC STUDY

I. General context

The component miniaturization which regulates the microelectronic industry evolution has led to a race toward the development of new lithographic techniques. Indeed, the lithographic resolution for a high density array is defined by the Rayleigh equation:

$$R = k_1 \frac{\lambda}{NA}$$

Where λ is the wavelength used for the lithographic process, *NA* the numerical aperture of the lens, and k_1 is a constant inherent of the process with a minimal value of 0.25.

It is important to note that during the last decades, the reduction of k_1 and λ revealed to be the main factor responsible for the large progress in photolithography. So far, the state of the art for the photolithography has been based on the 193nm lithography combined with an immersion process (NA = 1.35)[1]. Therefore, the microelectronic industry is nowadays able to produce components based on 32 nm node. These components are fabricated using the latest techniques of lithography using a double patterning process to further decrease the feature size.

In addition to the 32 nm node, others methodologies were considered, but nowadays, the industry focuses on the extreme UV lithography.[2] However, this methodology is far from complete, and serious problems inherent to the power of the sources remained to be tackled. Moreover, the choice of the lithographic technique is also limited by its cost. For instance, the scanners used in the 193nm lithography cost 50.000.000 $, and 125.000.000 $ for extreme UV lithography.[3–5] Interestingly, the same observation was done by the data storage industry which faced up to the same problematic.[6] This is why other techniques like maskless lithography or the self-assembly of block copolymer (BCP) thin films are seriously considered. Diblock copolymers (AB-type BCPs) are indeed considered thanks to their intrinsic self-assembling properties which leads to the formation of regular structures having a period in the range of 5-100 nm. BCPs have also the advantage to be cheap compared to other current technologies.

However, the pattern symmetries of AB-type BCPs are limited. While nanotemplates derived from the self-assembly of AB-type BCP thin films enable to achieve well-ordered features (*i.e.* dots, holes, pillars) within a common *p6mm* symmetry pattern due to packing frustration, linear ABC terpolymers provide access to more rich and complex patterns having *p2mm, p4mm, p3m1* or *p2* symmetries.[7–9] For that purpose, in this PhD thesis, we were interested by other block copolymer macromolecular architectures to achieve a panoply of more

complex pattern symmetries. To this aim, we have studied the self-assembly of linear and star miktoarm ABC terpolymers.

Some theoretical and experimental studies have shown that star miktoarm ABC terpolymers (noted hereafter 3 μ-ABC) give access to hierarchical morphologies and Archimedean tiling patterns.[10–14] Archimedean tiling patterns as presented by Johannes Kepler in Harmonices Mundi (1619) consist of regular polygons arranged on a plane without any interstice (gap). From this criteria, Kepler counted 11 tiling patterns (see Figure 1). The self-assembly of 3 μ-ABCs gives access to four of the eleven possible Archimedean tiling patterns which are: (6.6.6), (4.8.8), (4.6.12) and (3.4.6.4).[10,15,16]

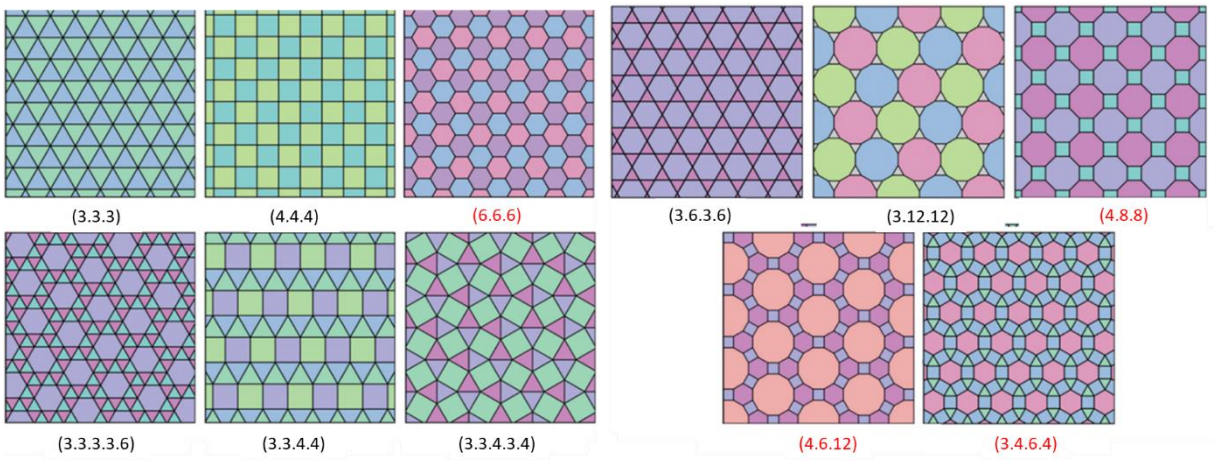

Figure 1: 11 possible Archimedean tilings. The red and black symbols give the notations of accessible and unaccesible Archimedean tilings using 3 µ-ABC chains, respectively. The first three tilings are usually called Platonic tilings or regular tilings because they use only one type of regular tiles. (Adapted from Ouyang et al.)[12]

These additional pattern symmetries formed by the microphase-separation of linear and star miktoarm ABC terpolymer thin films can be used to create surfaces with improved or new functionalities. Linear and star miktoarm terpolymers will be used in this thesis in order to generate “three-colored” hierarchical morphologies and Archimedean tiling patterns.

II. Block copolymer phase behavior

1. Block copolymer architecture

BCPs belong to one of the class of polymer in the wide class of soft matter. They consist of at least two chemically different polymers linked together with a covalent bond. Lots of BCP architectures exist such as linear, grafted, and star miktoarm. A schematic representation of some possible architectures for AB- and ABC-type BCPs is shown in Figure 2.

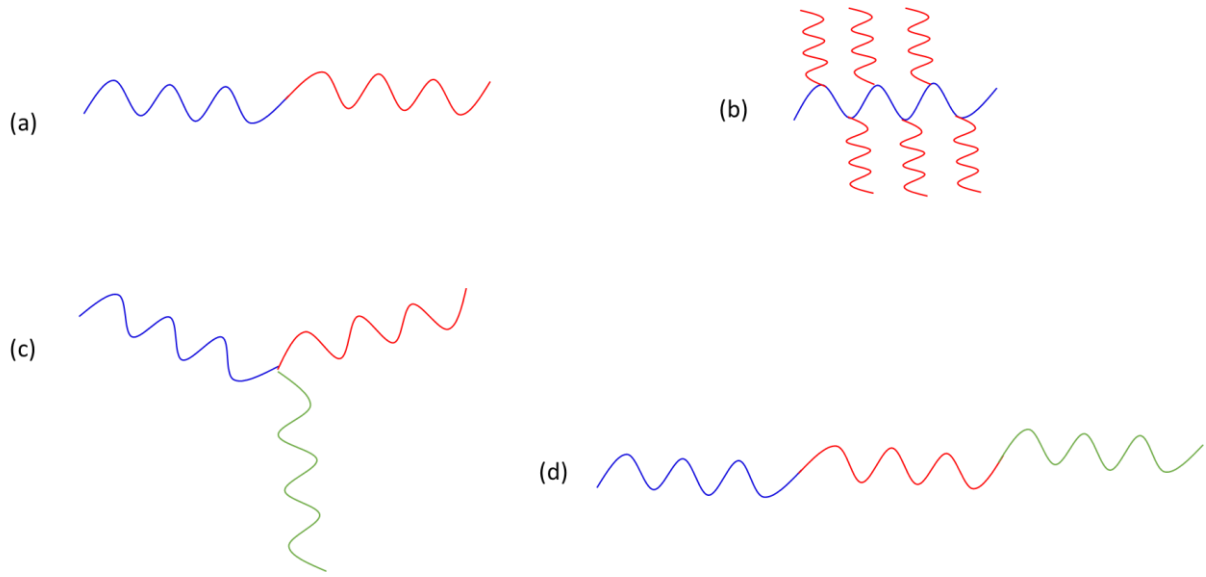

Figure 2: Schematic of some possible BCP architectures where each color represents a block: (a) linear AB-type BCP, (b) branched AB-type BCP, (c) star miktoarm ABC terpolymer and (d) linear ABC terpolymer.

The most studied BCP architecture is the linear AB-type BCP, which consists of two different blocks commonly named A and B. In our study, we rather decided to focus our interest on ABC-type BCPs such as linear and star miktoarm ABC terpolymers. These two kind of polymer architectures are named ABC-type because both of them are composed of three chemically different blocks. The linear ABC one is composed of three different blocks terminally connected, whereas the star miktoarm ABC one consists of three different arms linked all together to a core molecule.

Linear ABC terpolymers are noted A-*b*-B-*b*-C while star miktoarm ABC terpolymers are noted 3 μ-ABC.

2. Microphase separation of block copolymers

In the past decades, extensive research have been devoted toward the development of a molecular level understanding of microphase separation in block copolymers. The incompatibility between the different blocks leads to the phase separation which length scale is restrained by the covalent bounding between the two blocks. Thermodynamically the phase separation in block copolymer systems can be easily explained in terms of Gibbs free energy of mixing as follow:

$$\Delta G_m = \Delta H_m - T \Delta S_m$$

Where the enthalpy change of the process, ΔH_m, is largely determined by the Flory-Huggins parameter, χ, which relates to the interactions between the A and B blocks. The change in entropy of the process, ΔS_m, mainly depends (inversely related) on the polymerization degree of the chain, N. Here, the self-assembly of the AB-type BCP (demixing) spontaneously occurs if ΔG_m is positive and is (generally) accompanied by an entropy loss. When the temperature is increased, the self-assembly becomes progressively less effective as the magnitude of $T \Delta S_m$ approaches the magnitude of ΔH_m, and above a critical temperature will not occur. For an AB-type BCP, the incompatibility between the A and B blocks can be express by the product χN, and the microphase-separation occurs when $\chi N > 10.5$ (for a symmetric lamellar structure).[17]

Linear AB-type BCPs have been studied for over 30 years, and various structures have been identified depending on the volume fractions of each component. A close agreement between the theoretical predictions and the experimental results has been observed over the years. It was proven that the AB-type BCP self-assembly gives access to different morphologies including spheres, cylinders, lamellae, metastable hexagonally perforated lamellae, and complex networks (Q^{230} and O^{70}).[18] The theoretical phase diagram of a diblock copolymer is shown in Figure 3. Depending on the block volume fraction, f, and the incompatibility product, χN, the morphology can be predicted from the following phase diagram.

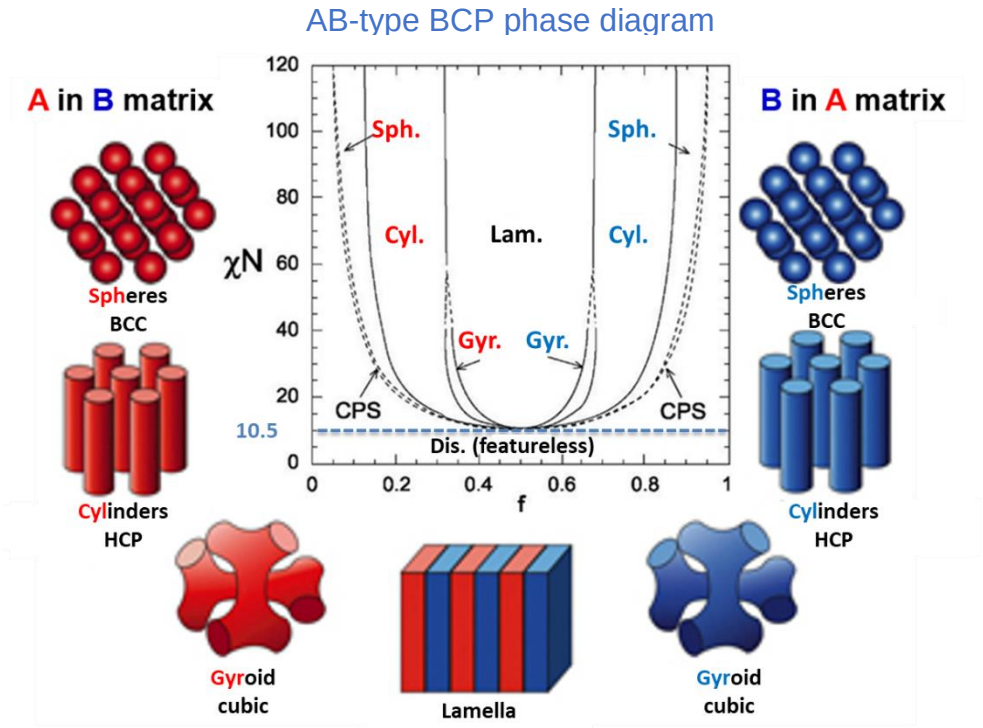

Figure 3: AB-type BCP phase diagram and schematic representation of some accesible morphologies. (Adapted from Matsen et al.)[17]

In the case of linear and star miktoarm ABC terpolymers, the equations are much more complicated and only few studies deal with the free energy of these systems. Nevertheless, the thermodynamic principles remain the same. Depending on the volume fractions of the A, B and C blocks, the different χN products, and the chain topology/architecture, linear and star miktoarm ABC terpolymers adopt different morphologies which are more rich and complex than those presented in Figure 3. In the next part, we will discuss about the self-assembly of bulk and thin film linear and star miktoarm ABC terpolymers.

III. Morphologies obtained from the self-assembly of linear and star miktoarm ABC terpolymers

In the literature, most of the works have been focused on the self-assembly of AB-type BCPs which is quite well understood now. Adding a C block to an AB-type BCP leads to the formation of linear or star miktoarm ABC terpolymers. In recent years, more interest was given to the self-assembly of linear or star miktoarm ABC terpolymer in bulk. These ABC-type terpolymers self-assemble into a wide spread of architectures compared with AB-type BCPs.

1. Bulk self-assembly of linear ABC terpolymers

In this part, we will describe the structures obtained from the self-assembly of bulk linear ABC terpolymers. After a brief general introduction, we will report on structures obtained depending on the chain topology.

a. Introduction

In 1980, Riess *et al.*[19] were the first to point out the possibility to achieve new morphologies with ABC-type terpolymers in comparison with those already observed from AB-type BCPs (see Fig. 3). In this study, they identified core-shell structures formed by a linear ABC terpolymer consisted of polystyrene (PS), polyisoprene (PI) and poly(methyl methacrylate) (PMMA) (PS-*b*-PI-*b*-PMMA). The microphase separation of linear ABC terpolymers is governed by the volume fractions of A, B, and C blocks (noted f_a, f_b, f_c, respectively), their degree of polymerization (noted N_A, N_B, N_C, respectively), the Flory-Huggins interaction parameters between the different pairs (noted χ_{AB}, χ_{BC}, χ_{AC}), and the chain topology (*i.e.* ABC, ACB, or BAC).

Bates and Fredrickson[20] demonstrated from theoretical studies some morphologies formed by linear ABC terpolymers (see Figure 4). As for AB-type BCP, the microphase separation depends on the local segregation driven by unfavorable interfaces and the tendency to maximize configurational entropy (*i.e.* minimize the chain stretching).

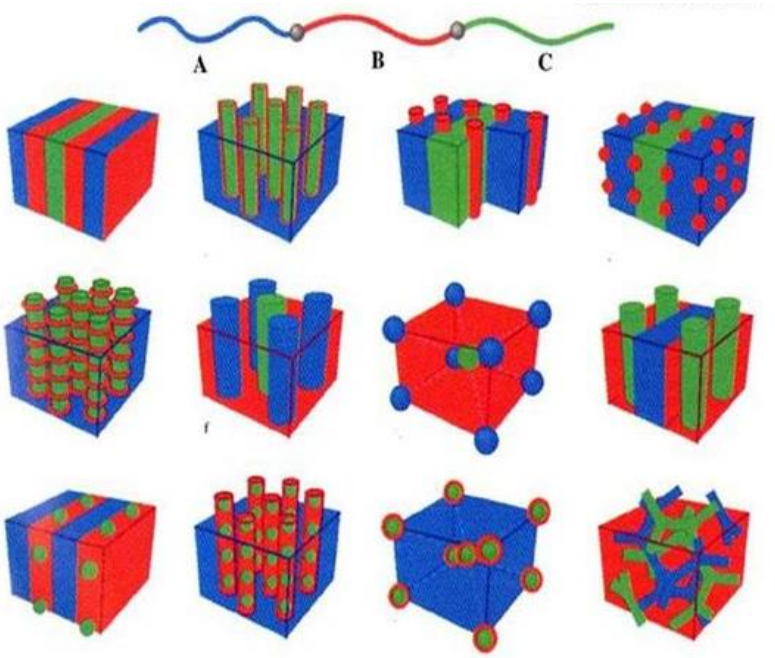

Figure 4: Morphologies for linear ABC terpolymers. A combination of block sequence (ABC, ACB, BAC), compositions and block molecular weights provides a wide parameter space for the creation of new morphologies. Microdomains are colored as shown on the copolymer strand at the top, with monomer types A, B and C confined to regions colored blue, red and green, respectively. (Adapted from Zheng et al.)[21]

Linear ABC terpolymers have two junction points (at the intersection of the mid-block). Therefore, the morphology depends on the position of each block. Different frustration types related to the topology of the terpolymer chain are described.

Bailey suggested a division of linear ABC terpolymers in three parts depending on the interaction between the different blocks.[22] When χ_{AC} is larger than the interaction parameters between the other blocks, it is so called a type 0 frustration. In contrast, if $\chi_{AB} \approx \chi_{AC} < \chi_{BC}$, it is a type I frustration, while if χ_{AC} is smaller than the other interaction parameters, it is a type II frustration ($\chi_{AC} < \chi_{BC} \approx \chi_{AB}$). Because of the incompatibility between end-blocks, in the case of a non-frustrated terpolymer the A/C interface is limited, whereas, for frustrated block copolymer, the A/C interface is energetically favorable. In the literature,[23] it was reported that depending on the frustration state, different morphologies can be obtained from the self-assembly of a linear ABC terpolymer as shown in Figure 4. In this part, we will discuss the morphologies obtained from some type 0, type I, and type II linear ABC terpolymers.

b. Type 0 frustration

A type 0 frustration linear ABC terpolymer ($\chi_{AC} > \chi_{AB} \approx \chi_{BC}$) exhibits an end-blocks Flory-Huggins parameter higher than other pairs. Consequently, interfaces between AB and BC blocks are promoted, which favor the formation of alternating morphologies. A few examples of morphologies experimentally produced from this kind of non-frustrated terpolymers will be described below.

In 1992, Mogi, Matshushita *et al.*[24–27] reported on the self-assembly in bulk of a non-frustrated polyisoprene-*b*-polystyrene-*b*-poly(2-vinylpyridine) (PI-*b*-PS-*b*-P2VP, ISP). In this study, they demonstrated the influence of the mid-block volume fraction on the attainable morphology. They reported a lamellar structure for symmetric volume fractions of PI, PS and P2VP blocks (I:S:P = 1:1:1), an ordered tricontinuous double-diamond (OTDD) phase for a composition of I:S:P = 1:2:1, an alternating cylindrical morphology arranged into a tetragonal array for I:S:P = 1:4:1, and an alternating spherical phase for I:S:P=1:8:1 as shown in Figure 5.

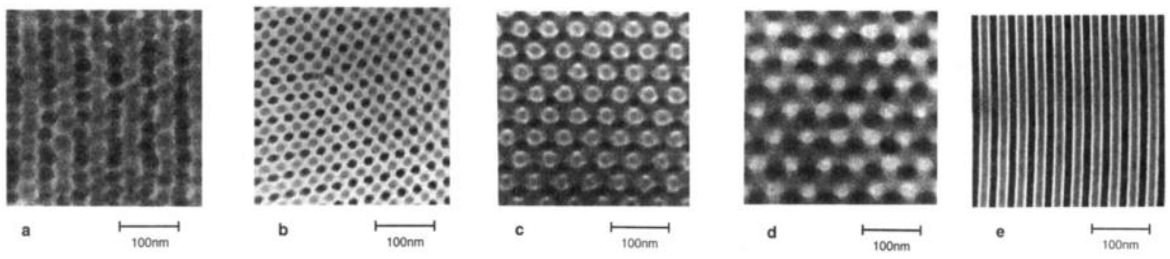

Figure 5: Typical examples of electron micrographs for different morphologies of microphase-separated structures of ISP triblock copolymers: (a) spherical (I:S:P = 1:8:1), (b) cylindrical (I:S:P = 1:4:1), (c and d) OTDD (I:S:P = 1:2:1), and (e) lamellar (I:S:P=1:1:1) structures. (Adapted from Mogi et al.)[25]

They highlighted that the shape of interfaces between I and S domains were similar to those between P and S domains because χ_{IS} and χ_{SP} are quasi-equivalent and the terpolymer chains are geometrically symmetric (*i.e.* equal volume of end-blocks). Some years later, Phan and Fredrickson[28] suggested that the morphology assigned to an OTDD network should be revisited. They pointed out that the alternative gyroid Q^{214} phase has a lower free energy than the OTDD network, and so the equilibrium mesostructure described by Mogi *et al.* should be considered as a gyroid Q^{214} phase.

Another non-frustrated linear ABC terpolymer consisting of polybutadiene, polystyrene and poly(methyl methacrylate) blocks (noted BSM) was studied by Jung and co-workers[29]. The non-frustrated BSM (B:S:M = 1:3:2), showed the formation of cylindrical domains of PB and

PMMA dispersed in a matrix of PS (the major component). The PB and PMMA cylinders show a tetragonal packing. As short-range order was obtained leading them to conclude that a mismatch between the cylinder dimensions brings a bending of cylinders, thus reducing the long range ordering.

In 2000, Hückstädt *et al.*[30] studied the self-assembly of polybutadiene-*b*-polystyrene-*b*-poly(2-vinylpyridine) (BSV) chains (B:S:V = 1:2:7 and B:S:V = 1:2:8). TEM images revealed a lamellar morphology as shown in Figure 6. The interfacial energies between the middle and the end-blocks are similar which lead to the promotion of a lamellar morphology even if the BCP composition was highly asymmetric.

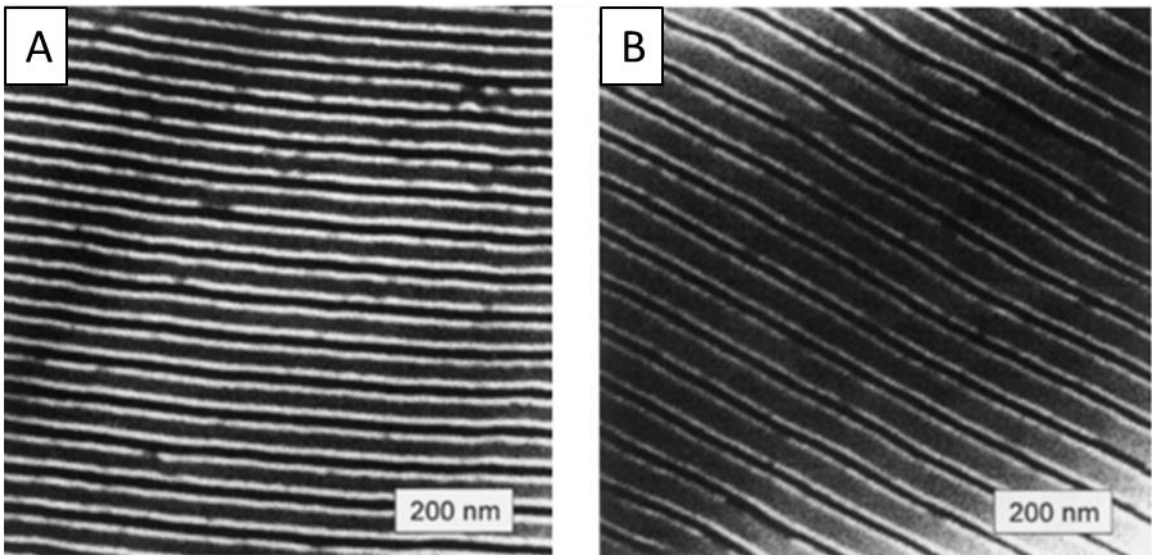

Figure 6: TEM micrographs of bulk BSV films stained with OsO_4 and CH_3I which have different compositions: (A) B:S:V = 1:2:7 (B) B:S:V = 1:2:8. (Adapted from Hückstädt et al.)[30]

In 2001, Bailey, Bates and co-workers[31–33] reported on the self-assembly of the non-frustrated polyisoprene-*b*-polystyrene-*b*-poly(ethylene oxide) (ISO). They built a phase diagram where different phases are obtained depending on the volume fractions (see Figure 7). In this paper, the authors showed that whatever the volume fraction of blocks the less incompatible blocks developed the largest interface (I/S and S/O interfaces).

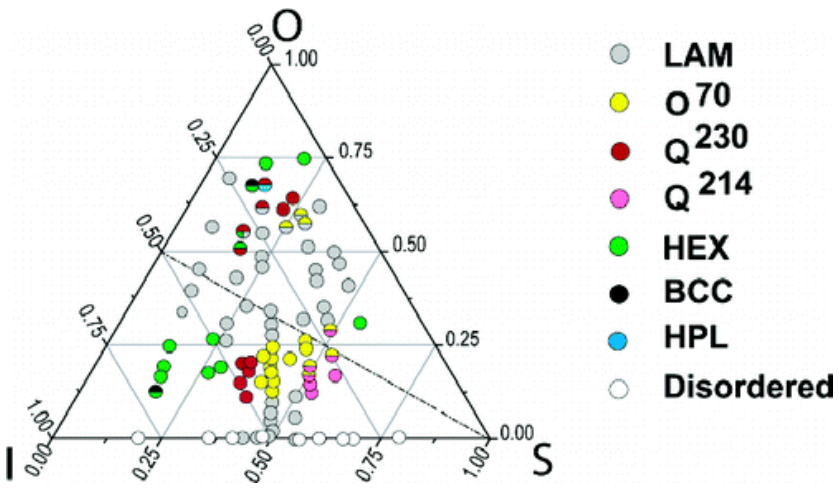

Figure 7: Phase map for poly(isoprene-b-styrene-b-ethylene oxide). The axes identify volume fractions of each block. Six stable ordered phases such as LAM (lamellar), HEX (hexagonal), Q^{230} (double gyroid), Q^{214} (alternating gyroid), BCC (body-centered cubic), O^{70} (Fddd orthorhombic network), the disordered state, and one metastable phase, HPL, are included.

To summarize, because of the topology of the terpolymer chain, core-shell and alternating morphologies are favored for non-frustrated linear ABC terpolymers. Indeed, since the A and C blocks have the largest Flory-Huggins parameter, the A/C interface tends to be minimized.

c. Type I frustration

Type I frustrated linear ABC terpolymers are characterized by a χ-parameter of the two end-blocks with an intermediate strength compared with the other pairs ($\chi_{AB} \approx \chi_{AC} < \chi_{BC}$).

In 1993, Gido and co-workers[34] reported on the self-assembly of a linear ABC terpolymer composed of PS, PI, and P2VP as Mogi and co-workers (previously described) but in a type I frustrated configuration. The obtained morphologies are different as shown on the TEM micrograph presented in Figure 8. The frustrated P2VP-*b*-PI-*b*-PS (P:I:S = 1:1:1) shows a PS matrix perforated by hexagonally-packed cylindrical cores of P2VP surrounded by a shell of PI. They showed that a non-constant mean curvature (non-CMC) could be obtained using a linear ABC terpolymer. The non-CMC morphology of this structure was explained by Matsen[17] and Semenov[35] for an asymmetric AB-type BCP. They demonstrated that the interface tends to curve because of the packing frustration. In the case of linear ABC terpolymers, Gido illustrated that the asymmetric interactions between blocks in a frustrated terpolymer theoretically leads to the formation of non-CMC cylinders.

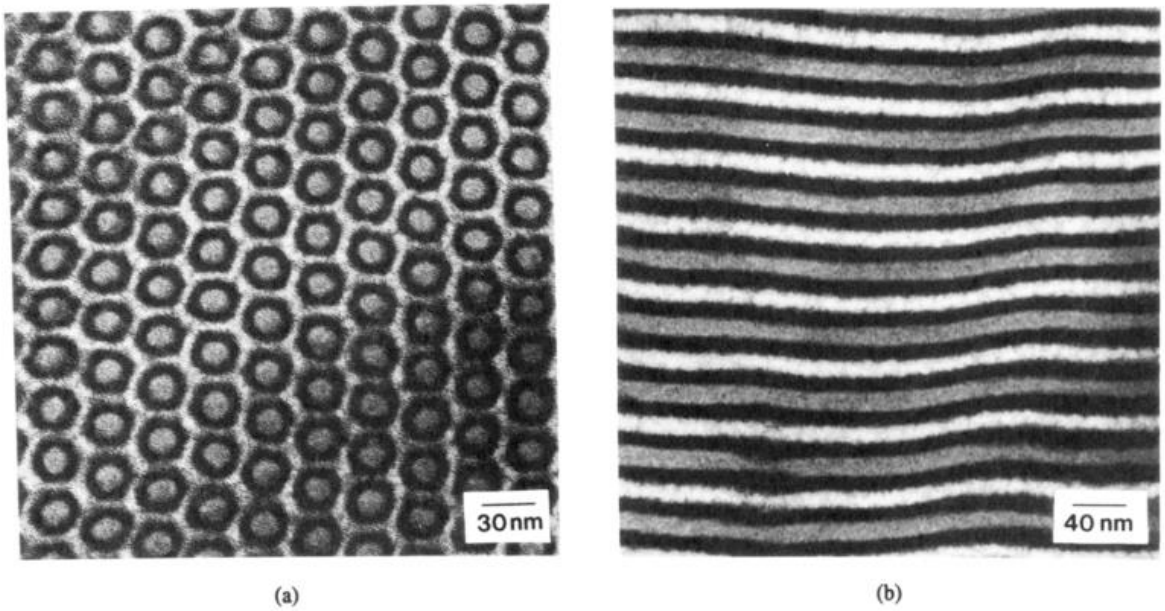

Figure 8: (a) Axial TEM projection of hexagonally-packed structural units. The darkest regions correspond to the OsO_4-stained PI domains, while the gray regions are CH_3I-stained P2VP domains. The non-CMC interface between this PI microdomain and the PS matrix phase has a hexagonal shape with corners. (b) Transverse TEM projection. The light, gray, and dark regions correspond to projections through the PS matrix, the P2VP core, and the PI annulus, respectively. (Adapted from Gido et al.)[34]

In 2000, Hückstädt and co-workers[8,30] described the morphology obtained from other type I frustrated PS-*b*-PB-*b*-P2VP (SBV) systems. For $S_{45}B_{32}V_{23}$ and $S_{44}B_{27}V_{29}$ (S:B:V = 1:0.7:0.5 and S:B:V = 1:0.6:0.7, respectively) they observed a core-shell double gyroid morphology with a P2VP core domain (the smallest block), a PB shell domain within a PS matrix, as shown in Figure 9. They highlighted that in the core-shell double gyroid, the smallest block (V) forms the core. This block is surrounded by a shell of the highest incompatible block (B). When the volume ratio of the P2VP was increased $S_{25}B_{17}V_{58}$ (S:B:V = 1:0.7:2.3), a lamellae morphology was produced. In both cases, a large interface between the two highest incompatible blocks was observed because of the topology of the chain. The core-shell double gyroid structure was not observed for non-frustrated BSV, and only a lamellar morphology was obtained.

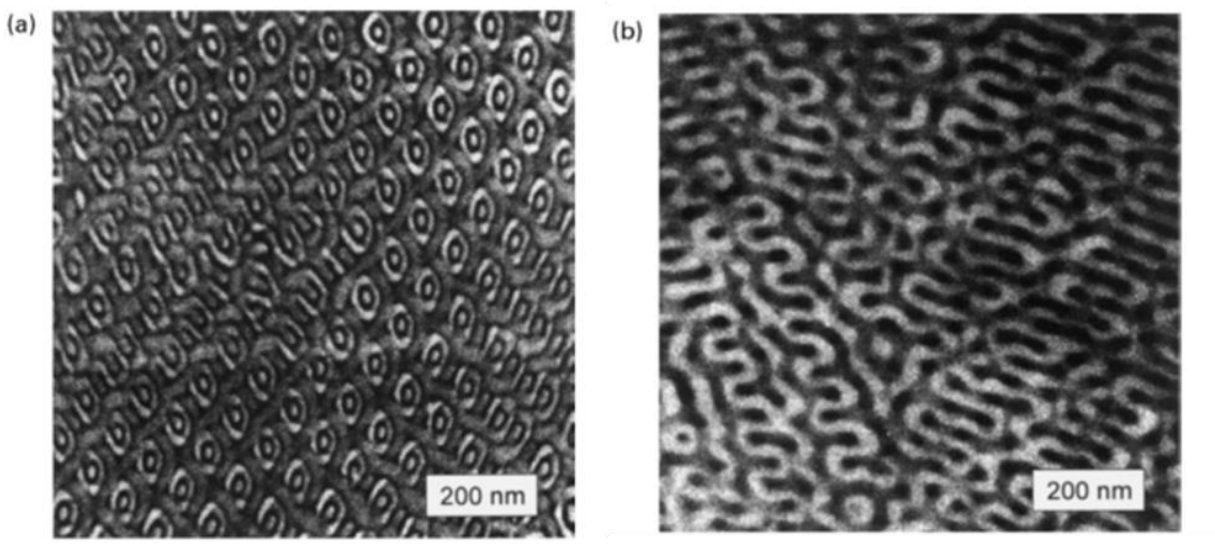

Figure 9: TEM micrographs of the gyroid structure obtained from the self-assembly in bulk of $S_{45}B_{32}V_{76}$: (a) stained with OsO4; (b) stained with I_2. (Adapted from Hückstädt et al.)[8,30]

In the case of the type I frustrated PS-*b*-PI-*b*-PEO (SIO),[36] a core-shell morphology of hexagonally-packed cylinders and gyroid morphologies (Q^{230} and Q^{214}) were observed, in addition to two lamellar structures (two- and three-domains), because of frustration conditions, as Bailey and co-workers expected.

Changing the order of polymers from a non-frustrated to a frustrated terpolymer led to a significantly different morphological behavior since in the case of frustrated terpolymer, the interface between two covalently bonded adjacent blocks in the chain is not energetically favorable.

d. Type II frustration

Linear ABC terpolymers with a type II frustration have a χ_{AC}-parameter smaller than the other pairs ($\chi_{AC} < \chi_{AB} \approx \chi_{BC}$). A type II frustrated polystyrene-*b*-polybutadiene-*b*-poly(methylmethacrylate) (S:B:M = 1:0.5:2.4) was studied by Krappe and co-workers[37]. Here PMMA is the major component and forms the matrix in which the PS phase forms cylinders surrounded by PB helices. Since the PS/PMMA interface is energetically favorable, this interface is promoted whereas the PS/PB and the PB/PMMA interfaces are unfavorable and tend to be reduced. In 1998, Brinkmann *et al*[38] studied the influence of the solvent casting on the bulk morphology of $S_{23}B_{57}M_{20}$ (S:B:M = 1:0.4:1.2). In this study, they proved that using solvent casting could stabilize certain structures. They described a new structure consisted of a new morphological hexagonal array, where PS and PMMA form two kinds of cylindrical

microdomains having a small and large diameter, respectively, in a PB matrix as shown in Figure 10.

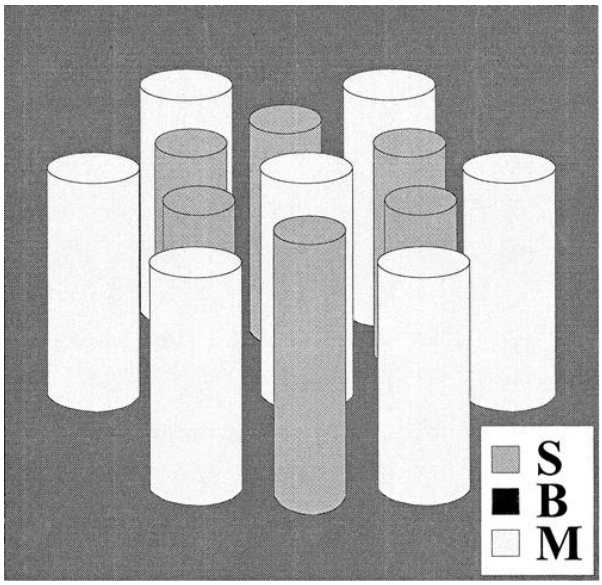

Figure 10: Schematic representation of the $S_{23}B_{57}M_{20}$ morphology. (Adapted from Brinkmann et al)[38]

Another example of self-assembled type II polystyrene-*b*-polybutadiene-*b*-poly(ε-caprolactone) (PS-*b*-PB-*b*-PCL) was described by Balsamo and co-workers[39]. In this study, they reported core-shell cylinders, with a PB shell, a PCL core, and a PS matrix. They also discussed about the introduction of a semicrystalline block in the self-assembled system. The introduction of a semicrystalline block did not changed the basic morphological pattern, but enhanced a deformation from a circular shaped cylinders to an unusual polygonal shape.

e. Theoretical studies

Some theoretical studies reported on the self-assembly of frustrated and non-frustrated linear ABC terpolymers. Li and co-workers[40,41] used a three-dimensional self-consistent field theory (SCFT) to predict morphologies adopted by frustrated linear ABC terpolymers. They demonstrated that frustrated ABC linear terpolymers can self-assemble into three-color lamellae (L_3), core–shell cylinders (CSC), perforated lamellae (PL), cylinders-*within*-lamellae (LC), triple/quadruple cylinders-*on*-cylinders (C_3/C_4), double/triple helices-*on*-cylinders (H_2C/H_3C), and perforated circular lamellae-*on*-cylinders (PC) as shown in Figure 11.

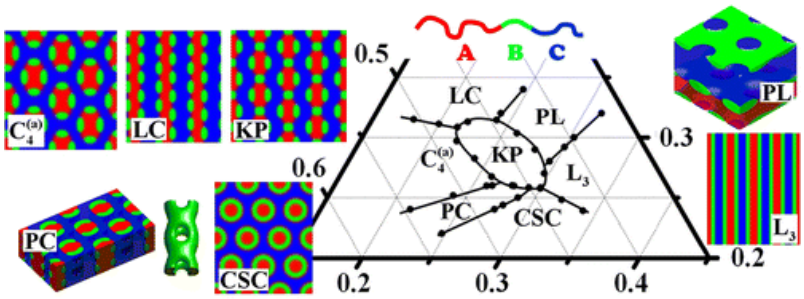

Figure 11: Density isosurface plots of morphologies formed by ABC linear triblock copolymers: (a) three-color lamellae (L_3), (b) cylinders-within-lamellae (LC), (c) knitting pattern (KP), (d) triple cylinders-on-cylinders (C_3), (e) and (f) quadruple cylinders-on-cylinders (C_4), (g) core–shell cylinders (CSC), (h) perforated lamellae (PL), (i) triple helices-on-cylinders (H_3C), (j) double helices-on-cylinders (H_2C), and (k) perforated circular layer-on cylinders (PC). The red, green, and blue colors denote the regions where the majority components are A, B, and C, respectively. (Adapted from Li and co-workers)[40,41]

These results were in accordance with experimentally obtained morphologies. The theoretical study of the self-assembly of non-frustrated linear ABC terpolymers was done in 2014 by Jiang *et al.* [42] In this work, they used the self-consistent field theory to predict the morphologies that could be obtained from the self-assembly of linear ABC terpolymers (see Figure 12). They showed that the three-color lamellar phase is predominant when the volume fraction of the three blocks are comparable. The lamellar phase region was found to be very large. Parallel lamellar phase with hexagonally packed pores at surfaces ($LAM_3^{//}$), perpendicular lamellar phase with cylinders at the interface ($LAM^{\perp}$), and perpendicular hexagonally packed cylinders phase with rings at the interface ($C_2^{\perp}$) were predicted. No core-shell structures were demonstrated for non-frustrated linear ABC terpolymers.

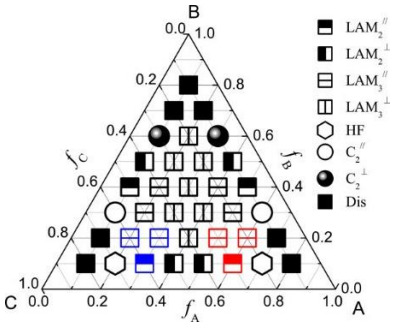

Figure 12: Phase diagram of ABC triblock terolymers with $\chi_{AB} = \chi_{BC} = 13$ and $\chi_{AC} = 35$ at grafting density $\sigma = 0.2$. Dis represents the disordered phase. The red, blue, or black icons showing the parallel lamellar phases discern the different arrangement styles of the triblock terpolymer with block A, block C, or block B adjacent to the brush layers, respectively. (Adapted from Jiang et al.)[42]

f. Conclusion

To summarize, varying the topology of a linear ABC terpolymer leads to the formation of different structures. We can note that in non-frustrated state alternative microstructures are obtained, while in the frustrated state (I or II), more complexes structures are described as reported in the Table 1. In the type II frustrated state, some spheres-*on*-spheres, spheres-*on*-cylinders, rings-*on*-cylinders, and cylinders-*in*-lamellae have been reported. In the case of type I frustrated linear ABC terpolymer, the interaction between end-blocks is of intermediate strength and structures are between those observed in the type II and type 0 frustration states. The morphologies observed include core-shell cylinders, core-shell double gyroid and lamellae. All the results are summarized in the Table 1.

Table 1: Morphologies obtained in bulk depending on the frustration state.

Morphology/frustration state	**Type 0**	**Type I**	**Type II**
Spheres-*on*-spheres			X
Spheres-*on*-cylinders			X
Rings-*on*-cylinders			X
Cylinders-*in*-lamellae		X	X
Core-shell cylinders		X	
Core-shell double gyroid		X	
Alternating spheres	X	X	
Alternating cylinders	X		
Alternating gyroid	X		X
Alternating lamellae	X	X	X
Helices-*on*-cylinders			X

2. Bulk self-assembly of star miktoarm ABC terpolymers

a. Introduction

As for linear ABC-type BCPs, the star miktoarm ABC terpolymer self-assembly is driven by the Flory-Huggins parameters of the different pairs (χ_{AB}, χ_{BC}, χ_{AC}), the volume fraction of blocks (f_a, f_b, f_c) and their degree of polymerization (N_A, N_B, N_C). For a star miktoarm architecture, the main difference resides in the fact that all blocks are connected at only one junction point. Because of this, A/B, B/C and C/A interfaces exist in the microstructure as described in Figure 13.[43]

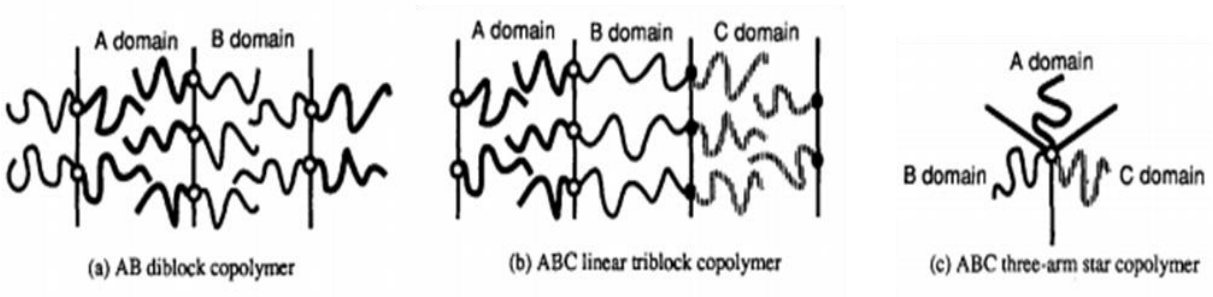

Figure 13: Schematic illustrations of the arrangement of copolymer chains. (a) AB-type BCP: the chemical junction points is confined to the AB interface, (b) linear ABC triblock copolymer: the chemical junction points are confined to the AB and B/C interfaces and (c) ABC star miktoarm: the chemical junction point is confined to a line. (Adapted from Okamoto et al.) [43]

This junction point is then localized along a line (one dimensional). This topological requirement allows the formation of morphologies that are not achievable with linear ABC terpolymers, such as Archimedean tiling patterns. Chen *et al.*[44] studied the theoretical phase diagram of star miktoarm ABC terpolymers depending on the block volume ratios (see Figure 13). They showed that hierarchical morphologies and Archimedean tiling patterns could be obtained. The nomenclature used in this thesis to define a star miktoarm ABC terpolymer is 3 μ-ABC with A, B, and C the three different arms of the chain.

Hadjichristidis was the first to report on the star miktoarm ABC terpolymer self-assembly in 1993.[45] The star miktoarm ABC terpolymer was a polystyrene-*arm*-polyisoprene-*arm*-polybutadiene (3 μ-SIB) with molar mass of 20.7, 15.6 and 12.2 kg.mol^{-1}, respectively. The 3 μ-SIB morphology obtained was a hexagonally close-packed array of cylinders with a period of 30 nm. The authors demonstrated a two-colored pattern since the PI and PB blocks were mixed. This result is undoubtedly due to the weak interaction parameter between the PI

and PB blocks. The morphology observed in this study has similarities with the structure of the AB-type or AB_2-type linear/star miktoarm BCPs.

The first three-colored pattern produced from a star miktoarm terpolymer was demonstrated 5 years later. In 1998, Okamoto and co-workers[43] studied the self-assembly of a star miktoarm ABC terpolymer composed of PS, PDMS and poly(tert-butyl methacrylate) (PtBMA) with approximatively the same volume ratio for each block. The large chemical nature differences of those three blocks led to the formation of three different microdomains. The TEM images of the cast-film revealed a three-fold symmetry confirmed by SAXS analysis, but no conclusion on the exact morphology could be drawn due to the lack of available information.

b. PS-*arm*-PI-*arm*-PMMA self-assembly

Star miktoarm ABC terpolymers composed of PS, PI and PMMA (3 μ-SIM) were widely studied. For instance, Sioula and co-workers[46] studied the effect of the composition on the morphology by keeping constant the molecular weight of the PI and PS blocks whereas they varied the PMMA block size. The nomenclature used in this paper is SIM-x/y/z with x, y, z the respective block molecular weight in kg/mol. TEM pictures of 3 μ-SIM chains (S:I:M = 1:1.1:2.6) revealed a hexagonal arrangement where PI cylinders were surrounded by a PS annulus in a PMMA matrix. The hexagonal arrangement was confirmed by SAXS. When the volume ratio of PMMA was decreased, the 3 μ-SIM (S:I:M = 1:1.1:2) and the 3 μ-SIM (S:I:M = 1:1.5:2.8) exhibited a inner core region of PI surrounded by a PS annulus in a matrix of PMMA. In this case, the interfaces between PI/PS and PS/PMMA had a rhombohedral shape, and the PI domain array did not have a *p6mm* symmetry but had a c*2mm* one (see Figure 14).

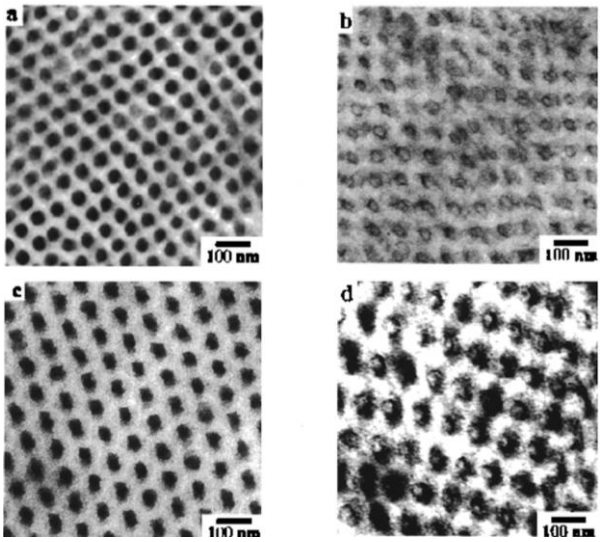

Figure 14: Bright field TEM images of (a) 3 μ-SIM (S:I:M = 1:1.1:2.6) stained with OsO_4, (b) 3 μ-SIM (S:I:M = 1:1.1:2.6) stained with RuO_4, (c) 3 μ-SIM (S:I:M = 1:1.1:2.6) stained with OsO_4, and (d) 3 μ-SIM (S:I:M = 1:1.1:2.6) stained with RuO_4. (Adapted from Sioula et al.)[46]

In any case, no-interfaces were observed between PI and PMMA in their study. PS formed a protective annulus between those two blocks, and PMMA partially mixed into the PS annulus. PI and PMMA tended to reduce their interfaces because of their highest χ-parameter compared with the other pairs, whereas the weak χ-parameter between PS and PMMA allowed for a partial mixing of those two blocks.

A few months later, the same team studied two other star miktoarm ABC terpolymers[47] composed of the same polymers but with different molecular weights: SIM-72/77/109 and SIM-92/60/94. Even if the molecular weight of those two 3 μ-ABC terpolymers was different, their volume ratios were quite equivalent and the morphology obtained was the same. The morphology observed in TEM images consisted of PMMA cylinders surrounded by six triangular prism-shaped cylinders of PI and six hexagonal-shape cylinders of PS, alternatively. The *p6mm* symmetry was confirmed by SAXS.

c. PS-*arm*-PI-*arm*-P2VP self-assembly

The star miktoarm ABC terpolymer composed of PS, PI, and P2VP have been extensively studied during the past decades. In 2004, Takano and co-workers[16] studied the self-assembly of this 3 μ-SIP by varying the volume ratio of the P2VP block, and keeping the volume ratios of PS and PI constant. The nomenclature used in this paper was 3 μ-SIP-x with x the volume ratio of the P2VP block. The PI and PS blocks have both a volume ratio of 1. Three star miktoarm ABC terpolymers were prepared with different P2VP volume ratios: 0.7,

1.2 and 1.9 (corresponding to 3 μ-SIP-0.7, 3 μ-SIP-1.2 and 3 μ-SIP-1.9, respectively). The 3 μ-SIP-0.7 showed a honeycomb-type microdomain structure with a (6.6.6) tiling pattern (see Figure 15a). The 3 μ-SIP-1.2 exhibited a cylindrical structure with a tetragonal symmetry. PI and PS formed octagonal domains and PS formed a square section. This structure was assigned to a (4.8.8) tiling pattern. The 3 μ-SIP-1.9 also exhibited a cylindrical structure forming an array with a hexagonal symmetry. The P2VP, PI and PS blocks formed dodecagonal-, hexagonal- and square-shaped domains, respectively. This structure was assigned to a (4.6.12) tiling pattern. In 2005, Takano and coworkers[11] studied the self-assembly of a blend of two 3 μ-SIP terpolymers. They blended 3 μ-SIP-1.2 with 3 μ-SIP-1.9 (weight ratio: 0.85/0.15 for 3 μ-SIP-1.2 and 3 μ- SIP-1.9, respectively) to obtain a 3 μ-SIP-1.3. The TEM pictures of the self-assembled 3 μ-SIP blend revealed a mesoscopic (3^2.4.3.4) Archimedean tiling pattern.

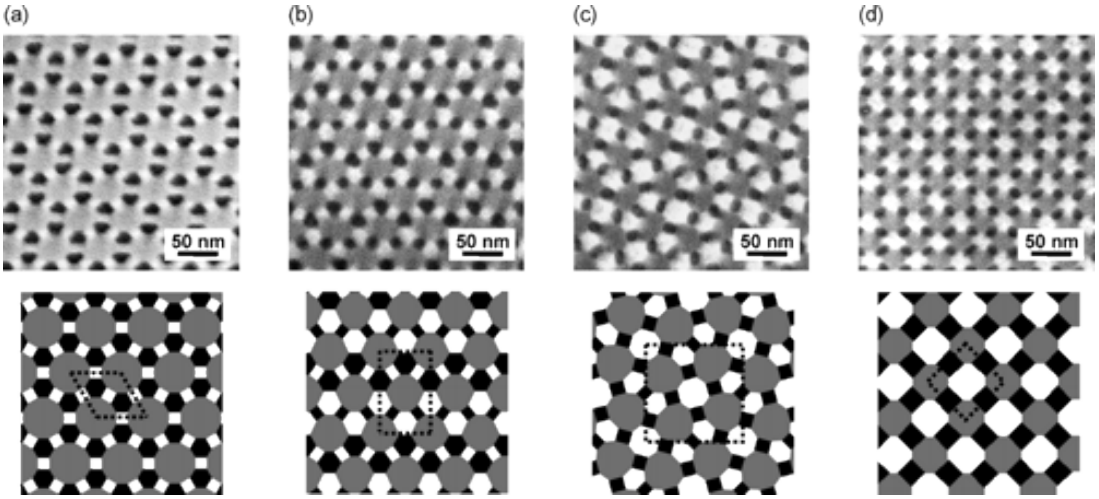

Figure 15: (top) TEM images of the four 3 µ-ISP star-shaped terpolymer samples and (bottom) their corresponding schematic tiling patterns: (a) $I_{1.0}S_{1.8}P_{1.0}$, (b) $I_{1.0}S_{1.8}P_{1.6}$, (c) $I_{1.0}S_{1.8}P_{2.0}$, (d) $I_{1.0}S_{1.8}P_{2.9}$. (Adapted from Takano et al)[11]

A few years later, in 2006, Hayashida[10] described morphologies obtained from the self-assembly of 3 μ-SIP varying the volume ratio of P2VP and keeping the volume ratios of PI and PS constant as 1 and 1.8, respectively. TEM images revealed (6.6.6) and (4.6.12) Archimedean tiling patterns for the 3 μ-ISP-1 and 3 μ-ISP-2.9, respectively. We can note that the (4.6.12) tiling pattern was already obtained by Takano in 2004 from a 3 μ-ISP-1.9. Other patterns, not assigned as Archimedean tiling patterns were observed for 3 μ-ISP-1.6 and 3 μ-ISP-2. For 3 µ-ISP-1.6, I and S domains consisted of one 4-fold and two 6-fold coordinated domains within the unit cell (see Figure 15b). Therefore, the average coordination number for I and S was 5.3 (=(4*1+6*2)/3) while P was 8-fold coordinated. Using the average coordination number (ACN), the tiling pattern for 3 μ-ISP-1.6 was described as (5.3, 5.3, 8). With the same

methodology, the authors defined the morphology of the 3 μ-ISP-2 as a (4.5, 6, 9) tiling pattern (see Figure 15c).

The effect of the PS volume ratio variation was also studied keeping constant the PI and the P2VP volume ratios as 1 and 2, respectively. For 3 μ-ISP-1.3 and 3 μ-ISP-2.7 terpolymers, the (4.6.12) and (4.8.8) Archimedean tiling patterns were obtained, respectively, while the ACN nomenclature was used for 3 μ-ISP-1.6 and 3 μ-ISP-2.3 which formed a (5, 5, 10) and (4, 6.7, 10) morphology.

In 2007, Hayashida[48] described the self-assembly of star miktoarm ABC terpolymers and their blends with either other star miktoarm ABC terpolymers or even with homopolymers. The summary of the neat and mixed polymers is given in Table 2 and Table 3, respectively.

Table 2: Characteristics of the ISP Star-Shaped Terpolymers

Sample	**Mn (10^3)**	**Mw/Mn [b]**	**I:S:P[d]**
I	13.3[a]	1.04	–
S	27.4[b]	1.01	–
$I_{1.0}$-*b*-$S_{1.8}$	40.7[c]	1.03	1:1.82:0
$I_{1.0}S_{1.8}P_{4.3}$	110[c]	1.01	1:1.8:4.3
$I_{1.0}S_{1.8}P_{6.4}$	147[c]	1.02	1:1.8:6.4
$I_{1.0}S_{1.8}P_{12}$	241[c]	1.03	1:1.8:12.2
$I_{1.0}S_{1.8}P_{22}$	401[c]	1.04	1:1.8:22.0

[a] Determined by ^{1}H-NMR. [b] Determined by SEC using polystyrene standard samples. [c] Estimated by ^{1}H-NMR based on M_n of the S precursor. [d] Volume ratios of I:S:P calculated using bulk densities of the components, *i.e.*, 0.926, 1.05, and 1.14 g/cm^3 for the I, S, and P components, respectively.

Table 3: Blend Ratios of the ISP Star-Shaped Terpolymers and homopolymer to obtain the $I_{1.0}S_{1.8}P_X$ Series

Sample	**Formulation**	**Weight fraction**	**I:S:P[a]**
$I_{1.0}S_{1.8}P_{9.6}$	$I_{1.0}S_{1.8}P_{6.4}$/$I_{1.0}S_{1.8}P_{12}$	0.35/0.65	1:1.8:9.6
$I_{1.0}S_{1.8}P_{11}$	$I_{1.0}S_{1.8}P_{6.4}$/$I_{1.0}S_{1.8}P_{12}$	0.16/0.84	1:1.8:11
$I_{1.0}S_{1.8}P_{32}$	$I_{1.0}S_{1.8}P_{22}$/hP	0.70/0.30	1:1.8:32
$I_{1.0}S_{1.8}P_{53}$	$I_{1.0}S_{1.8}P_{22}$/hP	0.44/0.56	1:1.8:53

[a] Volume ratios of I:S:P calculated using bulk densities of the components.

A cylinders-*in*-lamella morphology was observed on TEM images for $I_{1.0}S_{1.8}P_X$ with $4.3 \leq X \leq 11$. SAXS experiments confirmed the lamellar structure, and the lamellar d-spacing (48 nm) obtained by SAXS were in accordance with those measured on TEM images. Depending on the nature of the solvent casting, the morphology was a cylinders-*in*-lamella phase (with THF) or cylinders surrounded by as many as twenty I and S cylindrical domains (with toluene). The difference in the resulting morphology was due to the difference of polymer affinity with the solvent. When the volume ratio of P was increased ($12 \leq X \leq 32$), a lamellae-*in*-cylinders structure was obtained. When X = 53, the morphology obtained from the solvent-casting was a lamellae-*in*-sphere structure. In this study, they showed that depending of the solvent-casting and the block volume ratios, a wide range of morphologies could be obtained as shown in Figure 16.

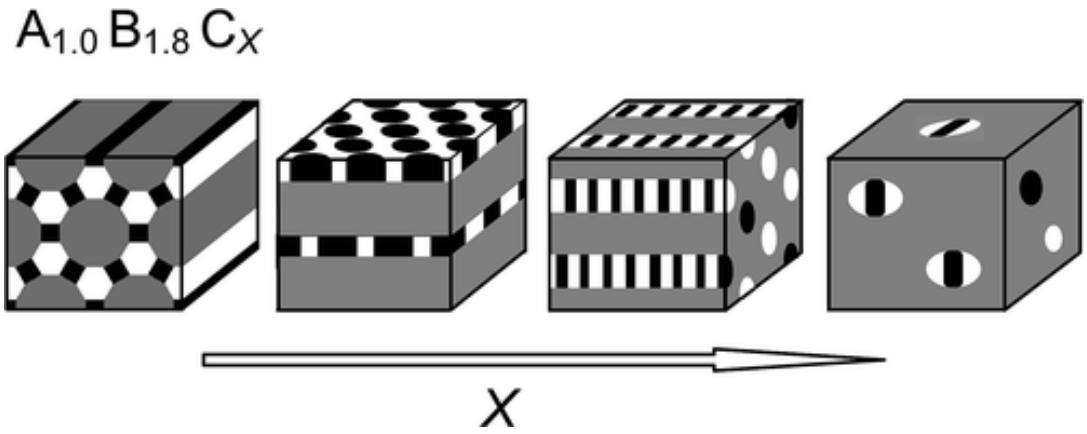

Figure 16: Schematic representation of morphologies obtained from the self-assembly of 3 μ-ISP terpolymers when the P block size is varied. (Adapted from Hayashida et al.)[48]

In 2007, Hayashida described the self-assembly of 3 μ-ISP chains blended with a PS homopolymer (hPS) having a molecular weight of 3 kg/mol.[49] The hPS was used to tune the PS block volume ratio of the star miktoarm terpolymers. They blended 3 μ-$I_1S_{1.8}P_2$ and 3 μ-$I_1S_{1.8}P_{2.5}$ with hPS to produce equivalent 3 μ-$I_1S_{2.3}P_2$ and 3 μ-$I_1S_{2.7}P_{2.5,}$ respectively. In both cases, a periodic pattern was observed with triangular and square arrangements of tiles. The square-triangle tiling superimposed upon the image were consistent with a dodecagonal symmetry. This result was in accordance with SAXS data. The morphology was assigned to the (3.3.4.3.4) Archimedean tiling pattern.

The (3.3.4.3.4) tiling pattern was also described by Takano[15] in 2007 for a self-assembled 3 μ-ISP (S:I:P = 1:1:1.3). In this paper, they studied the self-assembly of 3 μ-ISP-x

where the volume ratio of the P2VP block, *x*, was varied while the PS and PI volume ratios were equal to one. Results for *x* equals to 0.2, 0.4, 0.7, 1.2, 1.9, 3.0, 4.9, 7.9 and 10 are summarized in Table 4.

Table 4: Summary of the structures obtained from the self-assembly of 3 μ-ISP-x

Morphology	**(4.6.12)**	**(6.6.6)**	**(4.8.8)**	**(3.3.4.3.4)**	**Cylinders-in-lamella**	**Columnar piled disk cylinder**
I:S:P volume ratio	1:1:0.2; 1:1:0.4; 1:1:1.9; 1:1:1.5	1:1:0.7	1:1:1; 1:1:1.2	1:1:1.3	1:1:3; 1:1:4.9	1:1:7.9; 1:1:10

Many star ISP terpolymers have been studied. The microphase-separated morphologies obtained from different volume ratios of polystyrene, polyisoprene and poly(2-vinylpyridine) are summarized in the ternary phase diagram showed in Figure 17.

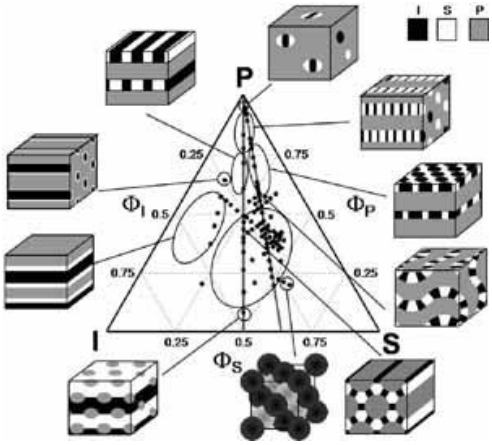

Figure 17: Ternary phase diagram of microphase-separated morphologies produced from a polystyrene-arm-polyisoprene-arm-poly(2-vinylpyridine) series. (Adapted from Takano et al.)[15]

d. Other systems

Both 3 *μ*-SIM and 3 *μ*-SIP systems have been widely studied is bulk, but other 3 *μ*-ABC were also reported is the literature. In 2000, Hückstädt, Göpfert and Abetz[50] described the self-assembly of a star miktoarm terpolymer composed of PS, PB and P2VP (see Figure 18). Archimedean tiling patterns and hierarchical morphologies were observed. Except for the

lamellar-like structure, the strong incompatibility between B and V blocks led to a small interface between those two polymers while the interfaces between other contents were larger.

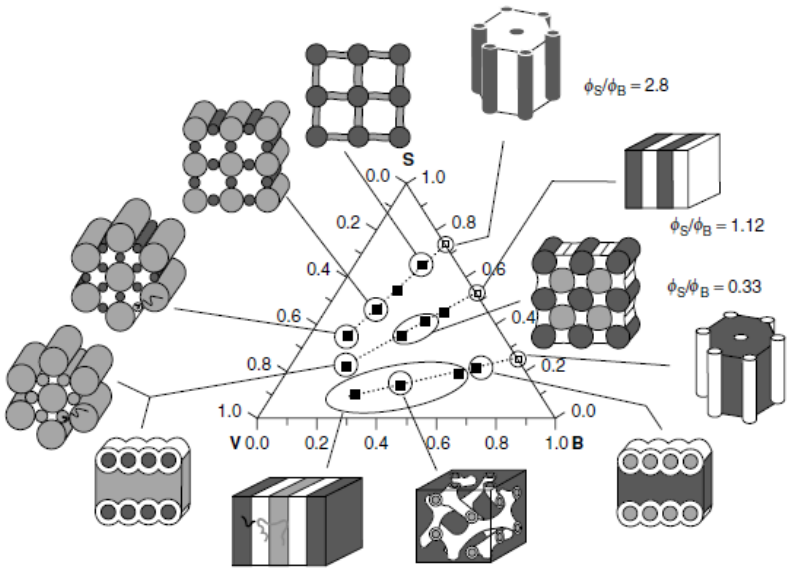

Figure 18: Ternary phase diagram of microphase-separated morphologies produced from a polystyrene-arm-polybutadiene-arm-poly(2-vinylpyridine) series. (Adapted from Abetz)[50]

In 2003, Yamauchi *et al.*[51] described the self-assembly of a star miktoarm ABC terpolymer composed of PI, PS and PDMS. The obtained morphology was composed of PI, PS and PDMS columns with different shapes: PDMS formed octagonal-cylindrical microdomains while the PS columns tended to expand their interface with PI, resulting in the concaved sides of the PI cylindrical domains. The coexistence of three types of cylindrical domains with different interface shapes is characteristic of St Andrew's cross morphology (see Figure 19).

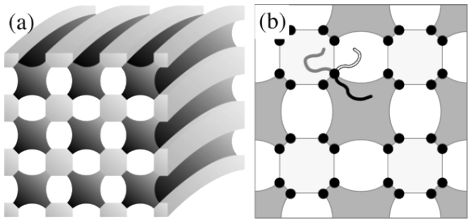

Figure 19: (a) Schematic illustration of the model for the microdomain structure of the (PI)(PS)(PDMS) 3-miktoarm star terpolymer consisting of dark (PI), gray (PDMS), and bright (PS) cylinders with characteristic shapes. (b) A cross-sectional view of the cylinders in (a). The junction points of the star miktoarm terpolymer are confined on the curved lines and designated by the filled circles in (b). (Adapted from Yamauchi)[51]

e. Theoretical studies

The bulk morphologies were also compared with simulation experiments. For instance, Gemma simulated the morphology of star miktoarm ABC terpolymers using Monte Carlo simulation (see Figure 20).[52] The volume ratios A and B blocks were kept constant and symmetric, while the volume fraction of the C block was changed (noted x).

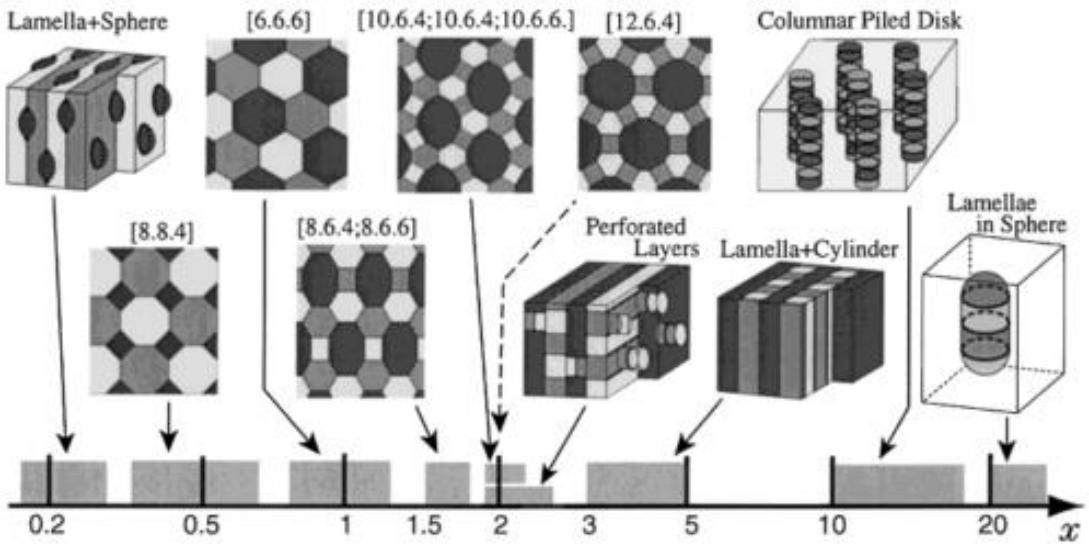

Figure 20: Phase diagram of ABC star miktoarm terpolymer systems with arm-length ratio 1:1:x and with symmetric interactions between three components. A (light gray), B (medium gray), and C (dark gray) are displayed. Junction point lines are drawn by thick lines or solid circles where three kinds of interfaces meet. (Adapted from Gemma et al.) [52]

For $0.17 \leq x \leq 0.33$, lamellae including spheres at their interfaces were obtained. When the volume ratio of the C block was increased ($0.37 \leq x \leq 0.7$), a (6.6.6) Archimedean tiling pattern was obtained. These simulated phases are in accordance with experimental results. For example, Takano observed the same structure for a 3 μ-ISP (S:I:P = 1:1:0.7).[13] When the volume ratio of the C block was close to two, different morphologies were close in term of energy. They reported the presence of a (4.6.12) tiling pattern which had been observed in bulk from a 3 μ-ISP (S:I:P = 1:1:1.9). 3 μ-ISP (S:I:P = 1:1:10) is another example of consistency between the experimental and simulated results since, in this case, a columnar piled disk structure was obtained. Some simulated predictions did not fully match with experimental data. Asymmetry of the interaction parameters for experimental data could be one of the reason of such a mismatch.

IV. Self-assembly of linear and star miktoarm ABC terpolymer thin film

Only few examples of self-assembly in thin films exist in the literature for ABC terpolymers (linear and star miktoarm). New parameters to explain the BCP phase behavior appear in thin films that are negligible in bulk. In thin film, the surface energy of polymers with regard to the surface energy of the substrate, the thickness, and post-treatments are some parameters that lead to the formation of different morphologies than in bulk. BCP thin films were obtained by solubilizing the linear or star miktoarm ABC terpolymers in a good solvent followed by the spin-coating of the solution on a substrate. In this part, the self-assembly of linear and star miktoarm self-assembly in thin film will be described.

1. Self-assembly of linear ABC terpolymer thin films

Elbs *et al.* reported on the self-assembly of polystyrene-*b*-poly(2vinylpyridine)-*b*-poly(t-butyl methacrylate)[53–58] (PS-*b*-P2VP-*b*-PtBMA) ($S_1V_{1.5}T_{3.4}$) thin films. Some interesting morphologies were obtained in thin film like core-shell cylinders, spheres-*in*-cylinders, helices-*on*-cylinders, core-shell double gyroid. In all cases PtBMA formed the matrix while P2VP formed the shell (cylinders), and PS the core. Depending on the solvent vapor annealing (SVA) post-treatment and the thickness of the film, morphologies differed for a given volume ratio between blocks. Thin films treated with tetrahydrofuran (THF) vapor showed a core-shell cylindrical morphology when the film was thick and helices-*on*-cylinders when the film was thinner. The helical structure was only obtained when the film thickness corresponded to a single layer of the cylinders. From solvent annealed thin films under a chloroform vapor, a core-shell double gyroid structure was obtained.

Deng *et al.*[59] also reported on a core-shell double gyroid morphology for a poly(ethylene oxide)-*b*-poly(ethyl acrylate)-*b*-polystyrene (E:A:S = 1:5.9:5.6) mixed with 25% of phenolic resin oligomers (resol). Herein, the PEO had the smallest volume ratio. The core of the network structure was once again formed of the polymer exhibiting the smallest volume ratio of the linear ABC terpolymer. The obtained structures are shown in Figure 21.

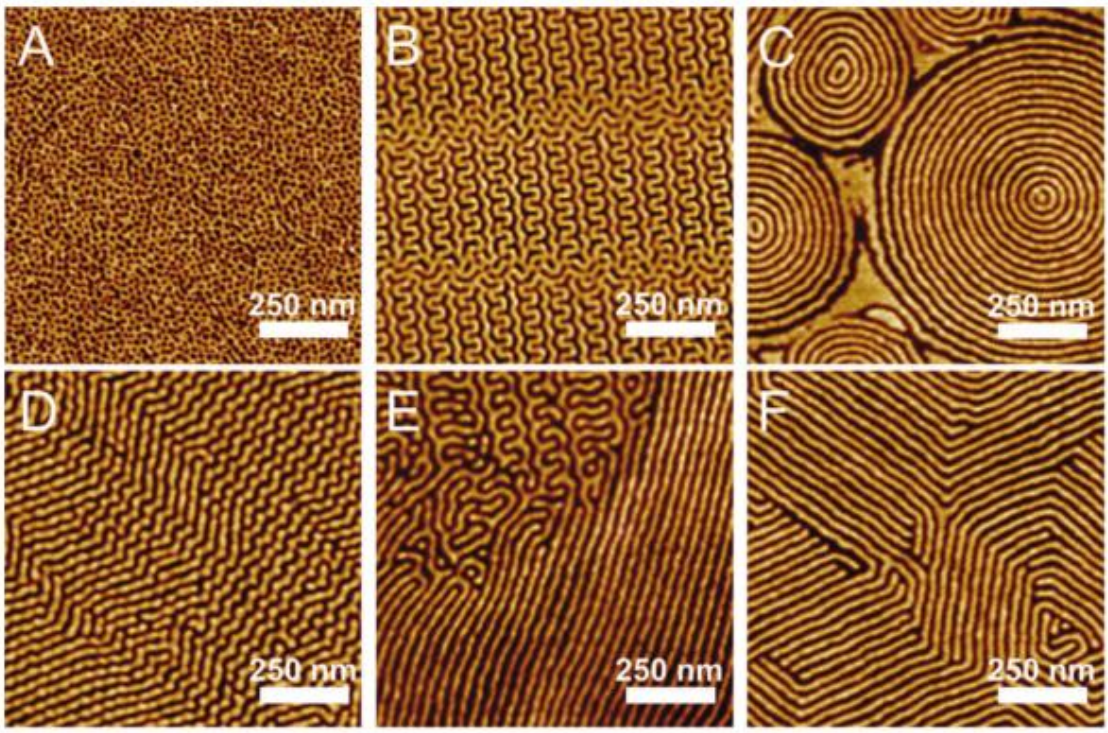

Figure 21: AFM phase images of films containing (a) 0 wt%; (b) 25 wt%; (c) 40 wt%; (d) 50 wt%; (e) 60 wt% and (f) 67 wt% resol after exposure to MEK using single SVA process. (Adapted from Deng et al.) [59]

Thin film core-shell cylinder structures were also reported by *Bang et al*.[60] in 2006, and by Chuang *et al*.[61] in 2009. Bang and co-workers studied the self-assembly of PEO-*b*-PMMA-*b*-PS thin films exposed to a benzene vapor while Chuang *et al*. reported on long-range ordered polystyrene-*b*-polyferrocenylsilane-*b*-poly(2-vinylpyridine) (PSF) thin films placed under solvent vapor consisting of a mixture of chloroform and acetone. They demonstrated that the solvent choice for the post-treatment was a key parameter to obtain long-range ordered structures.

Recently, Aissou *et al*.[62] reported on highly-ordered nanorings (core-shell cylinders) produced from poly(1,1-dimethylsilacyclobutane)-*b*-polystyrene-*b*-poly(methyl methacrylate) (PDMSB-*b*-PS-*b*-PMMA) thin films with different cylinder orientations depending on the film thickness. From a thickness of about 29 to 31 nm out-of-plane nanorings were observed, while in-plane nanorings were obtained when the thickness was increased (from 47 to 65 nm). They highlighted a clear dependence between the domain orientation and the film thickness. The

PDMSB-*b*-PS-*b*-PMMA thin films were also deposited on topographical substrates which revealed an increase of the long-range order of the core-shell features (see Figure 22).

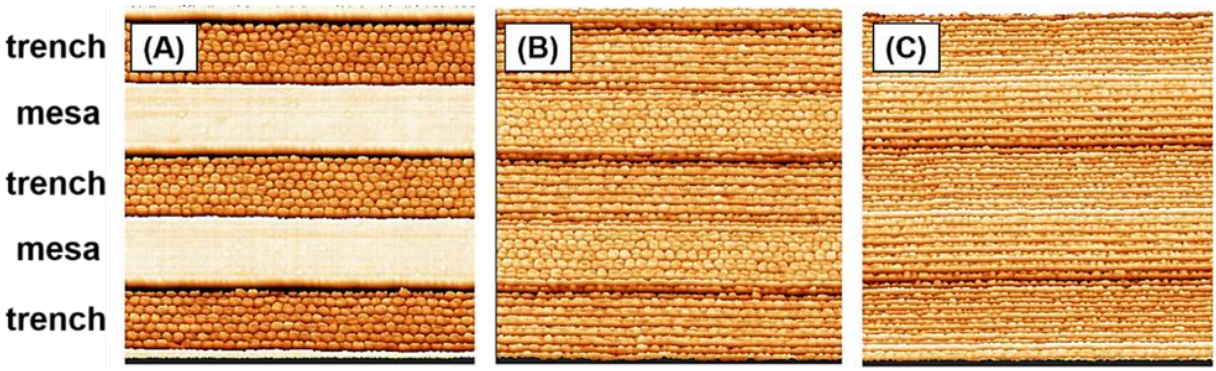

Figure 22: (1.25 × 1.25 µm) AFM phase views of templated DSM thin layers with different film thicknesses: a) $t_{trench} \approx 31$ nm, b) $t_{trench} \approx 47$ nm and $t_{mesa} \approx 29$ nm, and c) $t_{trench} \approx 65$ nm and $t_{mesa} \approx 47$ nm. DSM thin films were annealed under $CHCl_3$ vapor for 3 h then etched by a CF_4/O_2 RIE plasma prior to be imaged by AFM. Positions of trenches and mesas are indicated on the left of the figure. (Adapted from Aissou et al.)[62]

To summarize, only few structures have been obtained in thin film configuration. Important parameters like the solvent used for the SVA process and the film thickness must be taken into account to control the long-range order of the structure and the domain orientation.

2. Self-assembly of star miktoarm ABC terpolymer thin films

Only few papers reported on the self-assembly of star miktoarm ABC terpolymer thin films. To the best of my knowledge, the first example of self-assembled star miktoarm ABC terpolymer thin film was reported by Aissou *et al.* in 2013.[63,64] A star miktoarm ABC terpolymer composed of polyisoprene, polystyrene and polyferrocenylethylmethylsilane (3 µ-ISF, I:S:F = 1:0.9:0.7) was used to achieve Archimedean tiling patterns. The star miktoarm terpolymers (unblended or blended with hPS) was spin-coated on a silicon wafer (treated or untreated) and solvent-annealed under a chloroform vapor. They reported a morphological change from a (4.8.8) to a (6.6.6) tiling pattern induced by a greater swelling of the PI achieved by increasing the vapor pressure during the solvent vapor annealing (SVA) process (see Figure 23). Both morphologies were used as nanolithographic masks to transfer square and triangle hole arrays into the substrate.

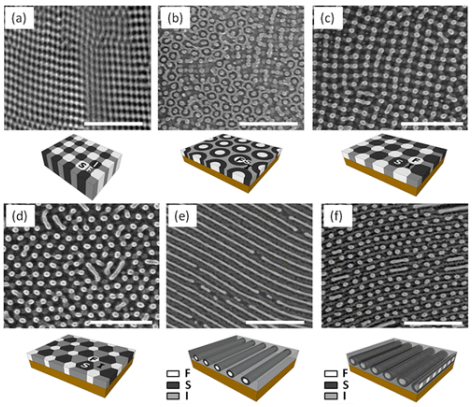

Figure 23: (a) TEM image of an unblended bulk 3 μ-ISF film and (b–d) SEM images of 3 μ-ISF/hS15 thin films on untreated Si wafer at (b) 0.7P_0, (c) 0.75P_0, and (d) 0.85 P_0. (e,f) 3 μ-ISF/hS15 thin films on a P2VP-coated surface at (e) 0.75P_0 and (f) 0.8P_0. Samples were stained with OsO_4 to enhance contrast for TEM and SEM imaging. Thin films (b–f) were etched by O_2 RIE before SEM observation, so PFS appears bright and regions formerly occupied by PS appear dark. (Adapted from Aissou et al. in 2013)[63,64]

In 2014, Choi *et al.*[65] reported the structure obtained from the self-assembly of the 3 μ-PFS (P:F:S=1:1.3:0.7). A hierarchical morphology composed of undulating lamellae of PFS separated by alternating cylinders of PI and PS was obtained after a chloroform SVA treatment (see Figure 24). Two different junction points are present in this morphology. On one hand, a junction point where polymers are well separated, and another one where the PS reduces the interface between PI and PFS. The presence of this two different junction points explained the undulation of the lamellae structure.

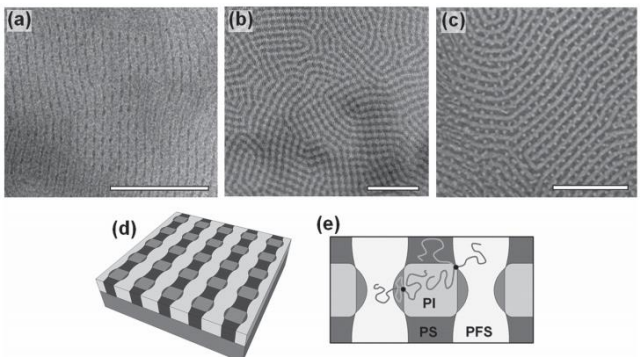

Figure 24: TEM images of 3μ-ISF thin films (a) before staining (b) after OsO_4 staining. PFS microdomains appear darkest in the unstained sample while PI microdomains appear darkest in the stained sample. (c) SEM image of bottom interface of 3μ-ISF thin film. The continuous bright regions indicate PFS and bright dots indicate PI. Scale bars in (a-c) are 300 nm. (d) Schematic description of thin film knitting pattern, and its chain conformation within the microdomains (e). (Adapted from Choi et al)[65]

In 2016, Aissou *et al.*[66] reported on the formation of Archimedean tiling patterns and another hierarchical morphology from the self-assembly of poly(1,1-dimethyl silacyclobutane)-*arm*-polystyrene-*arm*-poly(D,L-lactide acid) (3 μ-SDL). Herein, highly-oriented asymmetric hierarchical lamellar morphologies were produced from the 3 μ-SDL (S:D:L=1:2.1:0.6). The microstructure was composed of PDMSB lamellae separated by PS lamellae including PLA cylinders. Long-range order was obtained by templating the hierarchical morphology with topographical substrates (see Figure 25).

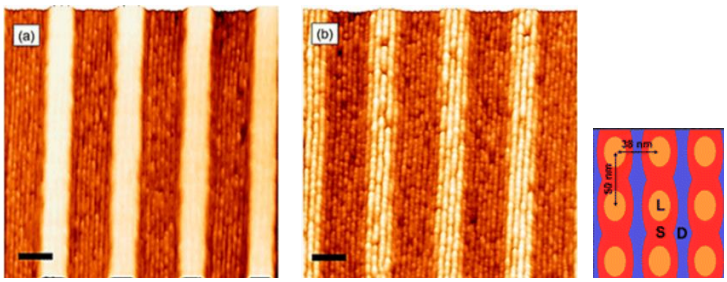

Figure 25: AFM topographic views of solvent-annealed 3 μ-DSL (D:S:L = 27:56:17) thin films deposited on topographical substrates followed by a CF_4/O_2 RIE treatment. Sample thicknesses are (a) $t_{trench} \sim 25$ nm and (b) $t_{mesa} \sim 20$ nm and $t_{trench} \sim 60$ nm. Scale bars: 250 nm. (Adapted from Aissou et al.)[66]

The volume ratio of the PLA was increased (S:D:L=1:2.1:1.5), and two morphologies were produced. The most stable one was the (6.6.6) tiling, but the step between terraces locally stabilized the (4.8.8) tiling pattern when the film dewetted (see Figure 26).

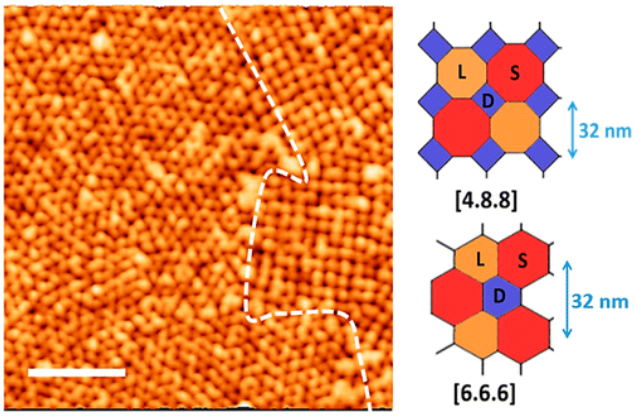

Figure 26: AFM topographic view of a solvent-annealed 3 μ-DSL (D:S:L = 22:46:32) thin film ($t \sim 45$ nm) treated with a CF_4/O_2 RIE plasma which includes two columnar morphologies indexed with a p6mm or p4mm symmetry. The dashed line delimits the regions occupied by the different phases. Schematic models showing (top) the p4mm and (bottom) the p6mm microstructures corresponding to the [4.8.8] and [6.6.6] tilings, respectively. (Adapted from Aissou et al.)[66]

3. Conclusion

Some morphologies have been described in thin film but much less than in bulk. Linear and star miktoarm ABC terpolymers give access to hierarchical structures and Archimedean tiling patterns. It should be noted that most of the morphological studies are done in bulk. Indeed, in thin film, the presence of boundary surfaces and confinement due to the film thickness, renders more difficult to obtain well-defined morphologies. Moreover, for star miktoarm ABC terpolymers, only few structures have been achieved due to the difficulty to synthetize the star miktoarm shaped polymers composed of three incompatible arms.

In the next part, we will discuss the synthesis of linear and star miktoarm ABC terpolymers.

V. Linear and star miktoarm ABC terpolymers synthesis

Several methods have been developed to synthetize linear and star miktoarm ABC terpolymers. One important parameter for the synthesis of a block copolymer is the precise control of the chain-growth polymerization, in order to avoid polydispersed polymers that create defects in the self-assembled structures. Consequently, most of the time, linear or star miktoarm ABC terpolymers are synthetized by living polymerization (anionic[67,68] or cationic[69]) or controlled polymerization (Nitroxide-Mediated Radical Polymerization,[70] Atom Transfer Radical Polymerization,[71–73] Reversible Addition-Fragmentation chain Transfer polymerization,[74] …).

In this study, we will focus our attention on the synthesis of linear and star miktoarm ABC terpolymers by anionic polymerization. This method allows the control of the chain growth by a fast and effective initiation step, prevents chain termination and transfer reactions which are common in classical radical polymerization. One limitation of the anionic polymerization comes from the harsh conditions needed. The reaction should takes place in a moisture and oxygen free reactor with highly purified monomers and solvents, and most of the time at low temperature. Whatever the drawbacks inherent to the anionic polymerization, it remains one of the most effective synthesis method for linear or star miktoarm ABC terpolymer.

1. Linear ABC terpolymer synthesis

For the synthesis of linear ABC terpolymers, one very common method consists in the synthesis of the different blocks successively *via* living polymerization (a three step sequential anionic polymerization process) as shown in Figure 27.[75] After initiation from an appropriate anionic initiator, monomers are sequentially added. Depending on their propagation rate, monomers should be added in a certain order: the initiation rate at each step should be faster than the corresponding propagation rate.[76]

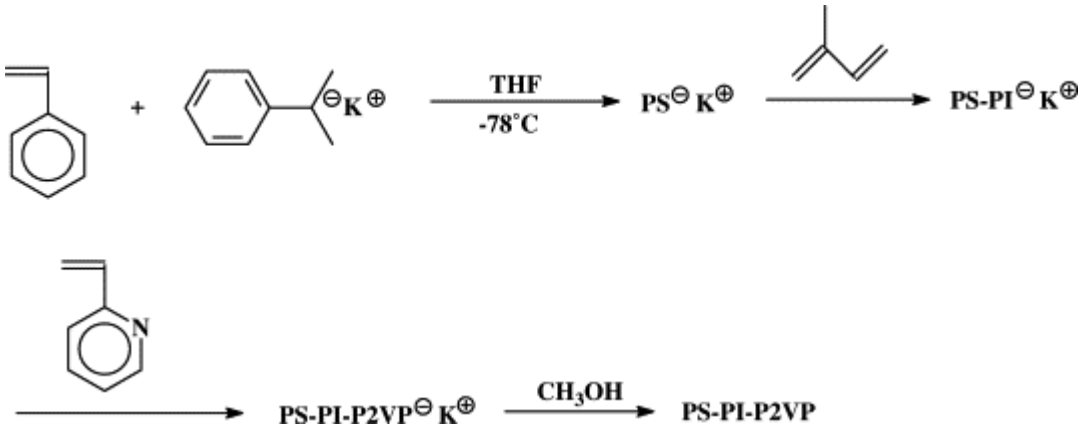

Figure 27: Synthesis of a PS-b-PI-b-P2VP triblock terpolymer by anionic polymerization.

Using this sequential approach, Matsushita *et al.*,[77, 26] synthetized a series of linear ABC terpolymers composed of PS, P2VP, and PI (SIP and ISP). Both polymerizations were done with cumylpotassium as an initiator in THF and monomers and solvents were highly purified. Polymers were characterized by both SEC (size exclusion chromatography) as showed in Figure 28 and proton NMR. Final linear ABC terpolymers exhibited a low dispersity, and the molecular weights obtained were closed to the ones expected from the stoichiometry.

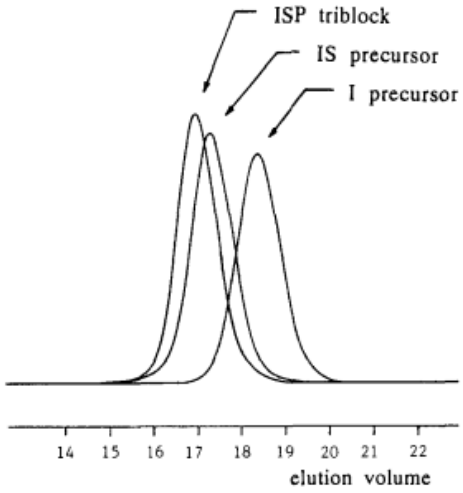

Figure 28: SEC traces of a triblock copolymer and its precursors.

Some examples of linear ABC terpolymer synthesis with a three-step-sequential-anionic polymerization described in the literature are reported in Table 5.

Table 5: Summary of the anionically polymerized linear ABC terpolymers.

Authors	**Linear ABC terpolymers**	**Initiator**	**Solvent**	**Dispersity**
Matsushita[26]	PI-*b*-PS-*b*-P2VP	cumylpotassium	THF	/
Matsushita[77]	PS-*b*-PI-*b*-P2VP	cumylpotassium	THF	/
Watanabee[78]	PS-*b*-P2VP-*b*-PB	*sec*-BuLi	THF	1.1
Stadler[37]	PS-*b*-PB-*b*-PMMA	*sec*-BuLi	THF	1.1
Stadler[79]	PS-*b*-PtBuMA-*b*-P4VP	*sec*-BuLi	THF	1.3
Abetz[80]	PI-*b*-PB-*b*-PS	*sec*-BuLi	benzene	1.02
Eisenberg[81]	PS-*b*-PMMA-*b*-PAA	*sec*-BuLi	THF	1.1
Liu[82]	PI-*b*-PCEMA-*b*-PtBA	*sec*-BuLi	THF/hexane	1.16
Bates[83]	PI-*b*-PS-*b*-PDMS	*sec*-BuLi	THF	1.18
Tsitsilianis[84]	PS-*b*-PANa-*b*-PnBMA	*sec*-BuLi	THF	1.16
Abetz[30]	PS-*b*-PBd-*b*-P2VP	*sec*-BuLi	THF/benzene	<1.3
Hadjichristidis[85]	PI-*b*-P2VP-*b*-PEO	Benzyl potassium	THF	1.05
Jérôme[86]	PS-*b*-P2VP-*b*-PEO	*sec*-BuLi	THF	1.1
Muller[87]	PDMAi-*b*-PS-*b*-PMMA	*sec*-BuLi	Toluene/THF	/
Tsitsilianis[88]	PS-*b*-P2VP-*b*-PMMA	*sec*-BuLi	THF	1.17
Manners[89]	PFP-*b*-PFS-*b*-PDMS	*n*-BuLi	THF	1.1

Regardless of the solvent polarity or the initiator, the obtained dispersity was close to one. This is a typical result observed in anionic polymerization due to the fast initiation and the absence of termination reactions.

2. Star miktoarm ABC terpolymer synthesis

The synthesis of star miktoarm ABC terpolymers is more complicated because each block needs to be attached to a core molecule. Herein, the three main methods for the synthesis of star miktoarm ABC terpolymers will be discussed.

a. Chlorosilane methology

One of the most well established methods for the synthesis of star miktoarm ABC terpolymers *via* anionic polymerization was reported for the first time in 1992 by Hadjichristidis.[90] They synthetized a 3 μ-ABC composed of PI, PS and PB using a chlorosilane method. Polymers were anionically polymerized using *sec*-BuLi as an initiator and a trifunctional chlorosilane compound was used as a core molecule according to the procedure presented in Figure 29.

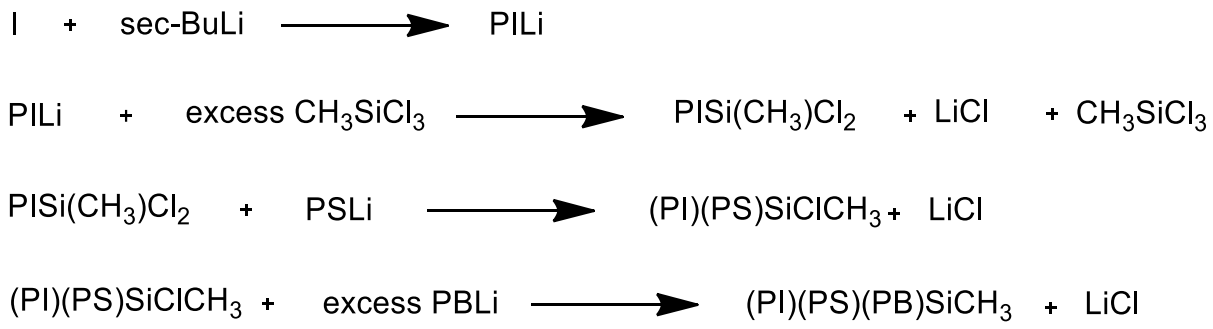

Figure 29: Synthesis of a PS-arm-PI-arm-PB by anionic polymerization using a chlorosilane method.

The first step consisted in the addition of $SiMeCl_3$ to a living PI block, then the PS living block was added, followed by the addition of a living PB block. Other star miktoarm ABC terpolymers such as PS-*arm*-PI-*arm*-PDMS,[91] PS-*arm*-PI-*arm*-P2VP,[92] PS-*arm*-PI-*arm*-PMMA[93] have been synthetized by Hadjichristidis and co-workers using this method. Those

reactions required a specific glassware, high vacuum and break-seal techniques, high purity compounds, and fractionation steps, making them difficult to reproduce in our laboratory.

b. Diphenylethylene methodology

Another synthesis procedure described by Fujimoto *et al*.[94] in 1992 deals with anionic polymerization and the use of a modified diphenylethylene (DPE) as a core molecule. A poly(styryl) anion and an end-reactive PDMS were coupled, followed by anionic polymerization of MMA as shown in Figure 30

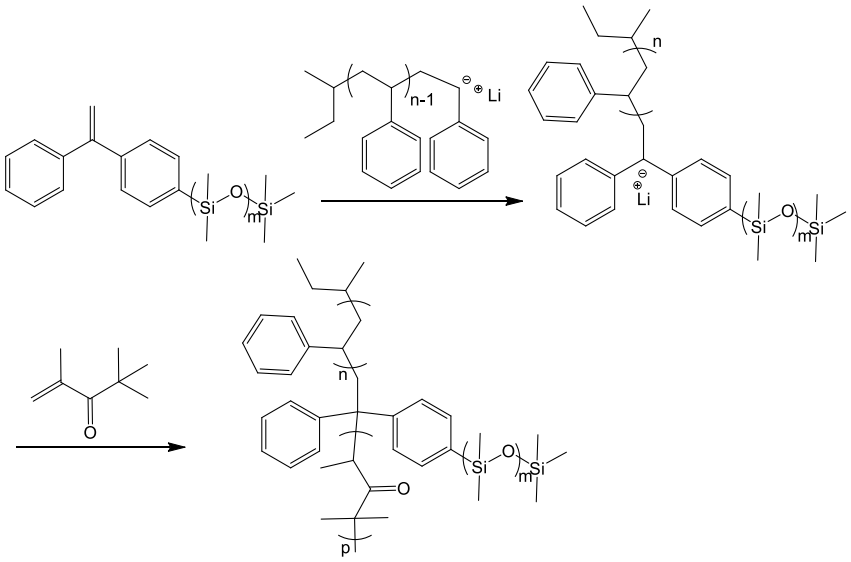

Figure 30: Synthesis of a star-shaped copolymer having three different arms, poly(styrene), poly(dimethylsiloxane) and poly(tert-butyl methacrylate).

Other groups reported on the preparation of star miktoarm ABC terpolymers using a modified DPE as the core molecule. Dumas *et al*.[95,96] reported on the synthesis of PS-*arm*-PEO-*arm*-PCL, PS-*arm*-PEO-*arm*-PLL and PS-*arm*-PMMA-*arm*-PEO. The synthesis involved a protected DPE (1-[4-(2-tert-butyldimethylsiloxy)ethyl]phenyl-1- phenylethylene) as the core molecule. The first arm was anionically polymerized, then, the hydroxyl protected DPE was added to the solution, followed by the polymerization of the second arm. Finally, the core molecule was deprotected, and the third arm was polymerized by ring opening polymerization from the hydroxyl reactive function. This method was very relevant, but the last step required a monomer that could be polymerized from a hydroxyl reactive function.

Stadler *et al*.[97] proposed another method using a modified DPE as core molecule. In this synthesis way, a living PS was end-capped with a bromo-subsituted DPE. Then, a living PB was added to the DPE-PS and reacted on the vinyl group of the DPE to produce a living

macroinitiator that could initiate the anionic polymerization of the MMA. The same methodology was used to prepare a PS-*arm*-PB-*arm*-P2VP.

In 2012, Muller et al[98] introduced a new synthesis route combining the use of DPE as a core molecule and click chemistry. In this route, the DPE bear a protected alkyne function. The two first arms were sequentially prepared by anionic polymerization using the modified DPE as core molecule. The third arm was then "clicked" on the alkyne function of the DPE after deprotection by Huisgen click chemistry[99] as shown in Figure 31.

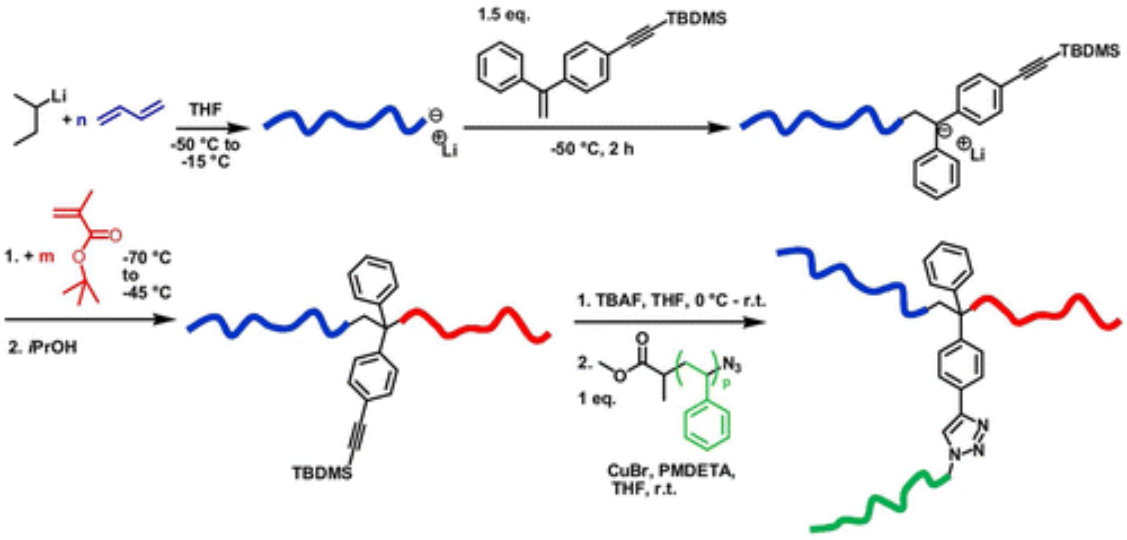

Figure 31: Synthetic route for the synthesis of an ABC miktoarm star terpolymer consisting of polybutadiene, poly(tert-butyl methacrylate), and polystyrene.

Those two methods involving modified DPE are very attractive for the synthesis of star miktoarm ABC terpolymers, and allows the synthesis of a wide range of 3 μ-ABC systems.

c. Combination of different polymerization routes

Combining different polymerization routes could be an effective way to achieve the desired star miktoarm ABC terpolymer. In 2006, Tunca *et al.*[100] reported on the synthesis of star miktoarm ABC terpolymers (PS-*arm*-PMMA-*arm*-PEO and PS-*arm*-PMMA-*arm*-PtBA) using a multifunctional initiating site core molecule. The core molecule was the succinic Acid 3-(2-bromo-2-methylpropionyloxy)-2-methyl-2-[2-phenyl-2-(2,2,6,6-tetramethyl piperidin-1-yloxy)-ethoxycarbonyl]-propyl ester prop-2-ynyl ester (see Figure 32). They prepared PMMA by ATRP using the Br-containing ATRP initiating group of the core molecule, the PS was done by NMP in the presence of TEMPO (2,2,6,6-tetramethylpiperidinyloxy) end-functionalized PMMA, and the third arm (PEO or PtBa) was linked to the azide function of the core molecule

using click-chemistry. They obtained well-defined star miktoarm ABC terpolymers. One limitation of this technique is the large number of synthesis and purification steps.

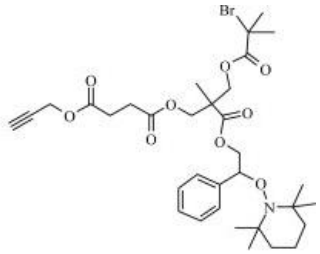

Figure 32: Core molecule was the succinic Acid 3-(2-bromo-2-methylpropionyloxy)-2-methyl-2-[2-phenyl-2-(2,2,6,6-tetramethyl piperidin-1-yloxy)-ethoxycarbonyl]-propyl ester prop-2-ynyl ester used for the synthesis of star miktoarm ABC terpolymer.

To overcome this drawback, in 2009, a one-pot synthesis of star miktoarm ABC terpolymers (PS-*arm*-PCL-*arm*-PDMA, PEO-*arm*-PCL-*arm*-PDMA) using a trifunctional core molecule bearing alkynyl, hydroxyl group and bromine moieties was reported by Liu *et al.*[101] The 2-(dimethylamino)ethyl methacrylate (DMA) was polymerized by ATRP, caprolactone (CL) by ROP, and azido-terminated PS or PEO was clicked to the core molecule in an one pot manner. Due to the orthogonality of the reactive functions of the core molecule, they obtained a well-defined star miktoarm ABC terpolymer. Other syntheses using a combination of polymerization route and a multifunctional initiator have been reported in the last few decades.[102–105]

3. Conclusion

Herein, we described some of the widely used synthesis route to produce linear and star miktoarm ABC terpolymers. The synthesis of linear ABC terpolymers are commonly done *via* sequential anionic polymerization with a good control of the dispersity. Regarding star miktoarm ABC terpolymers, the synthesis routes are more complicated and required more steps to prepare a multifunctional initiator or a core molecule.

Advancements in polymer chemistry allowed the synthesis of different 3 μ-ABC systems and provided access to chemically incompatible blocks. The synthesis of star miktoarm ABC terpolymers with chlorosilane compounds involves specific glasswares not available in our lab while metal catalyzed coupling reactions are hardly sustainable for the nanolithography industry. New synthesis ways are very desirable especially to prepare star miktoarm ABC terpolymers.

VI. Conclusion

In this bibliographic chapter, we saw that the self-assembly of linear and star miktoarm ABC terpolymers have been mostly studied in bulk. They allow to obtain a wide range of morphologies that give access to pattern symmetries not available with AB-type BCPs. Only few studies reported on the self-assembly of linear and star miktoarm terpolymer thin films. We saw that in the case of linear ABC terpolymer, morphologies obtained in thin films are in accordance with theoretical and bulk studies. For star miktoarm ABC terpolymers, very interesting structures including Archimedean tiling patterns have been identified both in bulk and in thin film configurations. Those patterns could open a broad array of applications in the nanoelectronic since Cartesian square arrays are accessible from self-assembled star miktoarm ABC terpolymers.

One limitation in the use of 3 μ-ABC systems is their synthesis. Actually, controlled polymerization and most of the time anionic polymerization are required to obtain well-defined terpolymers. Linear ABC terpolymers are mostly synthesized *via* a sequential anionic polymerization, but with this methodology, it is needed to take into account the reactivity of monomers in the sequence. Star miktoarm ABC terpolymers are synthesized using three main synthesis routes: the chlorosilane methodology, the diphenylethylene route, and a hybrid approach.

In the next chapters, an easy reproducible synthetic route will be described as well as the self-assembly of linear and star miktoarm ABC terpolymer thin films.

1. Berenschot, E. J. W. *et al.* 3D nanofabrication of fluidic components by corner lithography. *Small* **8,** 3823–3831 (2012).
2. Fan, D., Wang, L. & Ekinci, Y. Nanolithography using Bessel Beams of Extreme Ultraviolet Wavelength. *Sci. Rep.* **6,** 31301 (2016).
3. Lin, B. J. NGL comparable to 193-nm lithography in cost, footprint, and power consumption. *Microelectron. Eng.* **86,** 442–447 (2009).
4. Willson, C. G. & Roman, B. J. The future of lithography: SEMATECH Litho Forum 2008. in *ACS Nano* **2,** 1323–1328 (American Chemical Society, 2008).
5. Allen, R. D., Wallraff, G. M., Hofer, D. C. & Kunz, R. R. Photoresists for 193-nm lithography. *IBM J. Res. Dev.* **41,** 95–104 (1997).
6. Hu, H., Gopinadhan, M. & Osuji, C. O. Directed self-assembly of block copolymers: a tutorial review of strategies for enabling nanotechnology with soft matter. *Soft Matter* **10,** 3867 (2014).
7. Choi, H. K., Gwyther, J., Manners, I. & Ross, C. A. Square arrays of holes and dots patterned from a linear ABC triblock terpolymer. *ACS Nano* **6,** 8342–8348 (2012).
8. Hückstädt, H., Goldacker, T., Göpfert, A. & Abetz, V. Core-shell double gyroid morphologies in ABC triblock copolymers with different chain topologies. *Macromolecules* **33,** 3757–3761 (2000).
9. Krausch, G. & Magerle, R. Nanostructured thin films via self-assembly of block copolymers. *Adv. Mater.* **14,** 1579–+ (2002).
10. Hayashida, K. *et al.* Systematic transitions of tiling patterns formed by ABC star-shaped terpolymers. *Macromolecules* **39,** 9402–9408 (2006).
11. Takano, A. *et al.* A mesoscopic archimedean tiling having a new complexity in an ABC star polymer. *J. Polym. Sci. Part B Polym. Phys.* **43,** 2427–2432 (2005).
12. Ouyang, P., Zhao, W. & Huang, X. Beautiful Math, Part 5: Colorful Archimedean Tilings from Dynamical Systems. *IEEE Comput. Graph. Appl.* **35,** 90–96 (2015).
13. Matsushita, Y., Hayashida, K. & Takano, A. Jewelry box of morphologies with mesoscopic length scales - ABC star-shaped terpolymers. *Macromol. Rapid Commun.* **31,** 1579–1587 (2010).
14. Nunns, A., Ross, C. A. & Manners, I. Synthesis and bulk self-assembly of ABC star terpolymers with a polyferrocenylsilane metalloblock. *Macromolecules* **46,** 2628–2635 (2013).
15. Takano, A. *et al.* Composition dependence of nanophase-separated structures formed by

star-shaped terpolymers of the A1.0B1.0CX type. *J. Polym. Sci. Part B Polym. Phys.* **45,** 2277–2283 (2007).

16. Takano, A. *et al.* Observation of cylinder-based microphase-separated structures from ABC star-shaped terpolymers investigated by electron computerized tomography. *Macromolecules* **37,** 9941–9946 (2004).
17. Matsen, M. W. & Bates, F. S. Origins of Complex Self-Assembly in Block Copolymers. *Macromolecules* **29,** 7641–7644 (1996).
18. Leibler, L. Theory of Microphase Separation in Block Copolymers. *Macromolecules* **13,** 1602–1617 (1980).
19. Riess, G., Schlienger, M. & Marti, S. New Morphologies in Rubber-Modified Polymers. *J. Macromol. Sci. Part B* **17,** 355–374 (1980).
20. Bates, F. S. & Fredrickson, G. H. Block Copolymers—Designer Soft Materials. *Phys. Today* **52,** 32–38 (1999).
21. Stadler, R. *et al.* Morphology and Thermodynamics of Symmetric Poly(A-block-B-block-C) Triblock Copolymers. *Macromolecules* **28,** 3080–3097 (1995).
22. Bailey, T. S. Morphological behavior spanning the symmetric AB andABC block copolymer states. (University of Minnesota, 2001).
23. Radlauer, M. R. *et al.* Morphological consequences of frustration in ABC triblock polymers. *Macromolecules* **50,** 446–458 (2017).
24. Mogi, Y. *et al.* Molecular Weight Dependence of the Lamellar Domain Spacing of ABC Triblock Copolymers and Their Chain Conformations in Lamellar Domains. *Macromolecules* **26,** 5169–5173 (1993).
25. Mogi, Y. *et al.* Superlattice Structures in Morphologies of the ABC Triblock Copolymers. *Macromolecules* **27,** 6755–6760 (1994).
26. Mogi, Y. *et al.* Preparation and Morphology of Triblock Copolymers of the ABC Type. *Macromolecules* **25,** 5408–5411 (1992).
27. Matsushita, Y., Suzuki, J. & Seki, M. Surfaces of tricontinuous structure formed by an ABC triblock copolymer in bulk. *Phys. B Condens. Matter* **248,** 238–242 (1998).
28. Phan, S. & Fredrickson, G. H. Morphology of symmetric ABC triblock copolymers in the strong segregation limit. *Macromolecules* **31,** 59–63 (1998).
29. Jung, K., Abetz, V. & Stadler, R. Thermodynamically controlled morphological disorder in a microphase-separated cylindrical block copolymer. *Macromolecules* **29,** 1076–1078 (1996).

30. Hückstädt, H., Göpfert, A. & Abetz, V. Influence of the block sequence on the morphological behavior of ABC triblock copolymers. *Polymer (Guildf).* **41,** 9089–9094 (2000).
31. Bailey, T. S., Hardy, C. M., Epps, T. H. & Bates, F. S. A noncubic triply periodic network morphology in poly(isoprene-b-styrene-b-ethylene oxide) triblock copolymers. *Macromolecules* **35,** 7007–7017 (2002).
32. Chatterjee, J., Jain, S. & Bates, F. S. Comprehensive phase behavior of poly(isoprene-b-styrene-b-ethylene oxide) triblock copolymers. *Macromolecules* **40,** 2882–2896 (2007).
33. Epps, T. H., Bailey, T. S., Waletzko, R. & Bates, F. S. Phase behavior and block sequence effects in lithium perchlorate-doped poly(isoprene-b-styrene-b-ethylene oxide) and poly(styrene-b-isoprene-b-ethylene oxide) triblock copolymers. *Macromolecules* **36,** 2873–2881 (2003).
34. Gido, S. P., Schwark, D. W., Thomas, E. L. & do Carmo Gonçalves, M. Observation of a Non-Constant Mean Curvature Interface in an ABC Triblock Copolymer. *Macromolecules* **26,** 2636–2640 (1993).
35. Khokhlov, A. R. & Semenov, A. N. On the theory of liquid-crystalline ordering of polymer chains with limited flexibility. *J. Stat. Phys.* **38,** 161–182 (1985).
36. Bailey, T. S., Pham, H. D. & Bates, F. S. Morphological behavior bridging the symmetric AB and ABC states in the poly(styrene-b-isoprene-b-ethylene oxide) triblock copolymer system. *Macromolecules* **34,** 6994–7008 (2001).
37. Krappe, U., Stadler, R. & Voigt-Martin, I. Corrections: Chiral Assembly in Amorphous ABC Triblock Copolymers. Formation of a Helical Morphology in Polystyrene-block-polybutadiene-6/oc/c-poly(methyl methacrylate) Block Copolymers (Macromolecules (1995) 28(13) (4558–4561) (10.1021/ma00117a027)). *Macromolecules* **28,** 7583 (1995).
38. Brinkmann, S., Stadler, R. & Thomas, E. L. New structural motif in hexagonally ordered cylindrical ternary (ABC) block copolymer microdomains. *Macromolecules* **31,** 6566–6572 (1998).
39. Balsamo, V., von Gyldenfeldt, F. & Stadler, R. 'Superductile' Semicrystalline ABC Triblock Copolymers with the Polystyrene Block (A) as the Matrix. *Macromolecules* **32,** 1226–1232 (1999).
40. Liu, M., Li, W., Qiu, F. & Shi, A. C. Theoretical study of phase behavior of frustrated ABC linear triblock copolymers. *Macromolecules* **45,** 9522–9530 (2012).
41. Li, W., Qiu, F. & Shi, A. C. Emergence and stability of helical superstructures in ABC

triblock copolymers. *Macromolecules* **45,** 503–509 (2012).

42. Jiang, Z. *et al.* Complex microstructures of ABC triblock copolymer thin films directed by polymer brushes based on self-consistent field theory. *Nanoscale Res. Lett.* **9,** 359 (2014).
43. Okamoto, S. *et al.* Morphology of model three-component three-arm star-shaped copolymers. *Polymer (Guildf).* **38,** 5275–5281 (1997).
44. Li, S., Jiang, Y. & Chen, J. Z. Y. Morphologies and phase diagrams of ABC star triblock copolymers confined in a spherical cavity. *Soft Matter* **9,** 4843 (2013).
45. Hadjichristidis, N. *et al.* Morphology and Miscibility of Miktoarm Styrene-Diene Copolymers and Terpolymers. *Macromolecules* **26,** 5812–5815 (1993).
46. Sioula, S., Hadjichristidis, N. & Thomas, E. L. Novel 2-dimensionally periodic non-constant mean curvature morphologies of 3-miktoarm star terpolymers of styrene, isoprene, and methyl methacrylate. *Macromolecules* **31,** 5272–5277 (1998).
47. Sioula, S., Hadjichristidis, N. & Thomas, E. L. Direct Evidence for Confinement of Junctions to Lines in an 3 Miktoarm Star Terpolymer Microdomain Structure. *Macromolecules* **31,** 8429–8432 (1998).
48. Hayashida, K. *et al.* Hierarchical morphologies formed by ABC star-shaped terpolymers. *Macromolecules* **40,** 3695–3699 (2007).
49. Hayashida, K., Dotera, T., Takano, A. & Matsushita, Y. Polymeric quasicrystal: Mesoscopic quasicrystalline tiling in ABC star polymers. *Phys. Rev. Lett.* **98,** 195502 (2007).
50. Hückstädt, H., Göpfert, A. & Abetz, V. Synthesis and morphology of ABC heteroarm star terpolymers of polystyrene, polybutadiene and poly(2-vinylpyridine). *Macromol. Chem. Phys.* **201,** 296–307 (2000).
51. Yamauchi, K. *et al.* Microdomain morphology in an ABC 3-miktoarm star terpolymer: A study by energy-filtering TEM and 3D electron tomography. *Macromolecules* **36,** 6962–6966 (2003).
52. Gemma, T., Hatano, A. & Dotera, T. Monte Carlo simulations of the morphology of ABC star polymers using the diagonal bond method. *Macromolecules* **35,** 3225–3237 (2002).
53. Fukunaga, K., Elbs, H., Magerle, R. & Krausch, G. Large-scale alignment of ABC block copolymer microdomains via solvent vapor treatment. *Macromolecules* **33,** 947–953 (2000).

54. Fukunaga, K., Hashimoto, T., Elbs, H. & Krausch, G. Self-assembly of a lamellar ABC triblock copolymer thin film. *Macromolecules* **35,** 4406–4413 (2002).
55. Fukunaga, K., Hashimoto, T., Elba, H. & Krausch, G. Self-assembly of a lamellar ABC triblock terpolymer thin film. Effect of substrates. *Macromolecules* **36,** 2852–2861 (2003).
56. Elbs, H., Drummer, C., Abetz, V. & Krausch, G. Thin film morphologies of ABC triblock copolymers prepared from solution. *Macromolecules* **35,** 5570–5577 (2002).
57. Elbs, H., Abetz, V., Hadziioannou, G., Drummer, C. & Krausch, G. Antiferromagnetic ordering in a helical triblock copolymer mesostructure. *Macromolecules* **34,** 7917–7919 (2001).
58. Elbs, H. *et al.* Microdomain Morphology of Thin ABC Triblock Copolymer Films. *Macromolecules* **32,** 1204–1211 (1999).
59. Deng, G. *et al.* Bicontinuous mesoporous carbon thin films via an order-order transition. *Chem. Commun. (Camb).* **50,** 12684–7 (2014).
60. Bang, J. *et al.* Defect-free nanoporous thin films from ABC triblock copolymers. *J. Am. Chem. Soc.* **128,** 7622–7629 (2006).
61. Chuang, V. P., Ross, C. A., Cwyther, J. & Manners, I. Self-assembled nanoscale ring arrays from a polystyrene-b- polyferrocenylsilane-b-poly(2-vinylpyridine) triblock terpolymer thin film. *Adv. Mater.* **21,** 3789–3793 (2009).
62. Aissou, K. *et al.* Highly Ordered Nanoring Arrays Formed by Templated Si-Containing Triblock Terpolymer Thin Films. *Small* **13,** 1603184 (2017).
63. Aissou, K., Nunns, A., Manners, I. & Ross, C. A. Square and rectangular symmetry tiles from bulk and thin film 3-miktoarm star terpolymers. *Small* **9,** 4077–4084 (2013).
64. Aissou, K., Choi, H. K., Nunns, A., Manners, I. & Ross, C. A. Ordered nanoscale archimedean tilings of a templated 3-miktoarm star terpolymer. *Nano Lett.* **13,** 835–839 (2013).
65. Choi, H. K., Nunns, A., Sun, X. Y., Manners, I. & Ross, C. A. Thin film knitting pattern morphology from a miktoarm star terpolymer. *Adv. Mater.* **26,** 2474–2479 (2014).
66. Aissou, K. *et al.* Archimedean Tilings and Hierarchical Lamellar Morphology Formed by Semicrystalline Miktoarm Star Terpolymer Thin Films. *ACS Nano* **10,** 4055–4061 (2016).
67. Tsitsilianis, C., Roiter, Y., Katsampas, I. & Minko, S. Diversity of nanostructured self-assemblies from a pH-responsive BC terpolymer in aqueous media. *Macromolecules* **41,**

925–934 (2008).

68. Koutalas, G., Pispas, S. & Hadjichristidis, N. Micelles of poly(isoprene-b-2-vinylpyridine-b-ethylene oxide) terpolymers in aqueous media and their interaction with surfactants. *Eur. Phys. J. E* **15,** 457–464 (2004).
69. Kwon, Y. & Faust, R. Synthesis and Characterization of ABC Block Copolymers with Glassy (α-Methylstyrene), Rubbery (Isobutylene), and Crystalline (Pivalolactone) Blocks. *J. Macromol. Sci. Part A* **42,** 385–401 (2005).
70. Hawker, C. J. *et al.* Dual living free radical and ring opening polymerizations from a double-headed initiator. *Macromolecules* **31,** 213–219 (1998).
71. Bernaerts, K. V., Schacht, E. H., Goethals, E. J. & Du Prez, F. E. Synthesis of Poly(tetrahydrofuran)-b-Polystyrene Block Copolymers from Dual Initiators for Cationic Ring-Opening Polymerization and Atom Transfer Radical Polymerization. *J. Polym. Sci. Part A Polym. Chem.* **41,** 3206–3217 (2003).
72. Tang, Y., Liu, S. Y., Armes, S. P. & Billingham, N. C. Solubilization and controlled release of a hydrophobic drug using novel micelle-forming ABC triblock copolymers. *Biomacromolecules* **4,** 1636–1645 (2003).
73. Kubowicz, S. *et al.* Multicompartment micelles formed by self-assembly of linear ABC triblock copolymers in aqueous medium. *Angew. Chemie - Int. Ed.* **44,** 5262–5265 (2005).
74. Marsat, J. N. *et al.* Self-assembly into multicompartment micelles and selective solubilization by hydrophilic-lipophilic-fluorophilic block copolymers. *Macromolecules* **44,** 2092–2105 (2011).
75. Hadjichristidis, N., Iatrou, H., Pitsikalis, M., Pispas, S. & Avgeropoulos, A. Linear and non-linear triblock terpolymers. Synthesis, self-assembly in selective solvents and in bulk. *Prog. Polym. Sci.* **30,** 725–782 (2005).
76. Matsuo, Y., Konno, R., Ishizone, T., Goseki, R. & Hirao, A. Precise synthesis of block polymers composed of three or more blocks by specially designed linking methodologies in conjunction with living anionic polymerization system. *Polymers* **5,** 1012–1040 (2013).
77. Matsushita, Y., Tamura, M. & Noda, I. Tricontinuous Double-Diamond Structure Formed by a Styrene–Isoprene–2-Vinylpyridine Triblock Copolymer. *Macromolecules* **27,** 3680–3682 (1994).
78. Watanabe, H., Shimura, T., Kotaka, T. & Tirrell, M. Synthesis, Characterization, and

Surface Structures of Styrene—2-Vinylpyridine—Butadiene Three-Block Polymers. *Macromolecules* **26,** 6338–6345 (1993).

79. Giebele, E. & Stadler, R. ABC triblock polyampholytes containing a neutral hydrophobic block , a polyacid and a polybase. *Macromol. Chem. Phys.* **198,** 3815–3825 (1997).
80. Neumann, C., Abetz, V. & Stadler, R. Phase behavior of ABC-triblock copolymers with two inherently miscible blocks. *Colloid Polym. Sci.* **276,** 19–27 (1998).
81. Yu, G. & Eisenberg, A. Multiple Morphologies Formed from an Amphiphilic ABC Triblock Copolymer in Solution. *Macromolecules* **31,** 5546–5549 (1998).
82. Stewart, S. & Liu, G. Hollow Nanospheres from Polyisoprene-block-poly(2-cinnamoylethyl methacrylate)-block-poly(tert-butyl acrylate). *Chem. Mater.* **11,** 1048–1054 (1999).
83. Shefelbine, T. A. *et al.* Core-shell gyroid morphology in a poly(isoprene-block-styrene-block- dimethylsiloxane) triblock copolymer. *J. Am. Chem. Soc.* **121,** 8457–8465 (1999).
84. Tsitsilianis, C., Katsampas, I. & Sfika, V. ABC heterotelechelic associative polyelectrolytes. Rheological behavior in aqueous media. *Macromolecules* **33,** 9054–9059 (2000).
85. Ekizoglou, N. & Hadjichristidis, N. Benzyl potassium: An efficient one-pot initiator for the synthesis of block co- and terpolymers of ethylenoxide. *J. Polym. Sci. Part A Polym. Chem.* **39,** 1198 (2001).
86. Shell, R. *et al.* Core ± Shell ± Corona Micelles with a. *Angew. Chemie Int. Ed.* **40,** 3214–3216 (2001).
87. Bieringer, R., Abetz, V. & Müller, A. H. E. Triblock copolyampholytes from 5-(N,N-dimethylamino)isoprene, styrene, and methacrylic acid: Synthesis and solution properties. *Eur. Phys. J. E* **5,** 5–12 (2001).
88. Tsitsilianis, C. & Sfika, V. Heteroarm star-like micelles formed from polystyrene-block-poly(2-vinyl pyridine)-block-poly(methyl methacrylate) ABC triblock copolymers in toluene. *Macromol. Rapid Commun.* **22,** 647–651 (2001).
89. Wang, X. S., Winnik, M. A. & Manners, I. Synthesis and solution self-assembly of coil-crystalline-coil polyferrocenylphosphine-b-polyferrocenylsilane-b-polysiloxane triblock copolymers. *Macromolecules* **35,** 9146–9150 (2002).
90. Iatrou, H. & Hadjichristidis, N. Synthesis of a Model 3-Miktoarm Star Terpolymer. *Macromolecules* **25,** 4649–4651 (1992).

91. Bellas, V., Iatrou, H. & Hadjichristidis, N. Controlled anionic polymerization of hexamethylcyclotrisiloxane. Model linear and miktoarm star co- and terpolymers of dimethylsiloxane with styrene and isoprene. *Macromolecules* **33,** 6993–6997 (2000).
92. Tiatco, S. A. P. The possibilities and problems of entanglement in contemporary Manila theater: Pista as model, Rizal X as exemplar. *Humanit. Diliman* **13,** 127–162 (2016).
93. Sioula, S., Tselikas, Y. & Hadjichristidis, N. Synthesis of Model 3-Miktoarm Star Terpolymers of Styrene, Isoprene, and Methyl Methacrylate. *Macromolecules* **30,** 1518–1520 (1997).
94. Fujimoto, T. *et al.* Preparation and characterization of novel star-shaped copolymers having three different branches. *Polymer (Guildf).* **33,** 2208–2213 (1992).
95. Nasser-Eddine, M., Reutenauer, S., Delaite, C., Hurtrez, G. & Dumas, P. Synthesis of Polystyrene-Poly(tert-butyl methacrylate)-Poly(ethylene oxide) Triarm Star Block Copolymers. *J. Polym. Sci. Part A Polym. Chem.* **42,** 1745–1751 (2004).
96. Lambert, O., Reutenauer, S., Hurtrez, G., Riess, G. & Dumas, P. Synthesis of amphiphilic triarm star block copolymers. *Polym. Bull.* **40,** 143–149 (1998).
97. Hückstädt, H., Abetz, V. & Stadler, R. Synthesis of a polystyrene-arm-polybutadiene-arm-poly(methyl methacrylate) triarm star copolymer. *Macromol. Rapid Commun.* **17,** 599–606 (1996).
98. Hanisch, A., Schmalz, H. & Müller, A. H. E. A modular route for the synthesis of ABC miktoarm star terpolymers via a new alkyne-substituted diphenylethylene derivative. *Macromolecules* **45,** 8300–8309 (2012).
99. Huisgen, R. Kinetics and Mechanism of 1,3???Dipolar Cycloadditions. *Angew. Chemie Int. Ed. English* **2,** 633–645 (1963).
100. Altintas, O., Hizal, G. & Tunca, U. ABC-type hetero-arm star terpolymers through 'click' chemistry. *J. Polym. Sci. Part A Polym. Chem.* **44,** 5699–5707 (2006).
101. Zhang, Y., Li, C. & Liu, S. One-pot synthesis of ABC miktoarm star terpolymers by coupling ATRP, ROP, and click chemistry techniques. *J. Polym. Sci. Part A Polym. Chem.* **47,** 3066–3077 (2009).
102. He, T., Li, D., Sheng, X. & Zhao, B. Synthesis of ABC 3-miktoarm star terpolymers from a trifunctional initiator by combining ring-opening polymerization, atom transfer radical polymerization, and nitroxide-mediated radical polymerization. *Macromolecules* **37,** 3128–3135 (2004).
103. Guo, Y. M., Xu, J. & Pan, C. Y. Block and Star Block Copolymers by Mechanism

Transformation. IV. Synthesis of S-(PSt)2(PDOP)2 Miktoarm Star Copolymers by Combination of ATRP and CROP. *J. Polym. Sci. Part A Polym. Chem.* **39,** 437–445 (2001).

104. Li, Y. G., Wang, Y. M. & Pan, C. Y. Block and star block copolymers by mechanism transformation 9: Preparation and characterization of poly(methyl methacrylate)/poly(1,3-dioxepane)/polystyrene ABC miktoarm star copolymers by combination of reversible addition-fragmentation chain-transfer po. *J. Polym. Sci. Part A Polym. Chem.* **41,** 1243–1250 (2003).
105. Shi, P. J., Li, Y. G. & Pan, C. Y. Block and star block copolymers by mechanism transformation X. Synthesis of poly(ethylene oxide) methyl ether/polystyrene/poly(L-lactide) ABC miktoarm star copolymers by combination of RAFT and ROP. *Eur. Polym. J.* **40,** 1283–1290 (2004).

CHAPTER 2: SYNTHESIS AND CHARACTERIZATIONS OF LINEAR AND STAR MIKTOARM ABC TERPOLYMERS CONSISTING OF PS, PI, AND P2VP

I. Introduction

As it was discussed in the bibliographic part, a key parameter to produce "three-colored" patterns is to design ABC triblock terpolymers with highly incompatible blocks in order to promote their microphase-separation. Herein, we chose to work with PS, P2VP and PI where the χ-parameters between the different pairs are high: the χ_{SI}[1] and the χ_{SP}[2] were determined experimentally to be 0.1 while χ_{PI}[3] was determined theoretically to be 0.8. Such an incompatibility between the different blocks should allow their phase separation even for low degrees of polymerization. Our aim was to find an easy methodology to synthesize a library of linear and star miktoarm ABC terpolymers where the molecular weights of the PS and P2VP blocks were kept constant while the PI block size was varied in order to achieve different morphologies. To easily tune the PI molecular weight, we chose to work with a coupling method. The PS-*b*-P2VP synthesis involved a functionalized diphenylethylene (DPE)[4–8] as a core molecule for star miktoarm ABC terpolymers and an end-functionalized AB-type BCP for linear ABC terpolymers.[9–11] Different PI blocks were prepared with an end-function to allow their coupling with the mid- and end-functionalized PS-*b*-P2VP BCPs.

The mid- and end-functionalized PS-*b*-P2VP BCPs as well as the PI homopolymers having different molecular weights were prepared *via* an anionic polymerization.[8,12–19] Because of the living character of the anionic polymerization, the monomers and the solvents had to be highly purified, and vacuum techniques were also required. The order of monomers addition must be taken into account in the synthesis. It has been shown that monomers with the highest pKa must be added first.[18,20] Indeed, less-reactive chain-end anions derive from the more reactive monomer. Less stable monomers have higher pKa. Consequently, styrene had to be introduced first during the synthesis of the mid- and end-functionalized PS-*b*-P2VP BCPs followed by 2VP.

Once end-functionalized PI homopolymers were prepared, the next step consisted in their coupling with the mid- and end-functionalized PS-*b*-P2VP BCPs. For this purpose, we chose to work with a Steglich esterification[21,22] as a coupling method.

In this chapter, we will first describe the synthesis of the end-functionalized PI block, then we will present the synthesis of mid- and end-functionalized PS-*b*-P2VP BCPs. The last part of this chapter will be dedicated to the Steglich esterification.

II. End-functionalized polyisoprene homopolymer

The end-functionalized homopolyisoprene (hPI) chains were synthesized by anionic polymerization without any protection/deprotection step. For that purpose, a carboxylation was performed at the end of the synthesis of the living polyisoprene.[23,24] The general route for the synthesis of the end-functionalized hPI is presented in Figure 1.

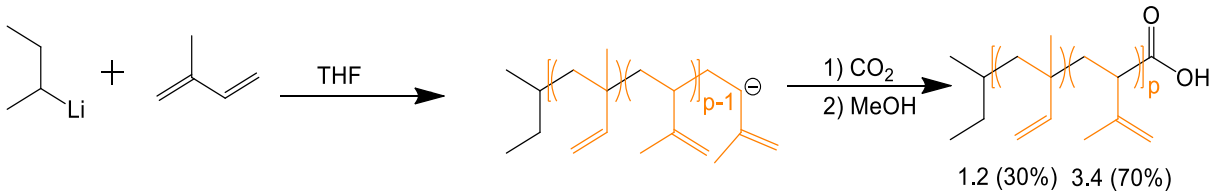

Figure 1: Synthesis route of carboxyl end-functionalized PI homopolymers by anionic polymerization in THF using sec-BuLi as an initiator.

PI homopolymers with different molecular weights (9, 13, 16, and 28 kg.mol^{-1}) were prepared using the same synthesis route. In the next part, the synthesis of the hPI having a molecular weight of 9 kg.mol^{-1} will be first described in detail. Results for the other PI homopolymers will be then presented.

1. Synthesis of a carboxyl-end-functionalized polyisoprene homopolymer model

The anionic polymerization of the PI homopolymer are conducted in THF at -30°C using *sec*-BuLi as initiator. For that purpose, THF (40mL) was introduced in a flame dried round 250 mL flask equipped with a magnetic stirrer.[25] The solution was cooled down to -30°C. *Sec*-butyllithium (0.45 mL, 0.0007 mol) was charged followed by the addition of isoprene (10 mL, 0.1 mol).[16,17] The slightly yellow reaction mixture was stirred for 3 hours. After complete conversion, the living polyisoprene was end-capped with carbon dioxide. The solution became colorless immediately. To ensure a complete end-capping of the polyisoprenyl anion, the solution was stirred at room temperature for 10 minutes. The reaction was then terminated by adding dried methanol in the flask. After concentration of the mixture, the hPI chains were precipitated in methanol and dried in an oven at 35°C. The concentration of carboxylic acid chain ends was determined by titrating a solution of 0.2 g of polymer in 20 mL of toluene with 0.01 M KOH in methanol with phenolphtalein. The resulted hPI-COOH was characterized by ^{1}H NMR (400 MHz, CD_2Cl_2).

^{1}H NMR spectrum of the carboxyl-end-functionalized hPI-COOH in CD_2Cl_2 is presented in Figure 2. The ^{1}H NMR spectrum shows the characteristic peaks of the 1.2 (δ = 5.5 – 6 ppm) and 3.4 (δ = 4.4 – 5 ppm) units of polyisoprene. According to the integration areas relative to the 1.2 and 3.4 units (5 and 1, respectively), the hPI-COOH contains 3.4 and 1.2 in-chain units in a 7/3 ratio.[16,17] This ratio is typical of the anionic polymerization of isoprene in THF. As THF is a polar solvent, the 1.4 addition is prevented and only 3.4 and 1.2 units are incorporated within the living PI chains.

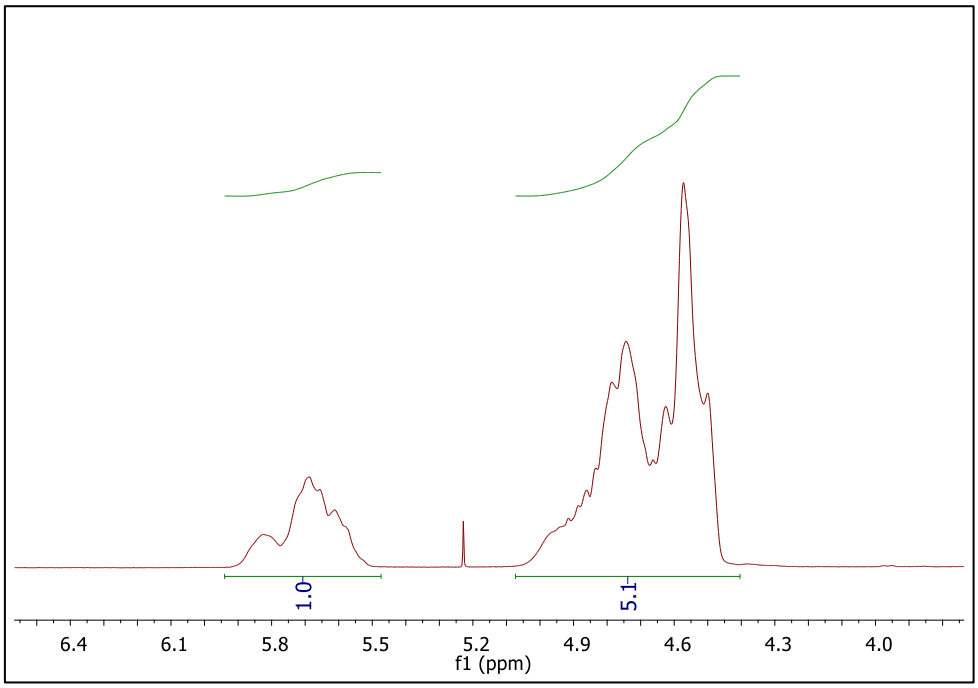

Figure 2: ^{1}H NMR spectrum (400 MHz, CD_2Cl_2) of the carboxyl-end-functionalized hPI.

The hPI-COOH was also characterized by size exclusion chromatography (SEC) with universal calibration in THF. The SEC trace is presented in Figure 3. The SEC trace of the PI homopolymer shows an intense and narrow peak. This peak is attributed to the end-functionalized polyisoprene homopolymer. The molecular weight of the hPI-COOH is determined to be 9 $kg.mol^{-1}$ (PI_9), and the dispersity about 1.06.

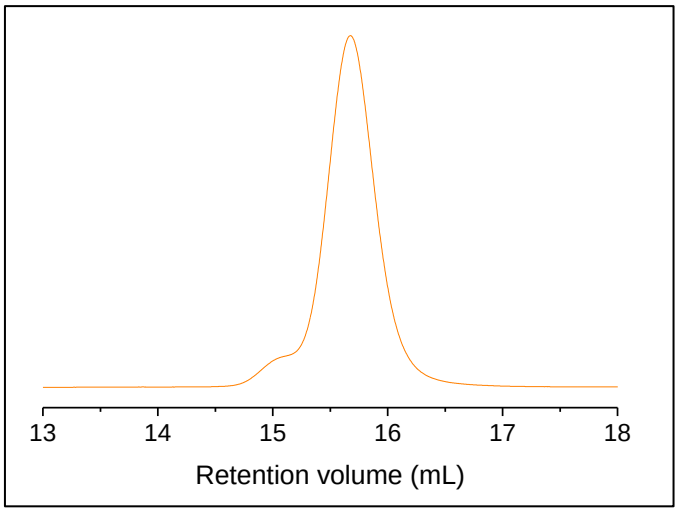

Figure 3: SEC trace of the hPI-COOH ($M_{n,PI}$ = 9 kg.mol^{-1}) in THF.

A small shoulder appears in the SEC trace of the hPI-COOH. This shoulder is attributed to the coupling between two living PI chains. At the end of the polymerization, the functionalization of the living PI chains was done by bubbling CO_2 in the media. Even after purging the tube between the gas bottle and the syringe, some traces of humidity or oxygen could still be present. The coupling between the living PI chains is probably due to those impurities. It is important to note that the coupled chains of PI are not carboxyl-end-functionalized. Coupled PI chains are terminated on both side by the butyl group of the initiator and therefore will not be involve in the Steglich esterification reaction.

The concentration of carboxylic acid chain ends was determined by titrating a solution of 0.2 g of polymer in 20 mL of toluene with 0.01 M KOH in methanol with phenolphtalein. The colorimetric titration of the PI chains confirms the presence of a carboxyl function. The colorimetric titration is not precise, but a functionalization yield higher than 90% was achieved.

2. Synthesis of carboxyl-end-functionalized polyisoprene homopolymers with different molecular weights

Three other carboxyl-end-functionalized polyisoprene chains were synthesized using the procedure described in the previous part. We only varied the molecular weight of the different PI homopolymers. For that purpose, the volume of *sec*-BuLi used to initialize the anionic polymerization was modified whereas the volume of isoprene introduced in the reactor was kept constant. PI homopolymers having different molecular weight were characterized by ^{1}H NMR (400 MHz, CD_2Cl_2), SEC chromatography and titration as previously. ^{1}H NMR

spectra of the three PI homopolymers are presented in the Figure 4. ^{1}H NMR spectra shows characteristic peaks of the 1.2 (δ = 5.5 – 6 ppm) and 3.4 (δ = 4.4 – 5 ppm) units of polyisoprene as for the hPI-COOH having a molecular weight of 9 kg.mol^{-1}. The three hPI-COOH also contain 3.4 and 1.2 in-chain units in a 7/3 ratio.

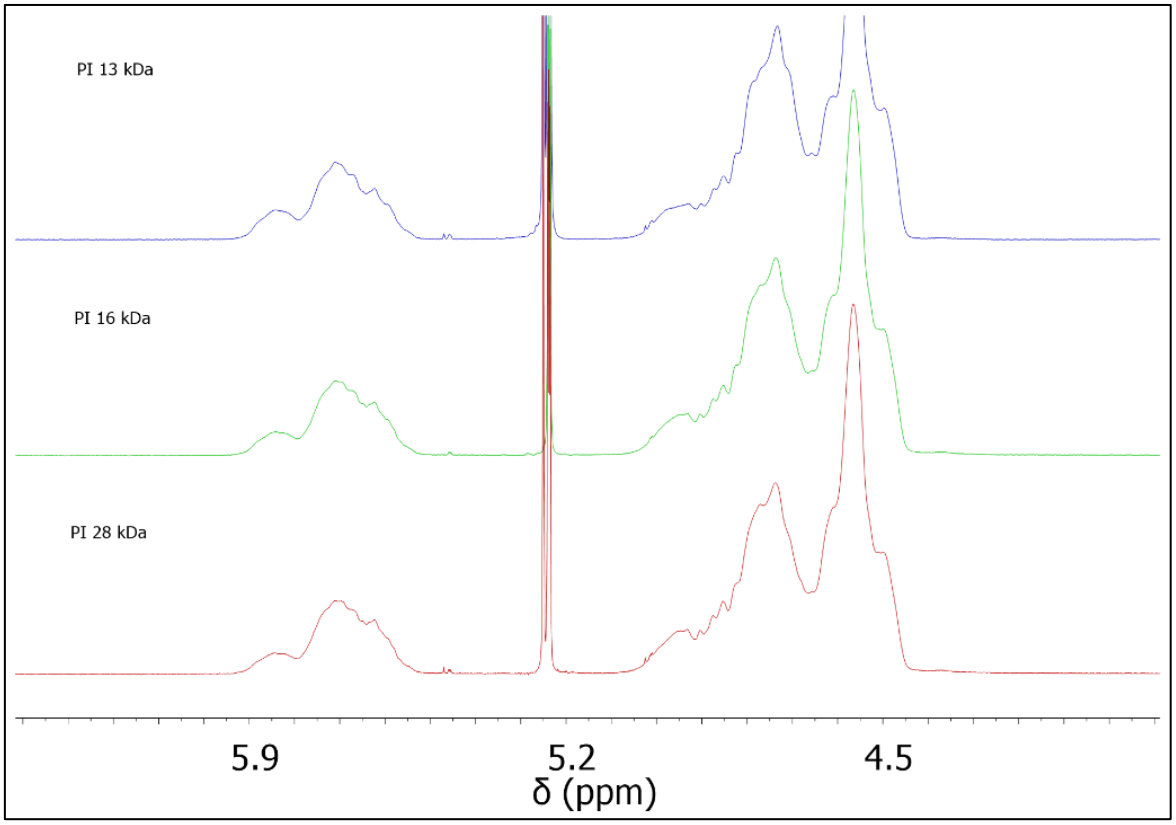

Figure 4: ^{1}H NMR (400 MHz) in CD_2Cl_2 of three carboxyl-end-functionalized hPI chains synthesized by anionic polymerization in THF.

The molecular weights of the other PI homopolymers were determined by SEC with universal calibration in THF. The SEC traces are presented in the Figure 5. The hPI-COOH molecular weights were determined to be 13, 16 and 28 kg.mol^{-1}. The dispersity of the PI homopolymers are below 1.1. For all the PI homopolymers, the SEC traces indicates that a small amount of coupled chains are formed due to some impurities.

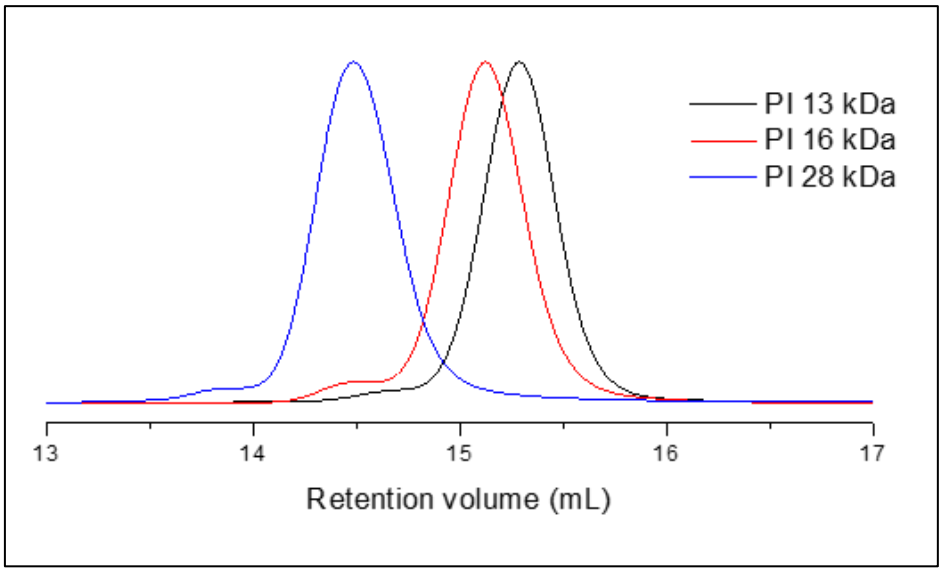

Figure 5: SEC traces of anionically synthetized PI homopolymers having different molecular weights (13, 16 and 28 kg.mol^{-1}).

3. Conclusion

In this part, the anionic polymerization of several PI homopolymers (9, 13, 16 and 28 kg.mol^{-1}) in THF is described. The end-functionalization of the polyisoprene, performed with carbon dioxide, revealed to be quantitative since more than 90% of hPI chains were functionalized with a carboxyl end-group as checked by titration using phenolphtalein as a colorant indicator.

This synthesis route is very convenient since the PI homopolymers have a narrow dispersity (< 1.1) and the carboxyl end-functionalization of hPI does not required any protection/deprotection step.

III. Synthesis of end- and mid- functionalized polystyrene-*block*-poly(2-vinylpyridine)

In this part, the anionic polymerization of the mid- and end-functionalized PS-*b*-P2VP chains will be described as they will be used for the synthesis of star miktoarm and linear ABC terpolymers, respectively. For this purpose, the PS-*b*-P2VP BCPs were prepared *via* a sequential anionic polymerization.[26] The end-functionalization of PS-*b*-P2VP was achieved by adding ethylene oxide on the living BCP chains at the end of the reaction.[18,27] The mid-functionalized PS-*b*-P2VP was synthesized using a core molecule inserted between the PS and P2VP blocks. The core molecule used for this synthesis is a diphenylethylene bearing a hydroxyl protected function. [6,9,28,29]

Monomers and solvents were distilled as previously described in the literature.[25,30] The 2VP monomer was cryo-distilled under vacuum over CaH_2 twice. The styrene was cryo-distilled over CaH_2 and stirred with dibutylmagnesium (1.0 M in heptane, Sigma-Aldrich). Tetrahydrofuran (THF, Sigma-Aldrich) was dried over Braun MB-SPS-800 solvent purification system, stored over sodium benzophenone ketyl under dry nitrogen and cryo-distilled prior to use.

As discussed in the bibliographic part, all the anionic polymerization must be realized in an inert atmosphere (here argon). To avoid the introduction of oxygen in the media, the reaction was carried out in the closed reactor. Monomers and solvents were put in a burette after their cryo-distillation, and the *sec*-BuLi initiator was introduced with a seal syringe through a septum surrounded of parafilm. The glassware was purified with three cycles of vacuum (flame)/argon before the beginning of the reaction, and then it was kept closed under argon pressure.

1. End-functionalized PS-*b*-P2VP synthesis

The hydroxyl-terminated PS-*b*-P2VP chains were synthesized using sequential living anionic polymerization. The general scheme of the reaction is presented in Figure 6.

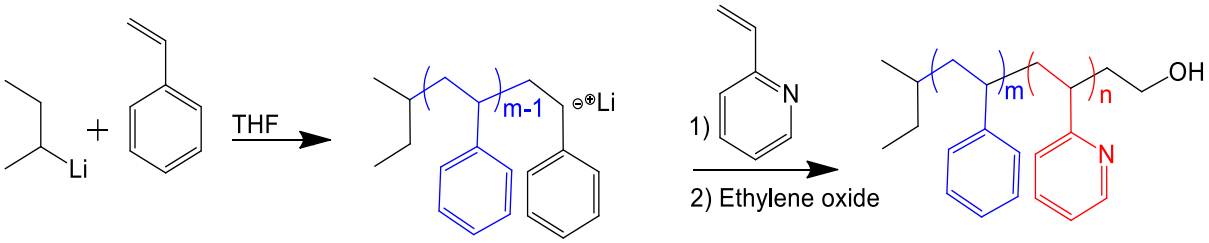

Figure 6: Synthesis route of hydroxyl end-functionalized PS-b-P2VP via anionic polymerization using sec-BuLi as an initiator in THF.

Tetrahydrofuran (THF, 40mL) was introduced in a flame dried round 250-mL-flask equipped with magnetic stirrer. The solution was then cooled down to -78°C. The synthesis was prepared at -78°C[8] to reduce the reactivity of monomers, and so to prepare PS-*b*-P2VP chains with a low dispersity. *Sec*-butyllithium (*Sec*-BuLi, 0.08mL, ~1.2M) was charged, which was followed by the addition of styrene (S, 2mL). The orange reaction was stirred for 1 hour. An aliquot of PS was taken before the addition of the second monomer and was analyzed by SEC with a universal calibration to check the PS molecular weight and its dispersity. The 2-vinylpyridine monomer (1.7mL) was then added in the reactive mild. After 20 minutes, ethylene oxide was added in the solution. The colorless mixture was kept under stirring. After 10 minutes, the reaction was terminated by the addition of degassed methanol. The mixture was concentrated, precipitated in cyclohexane and dried in an oven at 35°C for 12 hours. The PS-*b*-P2VP-OH was characterized by ^{1}H NMR (δ (ppm), 400MHz, CD_2Cl_2), 2D DOSY NMR (δ (ppm), 400MHz, THF), and SEC with a universal calibration in THF.

The aliquot of the polystyrene homopolymer (hPS) was characterized by SEC in THF and ^{1}H NMR (400 MHz, CD_2Cl_2) (see Fig. 8). The SEC trace shows an intense narrow peak with a small shoulder (see Fig. 8a). The peak having the largest intensity has a dispersity of 1.02. This peak attributed to the hPS corresponds to a molecular weight of 21 kg.mol^{-1}. We can note the presence of a small shoulder in higher molecular weight region (lower retention volume). This shoulder corresponds to the coupling between the two living hPS chains. The coupling occurs because the methanol used to quench the reaction was not degassed properly. The NMR spectrum of PS chains (1.3-2.3 ppm (m, 3H), 6.2-7.4 ppm (m, 5H)) shows the characteristic peaks of the styrenic protons (see Fig. 8b).

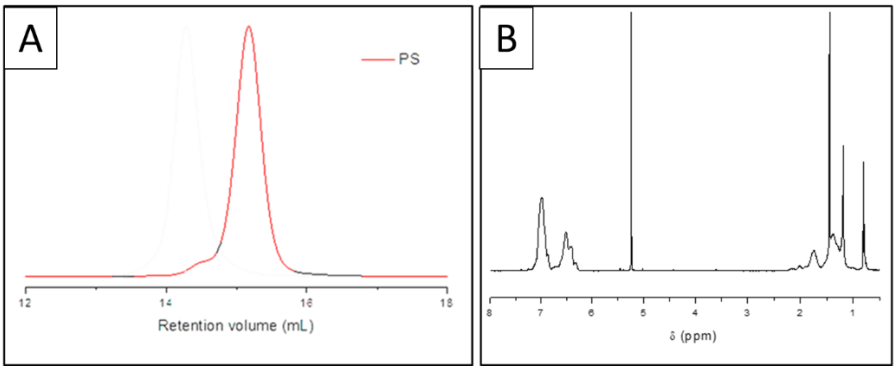

Figure 7: (a) SEC trace of the hPS aliquot in THF and (b) its corresponding ^{1}H NMR (400 MHz, CD_2Cl_2) spectrum.

Hydroxyl-terminated PS-*b*-P2VP chains were then similarly characterized (see Figure 8). After precipitation and purification of the PS-*b*-P2VP-OH chains, the NMR spectrum shows the appearance of the P2VP characteristic proton signals (1.3-2.3 ppm (m, 3H), 6.2-7.4 ppm (m, 5H), 8-8.5 ppm (m, ^{1}H)), in addition to those of PS which confirmed the formation of the PS-*b*-P2VP BCP (see Figure 8a). The proportion of different blocks within the PS-*b*-P2VP-OH chains was calculated by integration of their corresponding aromatic peaks on the NMR spectrum, and a ratio of PS:P2VP = 1:1.1 was determined.

The PS-*b*-P2VP-OH chains were also characterized by SEC with universal calibration in THF (see Figure 8b). The SEC trace shows a high intensity narrow peak attributed to the PS-*b*-P2VP-OH. The molecular weight of the Hydroxyl-terminated PS-*b*-P2VP is determined to be 45 $kg.mol^{-1}$, and its dispersity is about 1.06. The molecular weights of the hPS aliquot and PS-*b*-P2VP-OH determined by SEC are in accordance with the volume ratio calculated from the ^{1}H NMR spectrum.

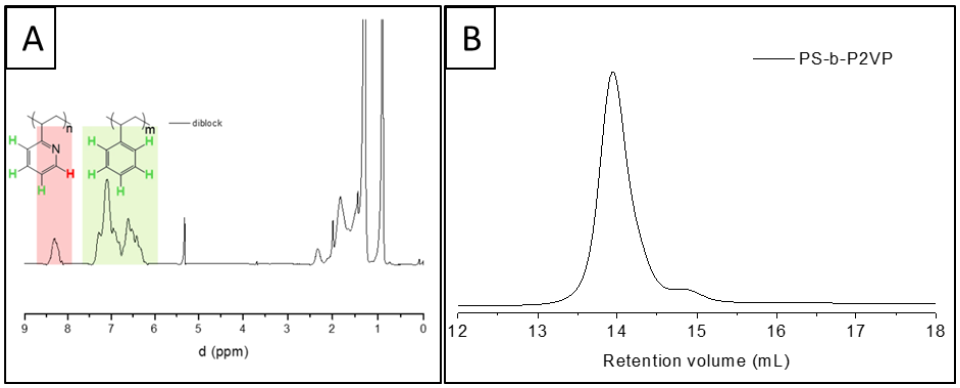

Figure 8: (a) ^{1}H NMR (400 MHz, CD_2Cl_2) spectrum of the PS-b-P2VP-OH chains and (b) their corresponding SEC trace in THF.

We can note the presence of a small shoulder on the SEC trace in low molecular weight region. This shoulder is observable on the SEC trace even after purification. This shoulder corresponds to some hPS that does not initiate the polymerization of 2VP. This hPS probably appears because some impurities are introduced in the reaction media by the syringe during the aliquot extraction. The hPS peak has a small intensity compared with the one of the peak assigned to the PS-*b*-P2VP-OH BCP and could be considered as negligible.

The ^{1}H NMR and SEC characterizations confirmed the synthesis of well-defined PS-*b*-P2VP-OH chains. A 2D DOSY NMR (400 MHz, THF) was also performed to bring another proof of the PS-*b*-P2VP BCP formation. The 2D DOSY NMR spectrum is showed in Figure 9. The proton signals assigned to the PS and P2VP blocks are aligned along the same line, which confirms this two blocks are linked together. The 2D DOSY NMR spectrum exhibits a single diffusion coefficient of about 1.7 x 10^{-10} $m^2.s^{-1}$. The others spots detected were assigned to solvents.

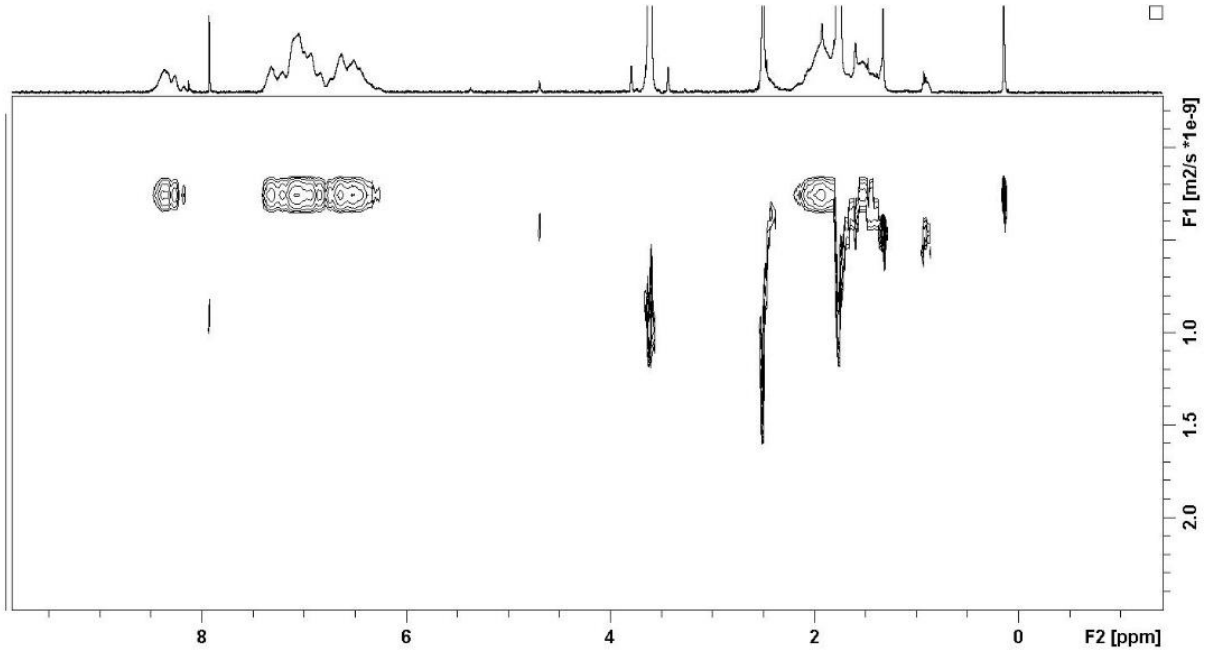

Figure 9: ^{1}H 2D DOSY NMR (400 MHz, THF) of the end-hydroxyl-functionalized PS-b-P2VP.

Unfortunately, we did not succeed in confirming the functionalization of the BCP either by ^{1}H NMR or even by FTIR because of the high molecular weight of the PS-*b*-P2VP-OH chains. However, as the quantitative functionalization of living P2VP with ethylene oxide was reported in the literature,[18] we considered that the PS-*b*-P2VP was totally functionalized, and this will be confirmed later by coupling these BCP chains with different PI homopolymers *via* an esterification reaction.

Herein, an end-functionalized PS-*b*-P2VP BCP was synthetized. It exhibited a low dispersity (1.06) and a quasi-symmetrical volume ratio (PS:P2VP = 1:1.1). This hydroxyl end-functionalized PS-*b*-P2VP will be used to prepare a linear ABC terpolymer series in order to explore the ternary phase diagram.

2. Mid-functionalized PS-*b*-P2VP synthesis

In the literature, three main methods are commonly employed for the synthesis of star miktoarm ABC terpolymers. The first one reported by Hadjichistidis *et al*. involves a chlorosilane compound as a core molecule,[31] and all arms prepared *via* an anionic polymerization are subsequently linked to this chlorosilane compound. This method requires specific glassware with a break-seal technology[25] which is too complicated to set-up in our laboratory. The second method consists in the use of a core molecule designed as a multifunctional initiator site with orthogonal reactive functions.[32,33] This method is easier than the previous one but it is limited since the different monomers must be selective. The last method involves a modified diphenylethylene as a core molecule which consists of initiating and terminating sites.[4,5,9,34,35] We choose to work with the last method by using a diphenylethylene bearing a tert-butyldimethylsilyl-protected hydroxyl functionality as a core molecule. The alkene function of the diphenylethylene allows to perform a sequential anionic polymerization to obtain a mid-functional AB-type BCP. The protected hydroxyl function will be use to attach the third arm after the deprotection step.[36] In this part, we will describe the synthesis of the core molecule and the preparation of the mid-functionalized PS-*b*-P2VP BCP.

a. Synthesis of the core molecule (DPE-Si)

The first step of the mid functionalized PS-*b*-P2VP synthesis requires the synthesis of the core molecule: 1-(4-(2-tert-Butyldimethylsiloxy)ethyl)phenyl-1-phenylethylene (DPE-Si) (see Figure 10).

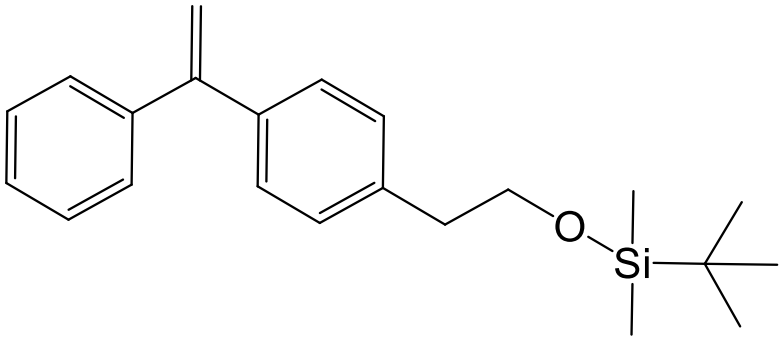

Figure 10: 1-(4-(2-tert-Butyldimethylsiloxy)ethyl)phenyl-1-phenylethylene (DPE-Si) core molecule used in this work.

All reactions were carried out with flame-dried glassware using standard Schlenk techniques under an inert atmosphere of dry argon. Heptane and ethyl acetate, with a reagent grade for chromatography, were procured from Aldrich and used as obtained. 1-(4-(2-*tert*-Butyldimethylsiloxy)ethyl)phenyl-1-phenylethylene was synthesized in a three-step manner according to a procedure described in the literature.[29] 1-(4-bromophenyl)-1-phenylethylene was synthesized by Wittig reaction. In the first step, methyltriphenylphosphonium bromide (20.8 g, 0.0582mol) was dissolved in dried THF (116 mL). To the suspension of methyltriphenylphosphonium bromide, *n*-butyllithium (1.6 M in hexane) was added dropwise at 0^{o}C under inert condition. The mixture was then allowed to stir for another two hours while it slowly warmed up to room temperature. 4-Bromobenzophenone (15 g, 0.0576 mol) in dried THF (29 mL) was then added dropwise to the solution with vigorous stirring at room temperature. The mixture was allowed to stir overnight under inert condition. The solution was filtered and washed by THF. If no powder was obtained, the solution was evaporated and diluted with water and then extracted three times with heptane. The organic phase was collected and washed with brine and then dried over Na_2SO_4. After filtration and removal of solvent, the residue was purified by column chromatography using heptane, giving 1-(4-bromophenyl)-1-phenylethylene as colorless liquid. Figure 11 presents the ^{1}H NMR spectrum (δ (ppm), 400MHz, $CDCl_3$): 7.50-7.23 (m, 9H, Ar-*H*), 5.50 (d, 2H, C=CH_2).

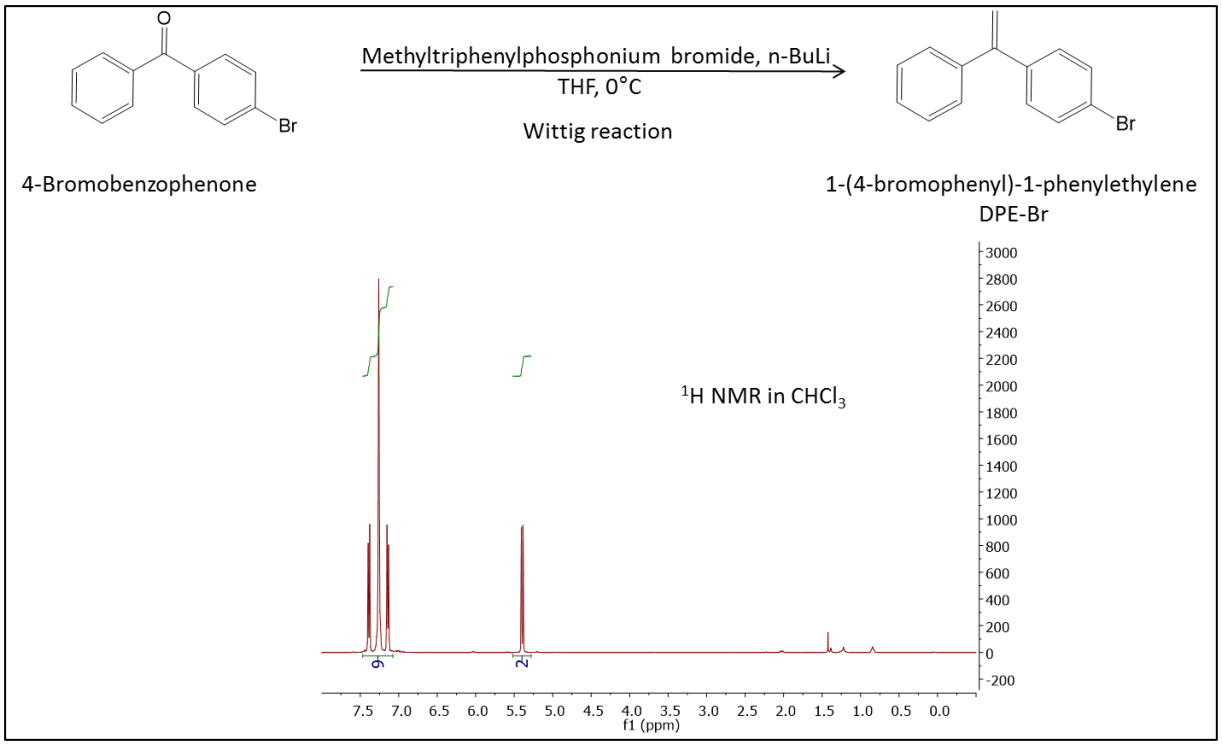

Figure 11: Reaction schema and ^1H NMR (400 MHz, $CDCl_3$) spectrum of the 1-(4-bromophenyl)-1-phenylethylene.

In the second step, 1-(4-bromophenyl)-1-phenylethylene was converted to 1-(4-(2-hydroxyethyl)phenyl-1-phenylethylene). 1-(4-bromophenyl)-1-phenylethylene (7.6g, 0.03 mol) was dissolved in dried THF (30 mL) and added dropwise to magnesium turning (0.86 g) at 60^{o}C and then refluxed for 2hrs to give a Grignard reagent. Ethylene oxide (2.93 mL, 0.058 mol) dissolved in dried THF (3 mL) was added dropwise to the Grignard reagent at 0^{o}C and then stirred at room temperature for 3 hours. After hydrolysis, the solution was extracted three times with ethyl acetate and washed by water and then dried over $MgSO_4$. After filtration and removal of solvent, the residue was purified by column chromatography using heptane : ethyl acetate = 2 : 1, giving 1-(4-(2-hydroxyethyl)phenyl-1-phenylethylene) as colorless liquid. ^1H NMR (δ (ppm), 400MHz, $CDCl_3$): 7.50-7.23 (m, 9H, Ar-*H*), 5.50 (d, 2H, C=CH_2), 3.93 (t, 2H, CH_2OH), 2.93 (t, 2H, CH_2CH_2OH) (see Figure 12).

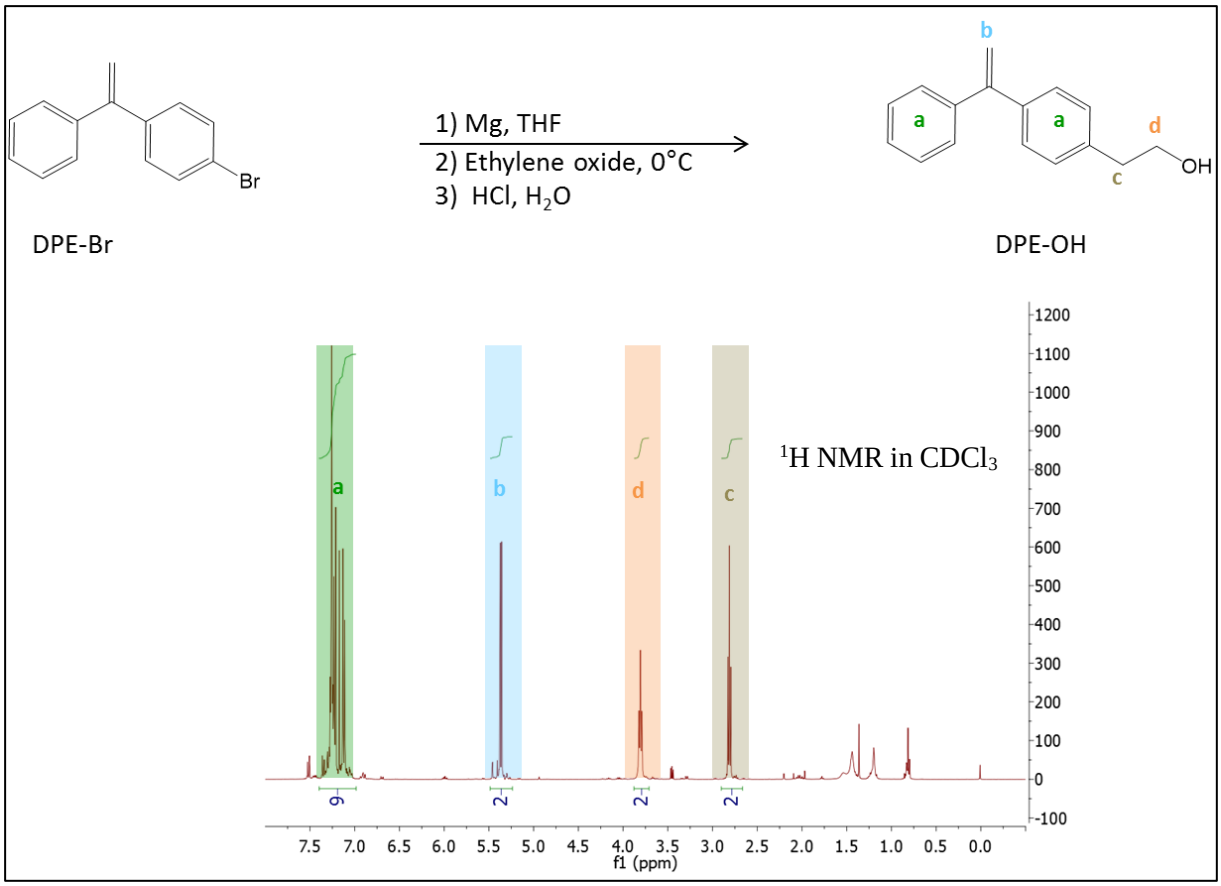

Figure 12: Reaction schema and ^{1}H NMR (400 MHz, $CDCl_3$) spectrum of the 1-(4-(2-hydroxyethyl)phenyl-1-phenylethylene).

In the final step, 1-(4-(2-hydroxyethyl)phenyl-1-phenylethylene) was further converted to 1-(4-(2-*tert*-Butyldimethylsiloxy)ethyl)phenyl-1-phenylethylene. 1-(4-(2-hydroxyethyl)phenyl-1-phenylethylene) (4.2 g, 0.018 mol) was dissolved in DMF (37.4 mL) and *tert*-butyldimethylsilyl chloride (3.39 g, 0.022 mol) and imidazole (3.83 g, 0.056 mol) were added and then stirred at 45 °C for 4 hours. The crude mixture was washed with an aqueous solution of sodium bicarbonate and extracted with heptane. Then 1-(4-(2-*tert*-Butyldimethylsiloxy)ethyl)phenyl-1-phenylethylene was purified by column chromatography using heptane : ethyl acetate = 9 : 1. The chemical structure and the purity was confirmed by 1H NMR spectroscopy. ^{1}H NMR (δ (ppm), 400MHz, $CDCl_3$): 7.42-7.23 (m, 9H, Ar-*H*), 5.50 (d, 2H, C=CH_2), 3.90 (t, 2H, CH_2O), 2.91 (t, 2H, CH_2CH_2O), 0.91 (s, 9H, (CH_3)$_3$CSi), 0.03 (s, 6H, (CH_3)$_2$Si) (Figure 13).

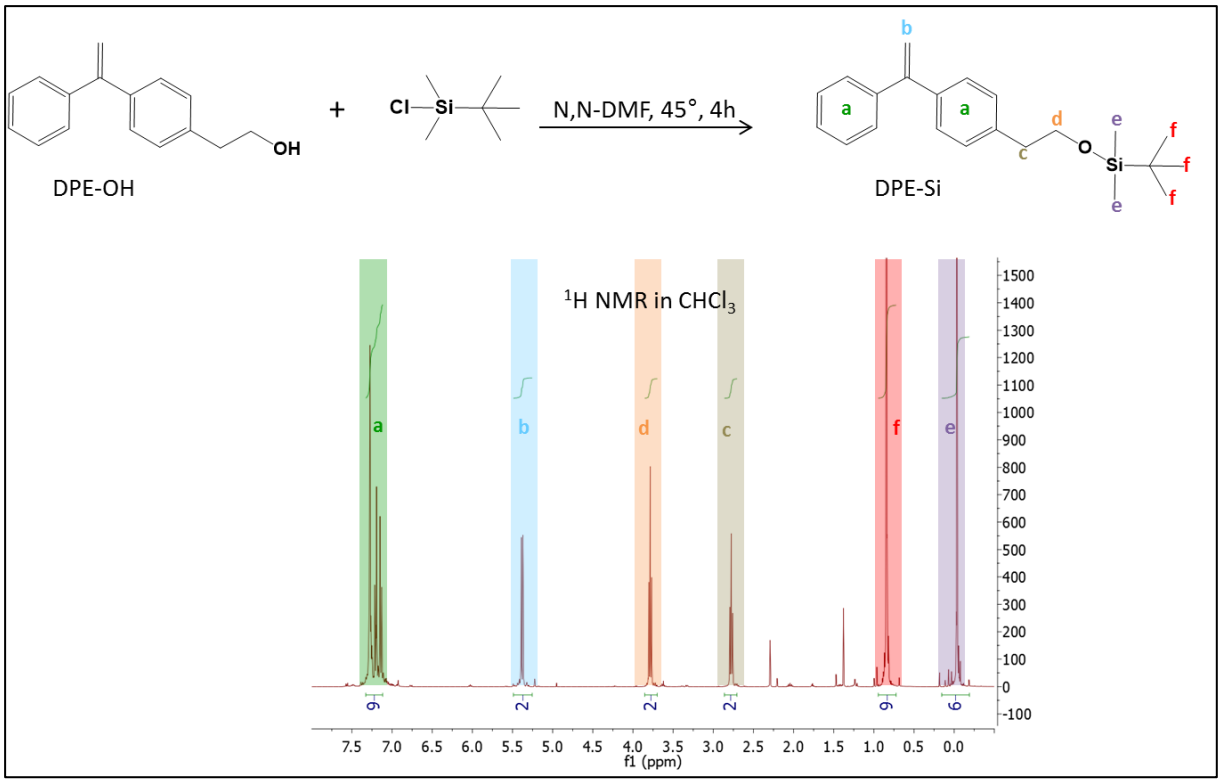

Figure 13: Schema of the reaction and ^{1}H NMR (400 MHz, $CDCl_3$) spectrum of the 1-(4-(2-tert-Butyldimethylsiloxy)ethyl)phenyl-1-phenylethylene.

b. Synthesis of the mid-functionalized PS-*b*-P2VP

Figure 14 shows the general scheme for the mid-functionalized PS-*b*-P2VP synthesis. The PS-*b*-P2VP chains were synthesized using a sequential living anionic polymerization. Tetrahydrofuran (THF, 40mL) was introduced in a 250 mL flame dried round flask equipped with magnetic stirrer.

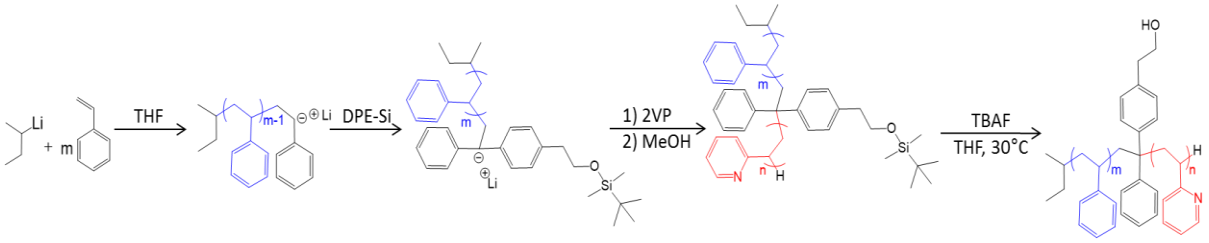

Figure 14: Synthesis route of hydroxyl mid-functionalized PS-b-P2VP via an anionic polymerization using sec-BuLi as an initiator and a modified DPE as a core molecule.

The solution was then cooled down to -78°C. *Sec*-butyllithium (Sec-BuLi, 0.085mL, ~1.2M) was charged, which was followed by the addition of styrene (S, 2mL). The orange reaction mixture was stirred for 1 hour. An aliquot of the anionic PS block was taken before addition of the core molecule 1-(4-(2-*tert*-Butyldimethylsiloxy)ethyl)phenyl-1-phenylethylene

(DPE-Si) and was analyzed by SEC to determine the molecular weight and the dispersity of the PS block. The living polystyryllithium anion was end-capped with 1-(4-(2-*tert*-Butyldimethylsiloxy)ethyl)phenyl-1-phenylethylene (0.04g, 1.2 equiv.). The addition of the DPE derivative led to an immediate change of the mixture color. The color of the solution changed from yellow to dark red. 2-vinylpyridine monomer (1.7mL) was then added. The brown reaction mixture was kept under stirring for 20 minutes. Finally, the reaction was terminated by the addition of degassed methanol, and the solution became colorless. The mixture was then concentrated, precipitated in cyclohexane and dried in oven at 35°C. The protected hydroxyl function beared by the DPE was hydrolyzed with tetrabutylammonium fluoride (TBAF, 3 eq) to generate a mid-functionalized diblock copolymers. After precipitation in cyclohexane, the mid-functionalized PS-*b*-P2VP was characterized by ^{1}H NMR (δ (ppm), 400MHz, CD_2Cl_2) and universal size exclusion chromatography in THF (see Fig. 16).

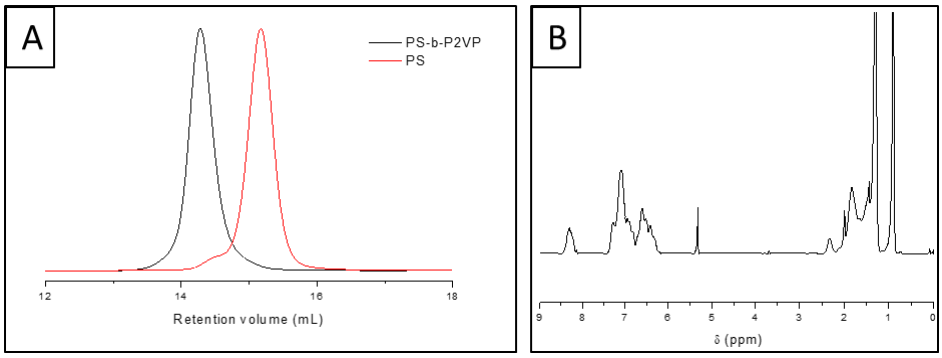

Figure 15: (a) SEC traces in THF of the hPS aliquot (red curve) and PS-b-P2VP (black curve) and (b) ^{1}H NMR spectrum (400 MHz, CD_2Cl_2) of the mid-functionalized PS-b-P2VP BCP.

The hPS aliquot and the PS-*b*-P2VP BCP were characterized by SEC with universal calibration in THF (see Fig. 16a). The SEC trace of the hPS exhibits a high intensity narrow peak. This peak corresponds to a PS molecular weight of 19 kg.mol^{-1} while the dispersity is determined to be 1.03. A small shoulder appears for a molecular weight that is the double of the one attributed to hPS. The living PS was quenched in a non-dry and undegassed methanol, which explains the coupling between two hPS chains. However, this coupling does not appear in the reactive media, and therefore will not interfere in with the reaction.

After the addition of the core molecule (DPE-Si) and the polymerization of the 2VP to the living PS, the SEC trace of the PS-*b*-P2VP exhibited one monomodal and narrow peak. The mid-functionalized PS-*b*-P2VP has a dispersity of 1.05, and the molecular weight was determined to be 43 kg.mol^{-1}. The P2VP/PS volume ratio determined to be 1.2 from SEC traces was also confirmed by ^{1}H NMR (see Fig. 16b).

A 2D DOSY NMR (400 MHz, THF) was also performed to verify the purity of the mid-functionalized PS-*b*-P2VP. The 2D DOSY NMR spectrum is shown in Figure 16. The proton signals assigned to PS and P2VP are aligned along the same line, which confirms that the two blocks are linked together. The 2D DOSY NMR spectrum exhibited a single diffusion coefficient of about 1.7 x 10^{-10} $m^2.s^{-1}$ while the other spots are assigned to solvents.

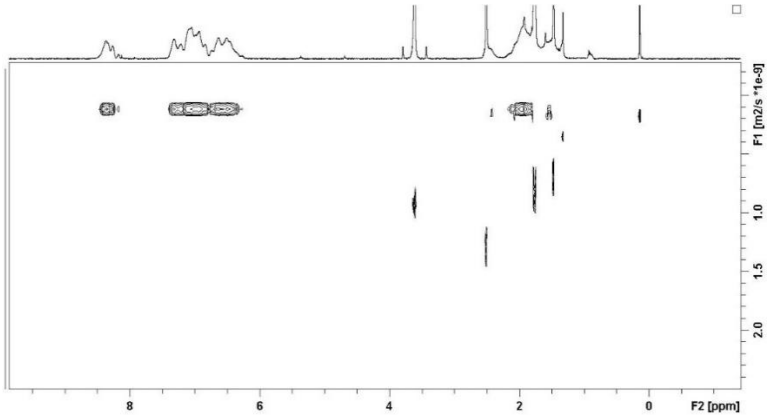

Figure 16: ^{1}H 2D DOSY NMR (400 MHz, THF) spectrum of the hydroxyl-mid-functionalized PS-b-P2VP BCP.

The deprotection of the PS-*b*-P2VP BCP was characterized by ^{1}H NMR (400 MHz, CD_2Cl_2). The NMR spectra was recorded before and after the deprotection of the hydroxyl function as shown in Figure 17. The disappearance of the proton signal characteristic of the methyl of the protecting silyl group at 0 ppm confirms the quantitative deprotection of the hydroxyl function.

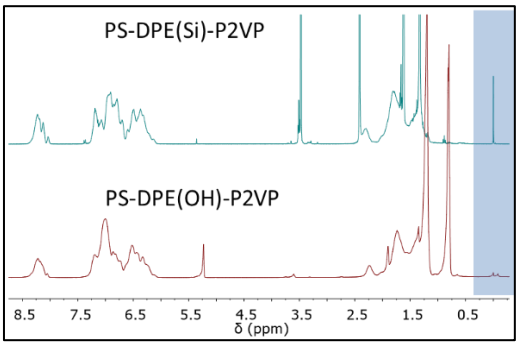

Figure 17: ^{1}H NMR spectra (400 MHz, CD_2Cl_2) of the mid-functionalized PS-b-P2VP before (green spectrum) and after (red spectrum) the deprotection step.

IV. Coupling reaction between end- and mid-functionalized PS-*b*-P2VP and end-functionalized hPI chains

1. Introduction

In the previous part, well-defined hydroxyl-mid/end-functionalized PS-*b*-P2VP BCPs as well as four well-defined carboxyl-end-functionalized PI homopolymers were synthesized. Here, the coupling between the mid/end-functionalized AB-type BCPs and the end-functionalized PI homopolymers will be discussed.

In most of cases, the coupling reaction involves the presence of a metal catalyst.[37,38] Here, it is better to avoid metal catalysts since the metallic salt could be chelated by the P2VP. For this purpose, the coupling between the different PS-*b*-P2VP BCPs and the PI homopolymers was realized *via* a Steglich esterification to produce linear and star miktoarm ABC terpolymers.[21,22] This synthesis route was chosen because it is a metal free coupling reaction but also because an efficient coupling can be achieved.

A general scheme of the Steglich esterification mechanism is proposed in Figure 18.[22] The coupling reaction was catalyzed by 4-(Dimethylamino)pyridinium-4-toluene (DPTS) and *N,N'*-diisopropylcarbodiimide (DIC). Since DPTS is not soluble in THF, the reaction was performed in dichloromethane. DIC and the carboxylic acid beared by the diblock copolymers are able to form an O-acylisourea intermediate, which offers reactivity similar to the corresponding carboxylic acid anhydride. DPTS is a stronger nucleophile than the alcohol, and reacts with O-acylisourea leading to a reactive amide ("activated ester"). This intermediate cannot form intramolecular side products but reacts rapidly with alcohols. DPTS acts as an acyl transfer reagent in this way, and subsequent reaction with the alcohol gives the ester.

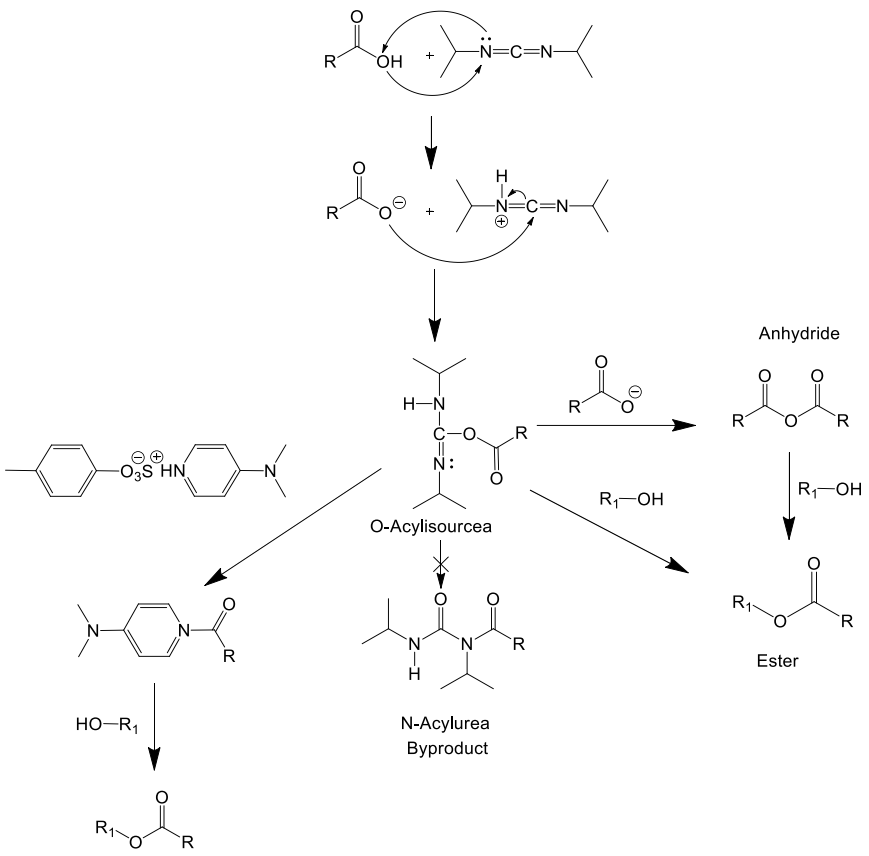

Figure 18: General scheme for the Steglich esterification mechanism.

Previously cryo-dried hydroxyl-mid/end-functionalized PS-*b*-P2VP (1 eq.) and hPI-COOH (3 eq.) were solubilized in dried dichloromethane. The *N,N*-Dimethyl-4-pyridinaminium 4-methylbenzenesulfonate (DPTS, 10 eq.) was added and stirred for 15 minutes at 40°C. Then, the *N,N'*-Diisopropylcarbodiimide (DIC, 10 eq.) was added, and the mixture was stirred at 35°C.[39] After 3 days, the solution was concentrated and the DPTS was precipitated in THF and recovered. The filtrate was then concentrated and the star miktoarm/linear ABC terpolymer chains were precipitated in heptane to remove the hPI-COOH excess.

2. Synthesis of PS-*b*-P2VP-*b*-PI linear terpolymers

a. Synthesis of a linear ABC terpolymers: PS-*b*-P2VP-*b*-PI (PI = 9 kg.mol^{-1})

Herein, we will first detail the coupling between the PS-*b*-P2VP-OH (45 kg.mol^{-1}) with the hPI-COOH (9 kg.mol^{-1}) as model synthesis before giving the results regarding the coupling of this AB-type BCP with different size PI homopolymers.

The general scheme to prepare the linear ABC terpolymer is presented in Figure 20. The esterification between the PS-*b*-P2VP-OH and the hPI-COOH was performed in dichloromethane with DIC as coupling reagent and DPTS as catalyst.

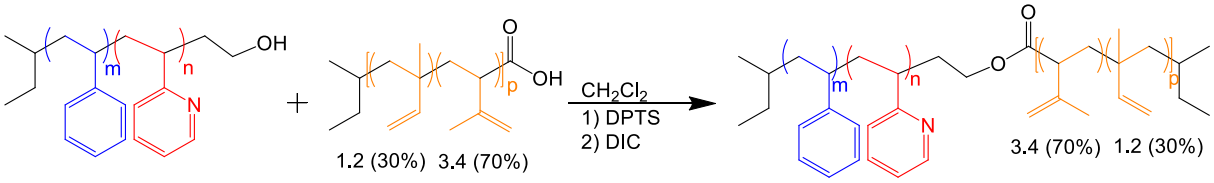

Figure 19: Steglich esterification between a hydroxyl end-functionalized PS-b-P2VP and a carboxyl end-functionalized PI in CD_2Cl_2.

Figure 20a shows the SEC traces (universal calibration in THF) of the hPI-COOH (9 kg.mol^{-1}), PS-*b*-P2VP-OH (45 kg.mol^{-1}), and PS-*b*-P2VP-*b*-PI (54 kg.mol^{-1}) chains. A complete shift of the molecular weight distributions of the terpolymer chains toward lower elution volumes compared to the PS-*b*-P2VP-OH and hPI-COOH ones was detected. Moreover, the SEC trace of the PS-*b*-P2VP-*b*-PI shows a narrow peak. The molecular weight of the PS-*b*-P2VP-*b*-PI is determined to be 54 kg.mol^{-1}, and the dispersity is about 1.06. On the SEC trace, we can note the presence of a low intensity shoulder at high retention volume. This small shoulder is overlapped by the peak of the hPS, which means that a small quantity of hPS chains is still present in the solution. The shoulder has a very low intensity and can be consider as negligible in comparison with the intense peak attributed to the PS-*b*-P2VP-*b*-PI chains. The volume ratios of PS, P2VP and PI were determined to be S:P:I = 1: 1.1:0.6. To confirm such volume ratios of the different blocks, NMR characterizations were also performed.

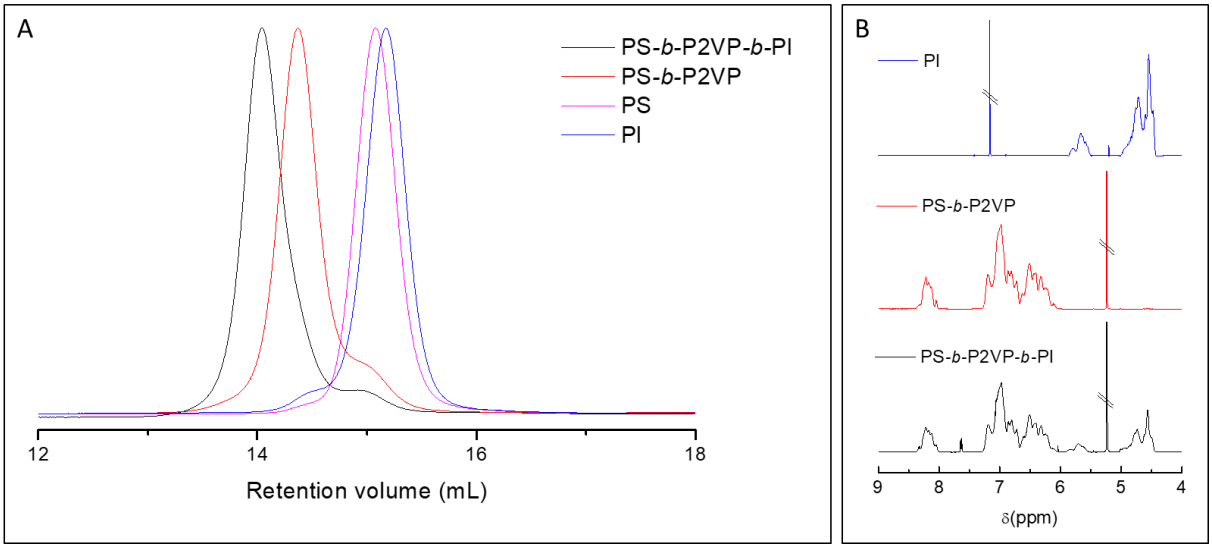

Figure 20: (a) THF-SEC traces (RI signal) of hPS, hPI-COOH, PS-b-P2VP-OH, PS-b-P2VP-b-PI. (b) ^{1}H NMR (400 MHz) spectra of hPI-COOH in $CDCl_3$, PS-b-P2VP-OH in CD_2Cl_2, and PS-b-P2VP-b-PI in CD_2Cl_2.

^{1}H NMR spectra of hPI-COOH, PS-*b*-P2VP-OH, and PS-*b*-P2VP-*b*-PI are presented in Figure 20b. After the esterification between the PI homopolymer and the PS-*b*-P2VP AB-type BCP, the characteristic peaks of the PI block (δ = 5.5 – 6 ppm and δ = 4.4 – 5 ppm), the aromatic protons of PS (δ = 6 - 7.5 ppm) and P2VP (δ = 6 -7.5 ppm and δ =8 - 8.5 ppm) were detected. The peaks were integrated, and the volume ratios between blocks were determined by NMR. The block volume ratios obtained by SEC and calculated ^{1}H NMR were similar, which confirmed the coupling between blocks.

A further evidence of the coupling between the hPI-COOH and PS-*b*-P2VP-OH chains was obtained by Diffusion Ordered Spectroscopy (2D-DOSY-NMR). From the 2D-DOSY spectrum presented in Figure 21, the diffusion coefficients of the PS-*b*-P2VP-OH BCP (D = 1.7 x 10^{-10} $m^2.s^{-1}$) and the PI homopolymer (D = 7.42 x 10^{-11} $m^2.s^{-1}$) are clearly different. Indeed, after the coupling reaction, the 2D-DOSY-NMR spectrum revealed that the proton resonances belonging to PS, P2VP and PI were aligned on the same horizontal line for the linear ABC terpolymer. This implies that all these signals are due to the same macromolecule which has a higher diffusion coefficient (D = 4.48 x 10^{-10} $m^2.s^{-1}$) than that of the hPI-COOH and PS-*b*-P2VP-OH chains. Signals which are not aligned with the horizontal line are due to solvents.

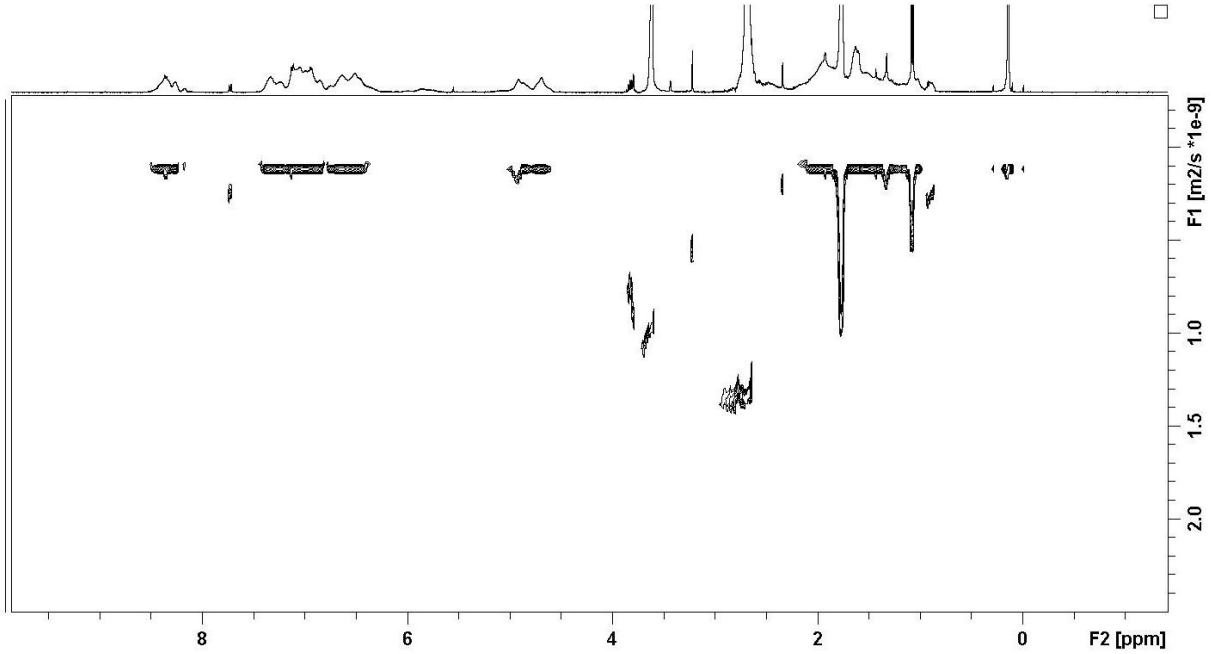

Figure 21: ^{1}H 2D DOSY NMR (400 MHz, THF) spectrum of the PS-b-P2VP-b-PI after purification.

b. Synthesis of other linear PS-*b*-P2VP-*b*-PI terpolymers

After we had proved the feasibility of the coupling method, the same route was used to couple the other hPI-COOH chains (13 and 16 kg.mol^{-1}) to the same PS-*b*-P2VP-OH BCP (45 kg.mol^{-1}). The reactions were conducted using the same conditions, and the linear ABC terpolymers were characterized by SEC.

Figure 23 shows the SEC traces of the four linear ABC terpolymers after the Steglich esterification step. As previously observed, the SEC traces of the different PS-*b*-P2VP-*b*-PI terpolymers shift towards lower retention volumes as that of the PS-*b*-P2VP-OH and hPI-COOH chains. All the PS-*b*-P2VP-*b*-PI terpolymers exhibit mainly one peak (with a small shoulder) confirming the efficiency of the coupling reaction while the dispersity of the different linear ABC terpolymers is found to be below 1.1.

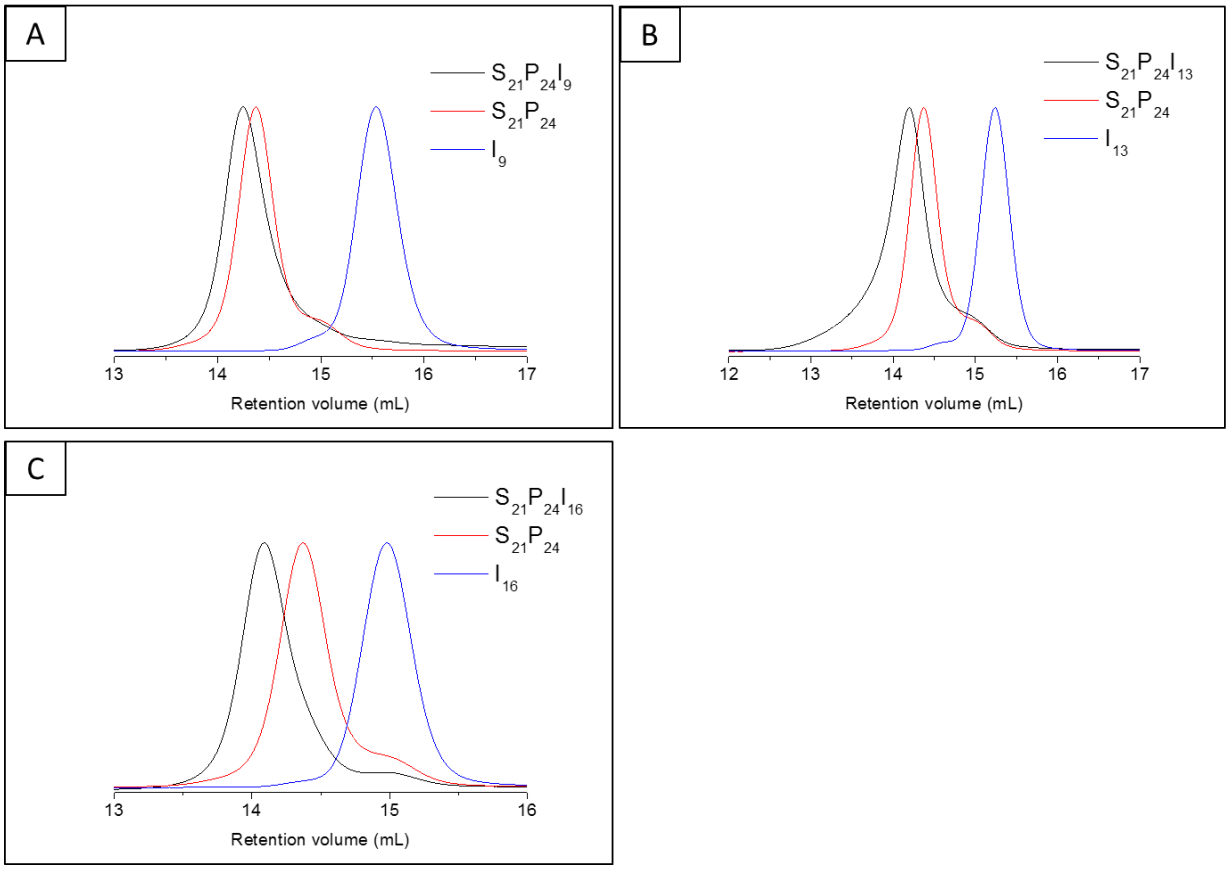

Figure 22: SEC traces in THF of (a) $S_{21}P_{24}I_9$ (black curve), $S_{21}P_{24}$ (red curve) and I_9 (blue curve); (b) $S_{21}P_{24}I_{13}$ (black curve), $S_{21}P_{24}$ (red curve) and I_{13} (blue curve); (c) $S_{21}P_{24}I_{16}$ (black curve), $S_{21}P_{24}$ (red curve) and I_{16} (blue curve).

We successfully synthesized three well-defined linear ABC terpolymers with different PI volume ratios. The molecular weights of the linear ABC terpolymers are summarized in the Table 1.

Table 1: Summary of the synthesized linear ABC terpolymers composed of PS, P2VP and PI (SPI) synthesized by combining the anionic polymerization with the Steglich coupling reaction.

	PS		**P2VP**		**PI**				
SAMPLE	M_n (kg/mol)	vol. frac.	M_n (kg/mol)	vol. frac.	M_n (kg/mol)	vol. frac.	S	P	I
$S_{21}P_{24}I_9$	21	0.39	24	0.41	9	0.20	1	1.1	0.5
$S_{21}P_{24}I_{13}$	21	0.36	24	0.38	13	0.26	1	1.1	0.7
$S_{21}P_{24}I_{16}$	21	0.34	24	0.36	16	0.30	1	1.1	0.9

3. Synthesis of the PS-*arm*-P2VP-*arm*-PI terpolymer

The star miktoarm ABC terpolymer was synthetized *via* an esterification between the hydroxyl-mid-functionalized PS-*b*-P2VP BCP and the carboxyl-terminated PI homopolymer according to Figure 23. First, we will describe the coupling reaction between the PS-*b*-P2VP-OH (43 kg.mol^{-1}) and hPI-COOH (16 kg.mol^{-1}) chains as a reaction model. After we will generalize this coupling reaction the other PI homopolymers.

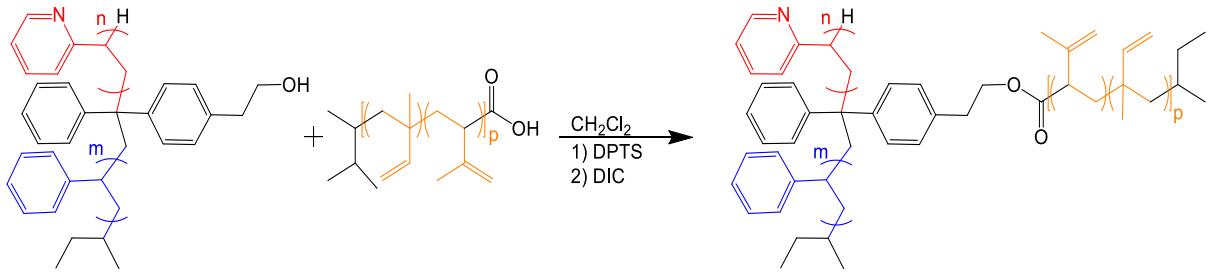

Figure 23: Scheme of the Steglich esterification between a hydroxyl mid-functionalized PS-b-P2VP BCP and a carboxyl end-functionalized PI homopolymer in CH_2Cl_2 to achieve a 3 μ-SPI.

a. Synthesis of a 3 μ-SPI having a PI block of 16 kg.mol^{-1}

The mid-functionalized PS-*b*-P2VP BCP (1 eq, 43 kg.mol^{-1}) and the hPI-COOH (3 eq, 16 kg.mol^{-1}) were solubilized in dried dichloromethane. The *N,N*-Dimethyl-4-pyridinaminium 4-methylbenzenesulfonate (DPTS, 10 eq) was added and let stirred for 15 minutes at 40°C. Then, the *N,N'*-Diisopropylcarbodiimide (DIC, 10 eq) was added, the mixture was stirred at 35°C. After 3 days, the solution was concentrated and precipitated in THF to recover the DPTS. The filtrate was concentrated and the desired 3 μ-SPI was precipitated in heptane to remove the excess of hPI-COOH.

The 3 μ-SPI was characterized by ^{1}H NMR (δ (ppm), 400 MHz, CD_2Cl_2), 2D DOSY NMR (δ (ppm), 400 MHz, THF) and SEC in THF.

Figure 24 shows the SEC traces with universal calibration of the hPI, hPS, PS-*b*-P2VP and 3 μ-SPI chains. Compared to the SEC traces of hPI, hPS, and PS-*b*-P2VP chains the SEC trace of the 3 μ-SPI terpolymer is shifted to low retention volumes corresponding to a higher molecular weight. The molecular weight of the 3 μ-SPI was found to be 59 kg.mol^{-1} which exactly corresponds to the addition of the PS-*b*-P2VP (43 kg.mol^{-1}) and hPI (16 kg.mol^{-1}) molecular weights. For this well-defined 3 μ-SPI, the volume ratios of the different blocks were determined to be S:P:I = 1:1.2:0.9. These ratios were also confirmed by the proton NMR characterization.

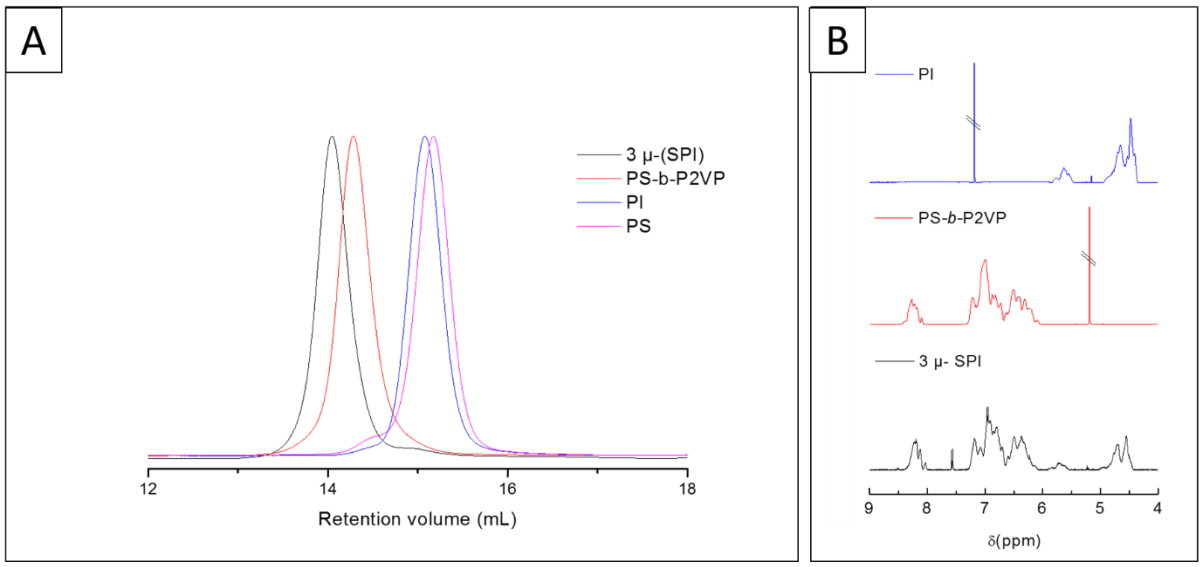

Figure 24: (a) SEC traces of hPS (pink), hPI (blue), PS-b-P2VP (red) and 3µ- SPI (black) chains. (b) ^{1}H NMR spectra (400 MHz) of hPI-COOH (blue), PS-b-P2VP (red,) and 3µ- SPI (black) chains.

^{1}H NMR spectra of hPI-COOH, PS-*b*-P2VP and 3 μ-SPI are presented in Figure 25. After the coupling step and purification in heptane, the NMR spectrum of the 3 μ-SPI shows the presence of the characteristic peaks of the three different blocks. Each specific peak was integrated and the different volume ratios were determined to be very close than those obtained from the SEC traces.

The coupling between the hPI-COOH and the end-functionalized PS-*b*-P2VP BCP was also evidenced by 2D-DOSY-NMR since the proton resonances belonging to PS, P2VP and PI blocks are aligned with the same horizontal line (see Figure 25). Here the macromolecule diffusion coefficient is $D = 4.48 \times 10^{-10}\ m^2.s^{-1}$ while the signals which are not aligned with the horizontal line are due to solvents.

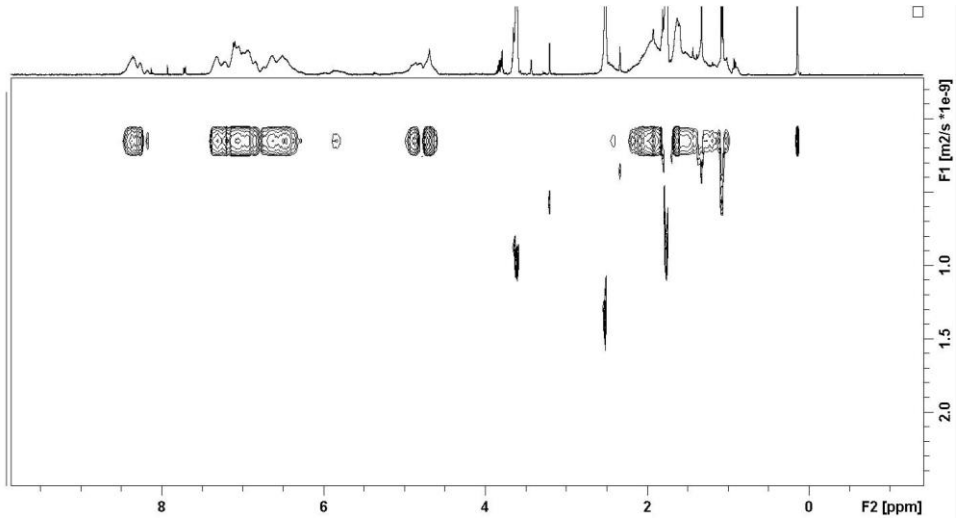

Figure 25: ^{1}H 2D DOSY NMR (400 MHz, THF) spectrum of 3 μ-SPI synthesized by combining the anionic polymerization with the Steglich coupling reaction.

b. Synthesis of other 3 μ-SPI terpolymers

Using the same strategy developed above, three other 3 μ-SPI terpolymers having different PI compositions have been synthetized. The SEC traces of the different star miktoarm ABC terpolymers are displayed in Figure 26.

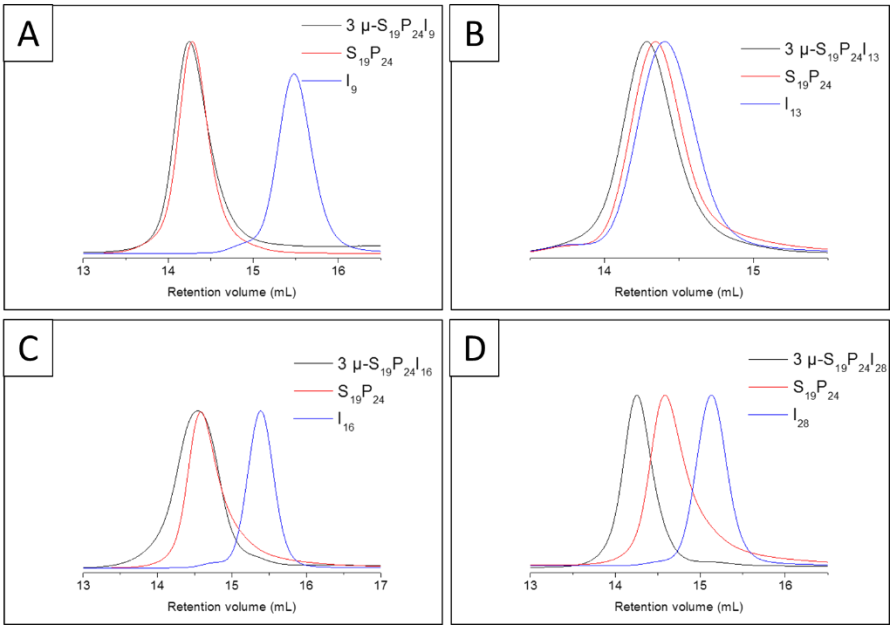

Figure 26: SEC curves in THF of (a) 3 μ-$S_{19}P_{24}I_9$ (black curve), $S_{19}P_{24}$ (red curve) and I_9 (blue curve); (b) 3 μ-$S_{19}P_{24}I_{13}$ (black curve), $S_{19}P_{24}$ (red curve) and I_{13} (blue curve); (c) 3 μ-$S_{19}P_{24}I_{16}$ (black curve), $S_{19}P_{24}$ (red curve) and I_{16} (blue curve); (d) 3 μ-$S_{19}P_{24}I_{28}$ (black curve), $S_{19}P_{24}$ (red curve) and I_{28} (blue curve).

As expected, the 3 μ-SPI SEC traces are shifted to low retention volumes and have a narrow and monomodal shape implying a low dispersity which is of about 1.1. The results are summarized in Table 2.

Table 2: Table summarizing the star miktoarm ABC terpolymer obtained from the after the coupling reaction.

	PS		**P2VP**		**PI**		**FRACTION/S**		
SAMPLES	M_n ($kg.mol^{-1}$)	vol. frac.	M_n ($kg.mol^{-1}$)	vol. frac.	M_n ($kg.mol^{-1}$)	vol. frac.	S	P	I
3 µ- $S_{19}P_{24}I_9$	19	0.37	24	0.43	9	0.20	1	1.2	0.6
3 µ- $S_{19}P_{24}I_{13}$	19	0.34	24	0.39	13	0.27	1	1.2	0.8
3 µ- $S_{19}P_{24}I_{16}$	19	0.32	24	0.37	16	0.31	1	1.2	1.0
3 µ- $S_{19}P_{24}I_{28}$	19	0,26	24	0.30	28	0.44	1	1.2	1.7

V. Conclusion

In this part, we synthesized two AB-type BCPs having a quasi-symmetric composition and bearing a mid- or an end-hydroxyl functionality. Four end-carboxyl-functionalized PI homopolymers with different molecular weights were also synthesized. The anionically polymerized PS-*b*-P2VP and hPI chains with a low dispersity revealed to be functionalized in high yields.

The mid- and end-functionalized PS-*b*-P2VP BCPs and the carboxyl-terminated PI homopolymers were coupled through a Steglich esterification to produce linear and star miktoarm ABC terpolymers. This efficient coupling method requiring with few purifications steps leads to well-defined terpolymers.

The advantage of this synthesis route is that the molecular weight of the nearly symmetric diblock copolymer PS-*b*-P2VP is kept constant and only the molecular weight of the hPI-COOH varies. This could be useful to achieve different phases resulted from the microphase separation of linear and star miktoarm ABC terpolymers. The phase behavior of microphase-separated linear and star miktoarm ABC terpolymers will be studied in the next chapters.

1. Ren, Y., Lodge, T. P. & Hillmyer, M. A. Synthesis, characterization, and interaction strengths of difluorocarbene-modified polystyrene-polyisoprene block copolymers. *Macromolecules* **33,** 866–876 (2000).

2. Hammond, M. R., Cochran, E., Fredrickson, G. H. & Kramer, E. J. Temperature dependence of order, disorder, and defects in laterally confined diblock copolymer cylinder monolayers. *Macromolecules* **38,** 6575–6585 (2005).

3. Funaki, Y. *et al.* Influence of casting solvents on microphase-separated structures of poly(2-vinylpyridine)-block-polyisoprene. *Polymer (Guildf).* **40,** 7147–7156 (1999).

4. Zhao, Y., Higashihara, T., Sugiyama, K. & Hirao, A. Synthesis of functionalized asymmetric star polymers containing conductive polyacetylene segments by living anionic polymerization. *J. Am. Chem. Soc.* **127,** 14158–14159 (2005).

5. Hanisch, A., Schmalz, H. & Müller, A. H. E. A modular route for the synthesis of ABC miktoarm star terpolymers via a new alkyne-substituted diphenylethylene derivative. *Macromolecules* **45,** 8300–8309 (2012).

6. Hückstädt, H., Abetz, V. & Stadler, R. Synthesis of a polystyrene-arm-polybutadiene-arm-poly(methyl methacrylate) triarm star copolymer. *Macromol. Rapid Commun.* **17,** 599–606 (1996).

7. Hückstädt, H., Göpfert, A. & Abetz, V. Synthesis and morphology of ABC heteroarm star terpolymers of polystyrene, polybutadiene and poly(2-vinylpyridine). *Macromol. Chem. Phys.* **201,** 296–307 (2000).

8. Higashihara, T., Hayashi, M. & Hirao, A. Synthesis of well-defined star-branched polymers by stepwise iterative methodology using living anionic polymerization. *Prog. Polym. Sci.* **36,** 323–375 (2011).

9. Lambert, O., Reutenauer, S., Hurtrez, G., Riess, G. & Dumas, P. Synthesis of amphiphilic triarm star block copolymers. *Polym. Bull.* **40,** 143–149 (1998).

10. Quirk, R. P., Guo, Y., Wesdemiotis, C. & Arnould, M. A. Functionalization of polymeric organolithium compounds with formaldehyde. *J. Polym. Sci. Part A Polym. Chem.* **41,** 2435–2453 (2003).

11. Guo, Y. M., Xu, J. & Pan, C. Y. Block and Star Block Copolymers by Mechanism Transformation. IV. Synthesis of S-(PSt)2(PDOP)2 Miktoarm Star Copolymers by Combination of ATRP and CROP. *J. Polym. Sci. Part A Polym. Chem.* **39,** 437–445 (2001).

12. Bellas, V., Iatrou, H. & Hadjichristidis, N. Controlled anionic polymerization of hexamethylcyclotrisiloxane. Model linear and miktoarm star co- and terpolymers of dimethylsiloxane with styrene and isoprene. *Macromolecules* **33,** 6993–6997 (2000).

13. Tsitsilianis, C., Katsampas, I. & Sfika, V. ABC heterotelechelic associative polyelectrolytes. Rheological behavior in aqueous media. *Macromolecules* **33,** 9054–9059 (2000).

14. Koutalas, G., Pispas, S. & Hadjichristidis, N. Micelles of poly(isoprene-*b*-2-vinylpyridine-*b*-ethylene oxide) terpolymers in aqueous media and their interaction with surfactants. *Eur. Phys. J. E* **15,** 457–464 (2004).

15. Tsitsilianis, C. & Sfika, V. Heteroarm star-like micelles formed from polystyrene-block-poly(2-vinyl pyridine)-block-poly(methyl methacrylate) ABC triblock copolymers in toluene. *Macromol. Rapid Commun.* **22,** 647–651 (2001).

16. Bywater, S. & Worsfold, D. J. Anionic polymerization of isoprene. Ion and ion-pair contributions to polymerization in tetrahydrofuran. *Can. J. Chem.* **45,** 1821–1824 (1967).

17. Worsfold, D. J.; Bywater, S. Anionic Polymerization of Isporene. *Can. J. Chem.* **42,** 2884–2892 (1964).

18. Quirk, R. P., Zhuo, Q., Jang, S. H., Lee, Y. & Lizarraga, G. Principles of Anionic Polymerization : An Introduction. *Symp. A Q. J. Mod. Foreign Lit.* (1998). doi:10.1021/bk-1998-0696.ch001

19. Nunns, A., Ross, C. A. & Manners, I. Synthesis and bulk self-assembly of ABC star terpolymers with a polyferrocenylsilane metalloblock. *Macromolecules* **46,** 2628–2635 (2013).

20. Baskaran, D. & Müller, A. H. E. Anionic vinyl polymerization-50 years after Michael Szwarc. *Progress in Polymer Science (Oxford)* **32,** 173–219 (2007).

21. Erothu, H. *et al.* Facile synthesis of poly(3-hexylthiophene)-block-poly(ethylene oxide) copolymers via Steglich esterification. *Polym. Chem.* **4,** 3652 (2013).

22. Neises, B. & Steglich, W. Simple Method for the Esterification of Carboxylic Acids. *Angew. Chemie Int. Ed. English* **17,** 522–524 (1978).

23. Quirk, R. P., Yin, J. & Fetters, L. J. Carbonation and Related Reactions of Poly(styryl)lithium. *Macromolecules* **22,** 85–90 (1989).

24. Quirk, R. P. Functionalization of Polymeric Organolithium Compounds. Carbonation. *Die Makromol. Chemie* **2076,** 2071–2076 (1982).

25. Uhrig, D. & Mays, J. W. Experimental techniques in high-vacuum anionic polymerization. *J. Polym. Sci. Part A Polym. Chem.* **43,** 6179–6222 (2005).

26. Schulz, M. F. *et al.* Phase Behavior of Polystyrene-Poly(2-vinylpyridine) Diblock Copolymers. *Macromolecules* **29,** 2857–2867 (1996).

27. Webster, O. W. Articles Living Polymerization Methods. *Science (80-.).* **251,** 887–893 (2014).

28. Nasser-Eddine, M., Reutenauer, S., Delaite, C., Hurtrez, G. & Dumas, P. Synthesis of Polystyrene-Poly(tert-butyl methacrylate)-Poly(ethylene oxide) Triarm Star Block Copolymers. *J. Polym. Sci. Part A Polym. Chem.* **42,** 1745–1751 (2004).

29. Ohata, M. & Isono, Y. Preparation of α-hydroxy-ω-carboxy-poly(methyl methacrylate) by anionic polymerization: 1. Utilization of initiator derived from 1-[4-(2-tert-butyldimethylsiloxy)ethyl]phenyl-1-phenylethylene. *Polymer (Guildf).* **34,** 1546–1548 (1993).

30. Ratkanthwar, K., Hadjichristidis, N. & Mays, J. W. High vacuum techniques for anionic polymerization. *Anionic Polym. Princ. Pract. Strength, Consequences Appl.* **38,** 19–59 (2015).

31. Sioula, S., Tselikas, Y. & Hadjichristidis, N. Synthesis of Model 3-Miktoarm Star Terpolymers of Styrene, Isoprene, and Methyl Methacrylate. *Macromolecules* **30,** 1518–1520 (1997).

32. Zhang, Z. & Fan, E. Solid phase synthesis of peptidotriazoles with multiple cycles of triazole formation. *Tetrahedron Lett.* **47,** 665–669 (2006).

33. Zhang, Y., Li, C. & Liu, S. One-pot synthesis of ABC miktoarm star terpolymers by coupling ATRP, ROP, and click chemistry techniques. *J. Polym. Sci. Part A Polym.*

Chem. **47,** 3066–3077 (2009).

34. Lambert, O., Dumas, P., Hurtrez, G. & Riess, G. Synthesis of an amphiphilic triarm star copolymer based on polystyrene, poly(ethylene oxide) and poly(ε-caprolactone). *Macromol. Rapid Commun.* **18,** 343–351 (1997).

35. Fujimoto, T. *et al.* Preparation and characterization of novel star-shaped copolymers having three different branches. *Polymer (Guildf).* **33,** 2208–2213 (1992).

36. Corey, E. J. & Venkateswarlu, A. Protection of Hydroxyl Groups as tert-Butyldimethylsilyl Derivatives. *J. Am. Chem. Soc.* **94,** 6190–6191 (1972).

37. Rostovtsev, V. V., Green, L. G., Fokin, V. V. & Sharpless, K. B. A stepwise huisgen cycloaddition process: Copper(I)-catalyzed regioselective 'ligation' of azides and terminal alkynes. *Angew. Chemie - Int. Ed.* **41,** 2596–2599 (2002).

38. Iskin, B., Yilmaz, G. & Yagci, Y. Synthesis of ABC type miktoarm star copolymers by triple click chemistry. *Polym. Chem.* **2,** 2865 (2011).

39. Albrecht, S., Defoin, A. & Tarnus, C. Simple preparation of O-substituted hydroxylamines from alcohols. *Synthesis (Stuttg).* **2006,** 1635–1638 (2006).

CHAPTER 3: SELF-ASSEMBLED PS-*b*-P2VP-*b*-PI THIN FILMS

I. Introduction

The phase behavior of linear ABC terpolymer thin films is studied in this chapter. The aim of this work was to achieve different structures in thin films than the regular phases formed from AB-type or ABA-type BCPs. As reported in chapter II, the synthesis of the linear ABC terpolymers was done by combining the anionic polymerization with a coupling reaction. PS, P2VP and PI blocks were used for their intrinsic properties. Firstly, the Flory-Huggins parameters between the different pairs are high which allow a "full" microphase-separation of the PS-*b*-P2VP-*b*-PI chains, resulting in the formation of three colored patterns.[1] Another advantage of those polymers is that they have a different etching resistance under a CF_4/O_2 RIE plasma[2,3] as it was evidenced from PM-IRRAS[4,5] measurements. Indeed, PI domains were etched more quickly than the P2VP and PS ones. The selectivity of blocks towards a fluorine riche plasma is an important parameter to obtain contrast for the microscopy analysis.

As the χ-parameters between the different pairs are $\chi_{SI} \approx \chi_{SP} \approx 0.1 << \chi_{PI} \approx 0.8$,[6–8] the PS-*b*-P2VP-*b*-PI chains are in a type II frustrated state. Although the self-assembly of linear ABC terpolymers in a type II frustration state has been reported in bulk[9,10] or theoretically,[11] there has been no investigation of their thin film behavior.

A thermal treatment of those kinds of polymers did not appear relevant to achieve well-defined structures. So, the effect of the thermal annealing process will not be studied in this thesis. The self-assembly of linear ABC terpolymers was achieved by exposing the spin-coated thin films to a chloroform vapor. The morphologies obtained will be described in the following part.

II. Q^{230} gyroid structure produced from the self-assembly of PS-*b*-P2VP-*b*-PI thin films

The thin film phase behavior of frustrated PS-*b*-P2VP-*b*-PI (S:P:I = 1:1.1:0.5) chains was studied. For that purpose, a 2 wt. % polymer solution in toluene was spin-coated on smooth silicon substrates and the film thickness was controlled through the speed-coating speed (1.5krpm). The PS-*b*-P2VP-*b*-PI self-assembly was promoted by exposing samples to a continuous stream of a $CHCl_3$ vapor produced by bubbling nitrogen gas through the liquid solvent as described previously.[12–14] The morphology of the solvent-annealed PS-*b*-P2VP-*b*-PI thin films was frozen by fast removal of the chamber lid. As the solvent annealing process under a $CHCl_3$ vapor favors the formation of a PI top surface layer, a fluorine-rich plasma (plasma conditions are: 40 W, 17 sccm CF_4 and 3 sccm O_2, 45 s) was applied to remove this low surface energy layer (*i.e.* the PI top layer) which revealed the thin film morphology.

On the substrate corner, the film thickness was determined to be 190 nm. The AFM topographic view of the thicker part of the PS-*b*-P2VP-*b*-PI layer exposed to a $CHCl_3$ vapor is presented in Figure 1a. After preferentially removing the PI domains (black) with the fluorine plasma, the AFM topographic view shows a double-wave pattern with waves having different amplitudes. This pattern is characteristic of the (211) crystallographic plane[15] of the core-shell double gyroid Q^{230} structure[16,17] oriented parallel to the interface air/surface. From the associated 2D-fast Fourier transform (FFT), a long period of about 120 nm is determined (see Fig. 1b)

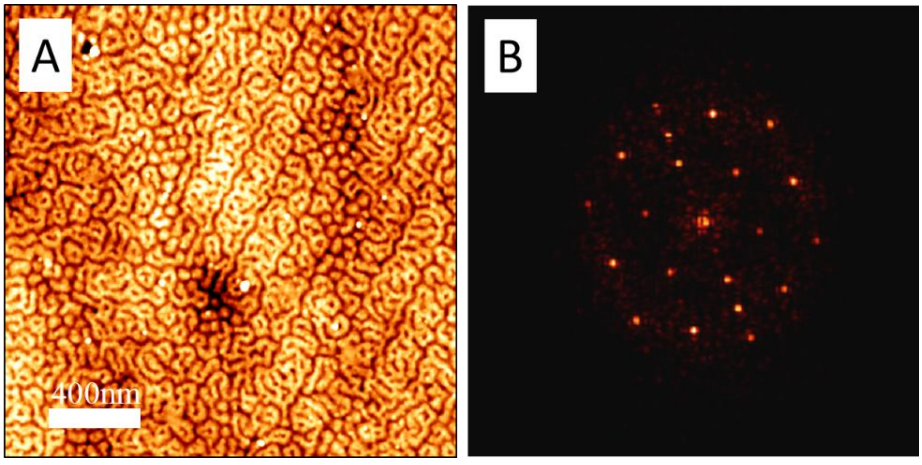

Figure 1: (a) (2 x 2 µm²) AFM topographic view of a solvent-annealed linear SPI (S:P:I = 1:1.1:0.5) thin film (190 nm) treated with a CF_4/O_2 RIE plasma which reveals the (211) plane of the core-shell double gyroid structure and (b) its corresponding 2D-FFT.

Different network structures have been reported in the literature: the Q^{230}, Q^{214}, and O^{70} structures (see Fig. 2).[16,18,19] The cubic Q^{214} phase is a single-gyroid morphology which refers to an alternating gyroid network. The O^{70} structure is an orthorhombic alternating network structure. For cubic Q^{230} phase, each of the two interpenetrating and independent lattices receives three segregated domains, resulting in five independent, triply periodic regions.

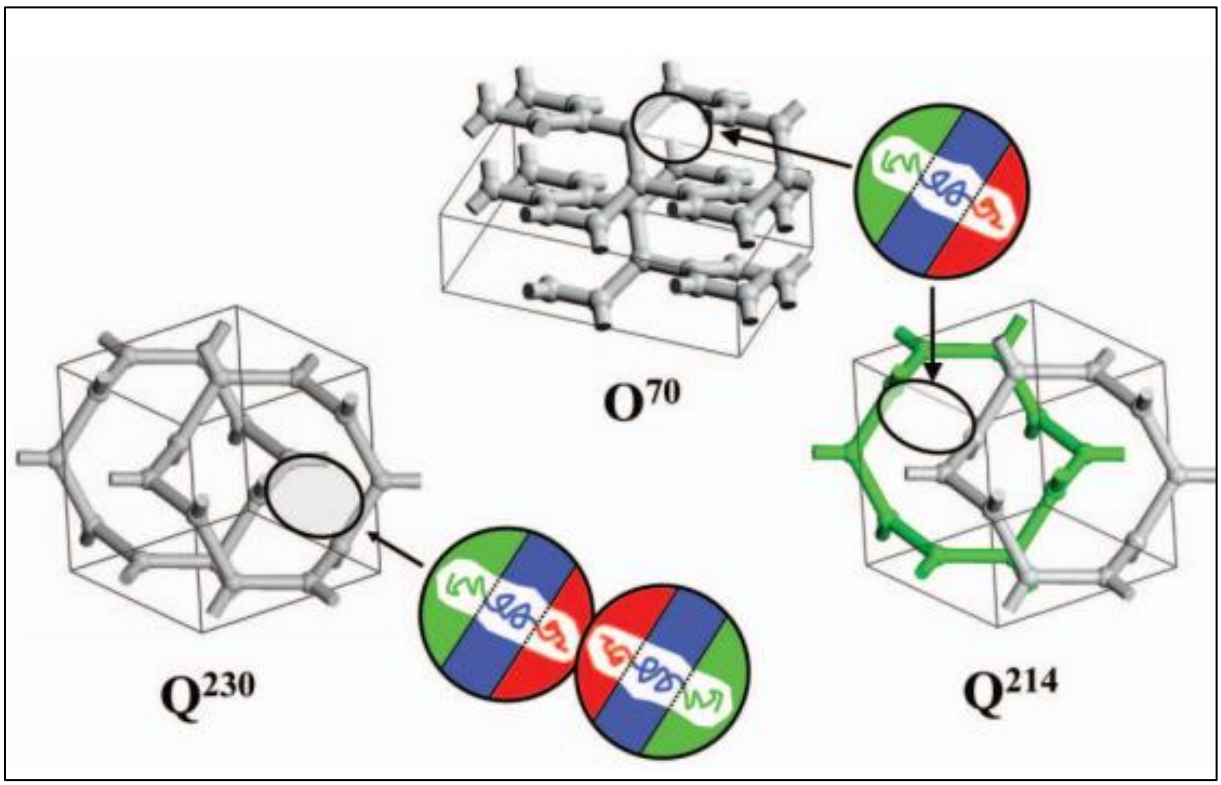

Figure 2: Lattice structures for the three network phases identified for linear ABC terpolymers. Cubic phases Q^{230} (far left) and Q^{214} (far right) are double- and single-gyroid networks, respectively, while phase O^{70} (center) is a single-orthorhombic network. The colored insets illustrate how triblock copolymer is added to these lattices, resulting in pentacontinuous (Q^{230}) and tricontinuous (Q^{214} and O^{70}) morphologies.

In order to describe the gyroid structure in details, the notion of crystallographic planes is introduced. The planes described in this part correspond to the (*hkl*) crystallographic planes.[20] For instance, the plane (211) of the gyroid structure is a cross section along the (211) crystallographic plane with $h = 2$, $k = 1$ and $l = 1$. Other plane examples are reported in Figure 3.

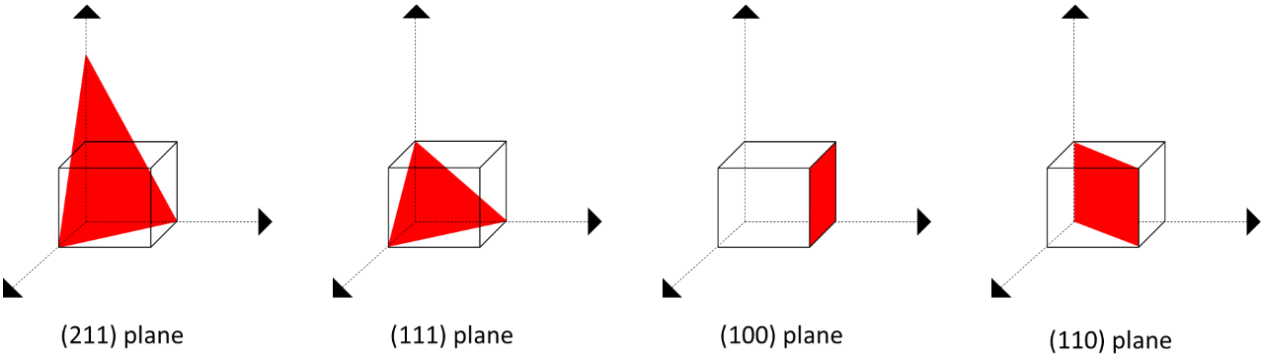

Figure 3: Four examples of crystallographic planes.

The (211) plane of the Q^{230} structure described above is present only in the thicker part of the film. In contrast, a *p6mm* symmetry pattern with a period of ~52 nm is produced in regions of the film having a thickness of about 90 nm as revealed by the AFM topographic view presented in Figure 4a. Here, the period was determined from the 2D-FFT showed in Figure 4b. This *p6mm* symmetry pattern is attributed to the (111)[15,20,21] plane of the core-shell gyroid structure.

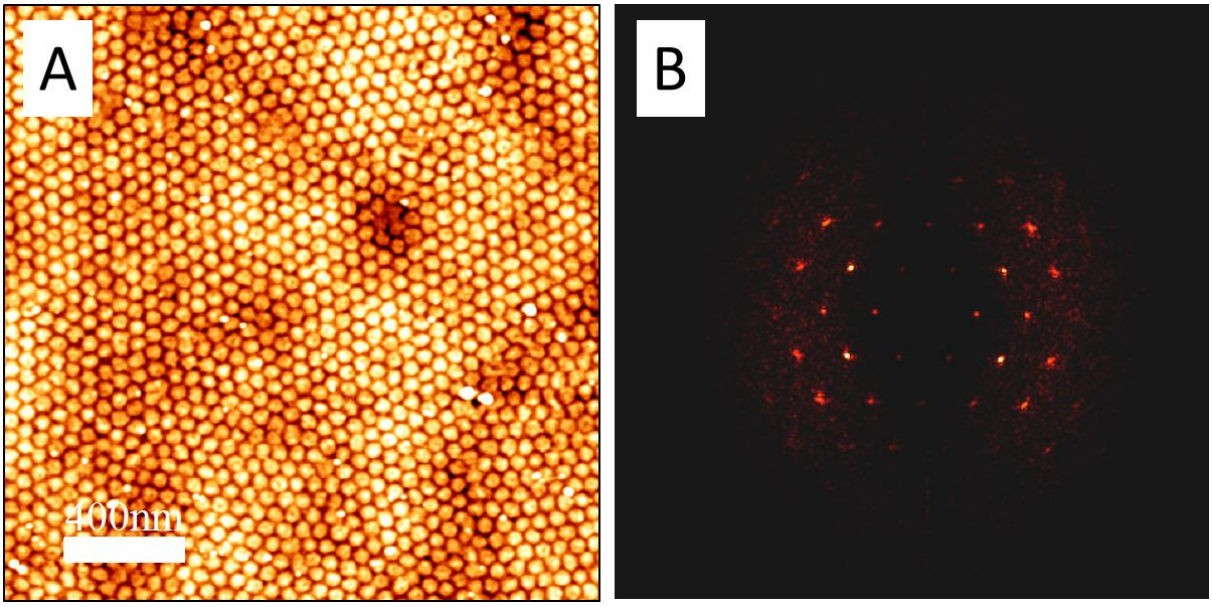

Figure 4: (a) (2 x 2 µm²) AFM topographic view of a solvent-annealed linear SPI terpolymer (S:P:I = 1:1.1:0.5) thin films treated with a CF_4/O_2 RIE plasma which reveals the (111) plane of the core-shell double gyroid structure and (b) its corresponding 2D-FFT.

Although the contrast of the AFM pictures presented in Figure 1 and 4 is sufficient to identify different planes of the core-shell double gyroid structure, the contrast between PS and P2VP blocks is too weak to investigate in more details the different patterns. To gain insight into the thin film morphologies developed within the (211) and (111) planes, the PS-*b*-P2VP-*b*-PI thin films were also dipped in a H_2PtCl_6 solution. As the platinum salt is chelated by the

pyridine moiety, it selectively stains the P2VP domains. The resist of H_2PtCl_6-stained P2VP domains under the RIE plasma conditions is increased, which improves the AFM topographic image contrast between PS and P2VP domains. Such additional treatment makes that PS appears in brown while the P2VP and PI domains are yellow and dark brown, respectively, on the AFM topographic views presented in Figure .

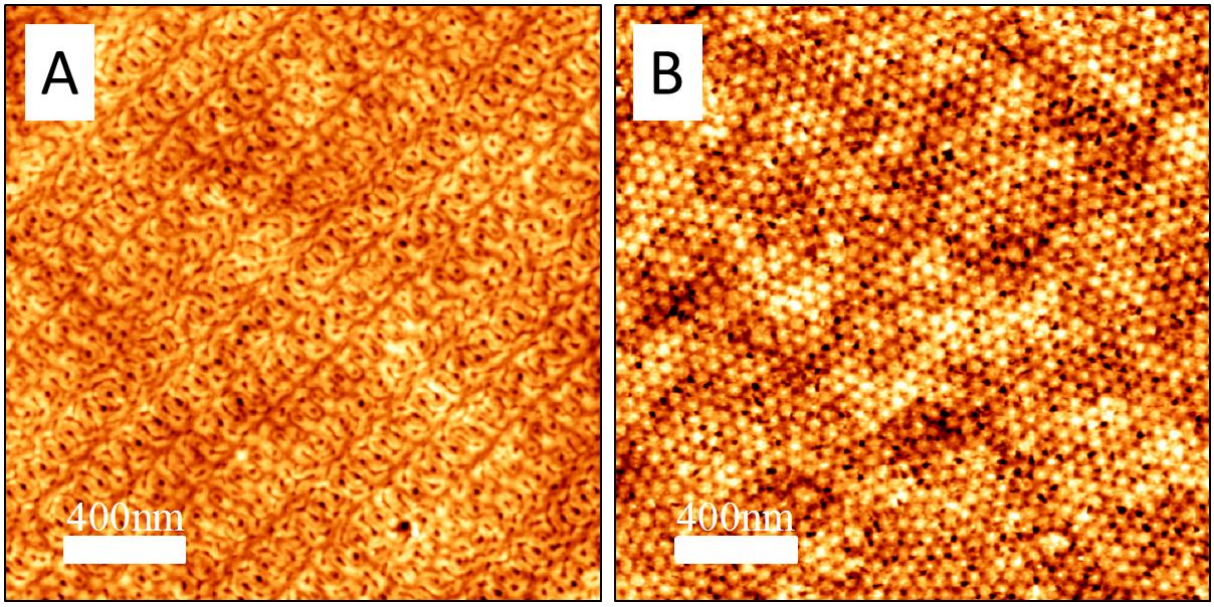

Figure 5: (2 x 2 µm²) AFM topographic views of solvent-annealed linear SPI terpolymer (S:P:I= 1:1.1:0.5) thin films treated with a CF_4/O_2 RIE plasma which reveals two planes of a H_2PtCl_6-stained core-shell double gyroid structure: (a) the (211) plane and (b) the (111) plane.

These AFM topographic views correspond to solvent-annealed (2h, $CHCl_3$) 190- and 90-nm-thick PS-*b*-P2VP-*b*-PI layers, immersed into an aqueous H_2PtCl_6 solution then subsequently treated by a CF_4/O_2 reactive ion etching (RIE) plasma. The (211) plane oriented parallel to the air surface with its typical "double-wave" pattern,[15] consisting of small- and large-amplitude oscillations, can be clearly observed in the 190 nm thick PS-*b*-P2VP-*b*-PI layer (see Figure a). This double wave pattern has a long period of ~120 nm which gives a good indication of the unit cell dimension, a_G. In contrast, a "wagon-wheel" pattern, consisting of 6-fold P2VP (bright) domains surrounded by smaller PS (brown) and PI (black) domains, is produced in the 90 nm thick PS-*b*-P2VP-*b*-PI layer (see Figure 5b).

In this core-shell double gyroid phase, the PI and P2VP domains form the core and the shell of the structure, respectively, while PS is the matrix.[17] Figure 6 shows a simulation of the (211) projection of a core-shell double gyroid morphology. In this figure, the P2VP shell and the PI core would correspond to the black and white domains drown in a PS gray matrix. This simulation is fully in accordance with the (211) plane demonstrated in this study.

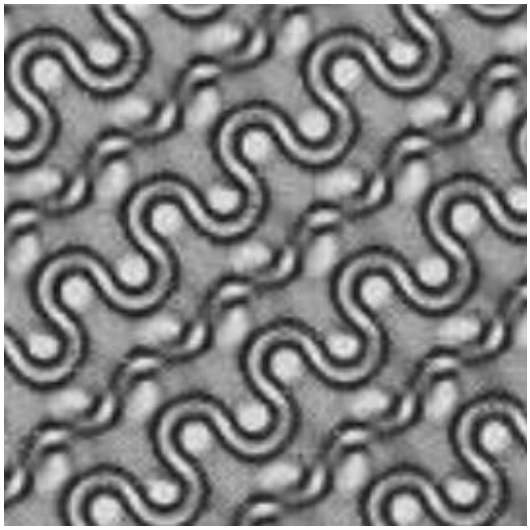

Figure 6: Simulation (211) projection of a core-shell double gyroid morphology. Reproduced from Goldacker et al.[16]

Scanning electron microscopy (SEM) images presented in Figure show additional plane orientations of the core-shell double gyroid structure produced from solvent-annealed (2h, $CHCl_3$) PS-*b*-P2VP-*b*-PI layers plunged into an aqueous H_2PtCl_6 solution and subsequently treated by CF_4/O_2 RIE plasma. The hexagonal pattern showed in Figure 7a is consistent with the "doughnut pattern" observed along the (110) projection of the Q^{230} structure. Here, etched PI core (black), ordered into a hexagonal array with a period of ~100 nm, are surrounded by a H_2PtCl_6-stained P2VP shell (light) including PS matrix (gray). Importantly, this pattern is stabilized in peculiar regions of the film where the film thickness is between the upper and lower terraces occupied by the double-wave and wagon-wheel patterns, respectively, as well as regions where the film thickness is between the upper and lower terraces occupied by the wagon-wheel pattern and the small amplitude wavy structure. Decreasing the film thickness well below the unit cell dimension ($t \approx 75$ nm $< a_G$) leads to the formation of an ordered structure which resembles to the "zigzagging lamellar" pattern formed along the (100) of the Q^{230} structure (see Fig. 7b).[20,22] This pattern with a period of ~50 nm consists of zigzagging PS (gray) and H_2PtCl_6-stained P2VP lamellar domains (light) with PI domains (black) not perfectly distributed within the P2VP lamellae. SEM images corresponding to the (111) and the (211) planes of the core-shell double gyroid already observed from AFM topographic images (see Fig. 5) are also displayed in Figures 7c-d.

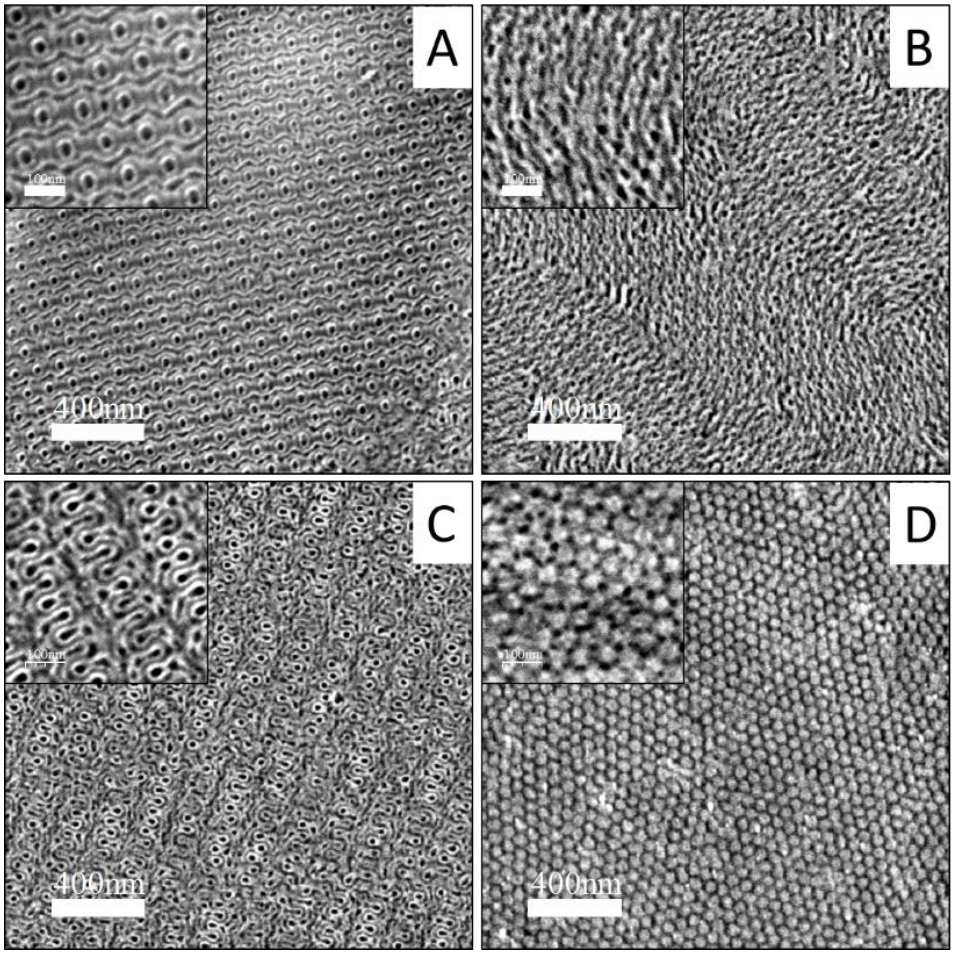

Figure 7: (2 x 2 μm^2, inset = 0.5 x 0.5 μm^2) SEM images of H_2PtCl_6-stained SPI (S:P:I = 1:1.1:0.5) thin films treated with a CF_4/O_2 RIE plasma which reveals four planes of a core-shell double gyroid structure: (a) (110), (b) (100), (c) (211), and (d) (111) planes.

Depending on the layer thickness, thin films of a Q^{230} structure with characteristic crystallographic planes such as (211), (110), (111) or (100) oriented parallel to the air surface are observed. When the film thickness is well-above the unit cell dimension, a double-wave (211) pattern maximizing the PI composition at the polymer-air interface is produced. As $CHCl_3$ preferentially attracts the PI block with its low surface tension to the film air-polymer interface, a PI top-coat layer with its (211) plane oriented parallel to the air surface appears on the Q^{230} morphology, similarly to the thermodynamically stable structure which is observed in the 190 nm thick PS-*b*-P2VP-*b*-PI layers. When the film thickness is in the order of the unit cell dimension, a hexagonal doughnut pattern with a higher surface PI composition ratio than that of PS-*b*-P2VP-*b*-PI chains is observed at the polymer-air interface. Although this Q^{230} (110) pattern does not optimize the PI composition at the polymer-air interface as the double wave pattern does, it exhibits a hexagonal array with a periodicity lower than a_G. Below the unit cell dimension, the plane orientation of the core-shell DG at the air surface is probably driven by a

commensurability effect. Further decreasing of the film thickness to 90 nm stabilizes a (111) plane orientation parallel to the air surface. However, this pattern, with a surface PI composition ratio just slightly higher than that of PS-*b*-P2VP-*b*-PI chains, exhibits a hexagonal array with a period two times smaller than that of the one formed on the Q^{230} (110) pattern. Finally, a zigzagging lamellar pattern with a period of ~50 nm and a PI composition at the polymer-air interface close to the one of the PS-*b*-P2VP-*b*-PI chains is produced when the film thickness is about 75 nm.

These results are in accordance with the numerical analysis of FE-SEM images done by Hashimoto *et al.* and Wu *et al.*.[15,20] Indeed, these authors reported that depending on the area fraction matrix ($S(x_0)$) cut along the planes parallel to various crystallographic planes and the position of the cross section (x_0), some crystallographic planes orientation are predominant as shown in Figure 8.

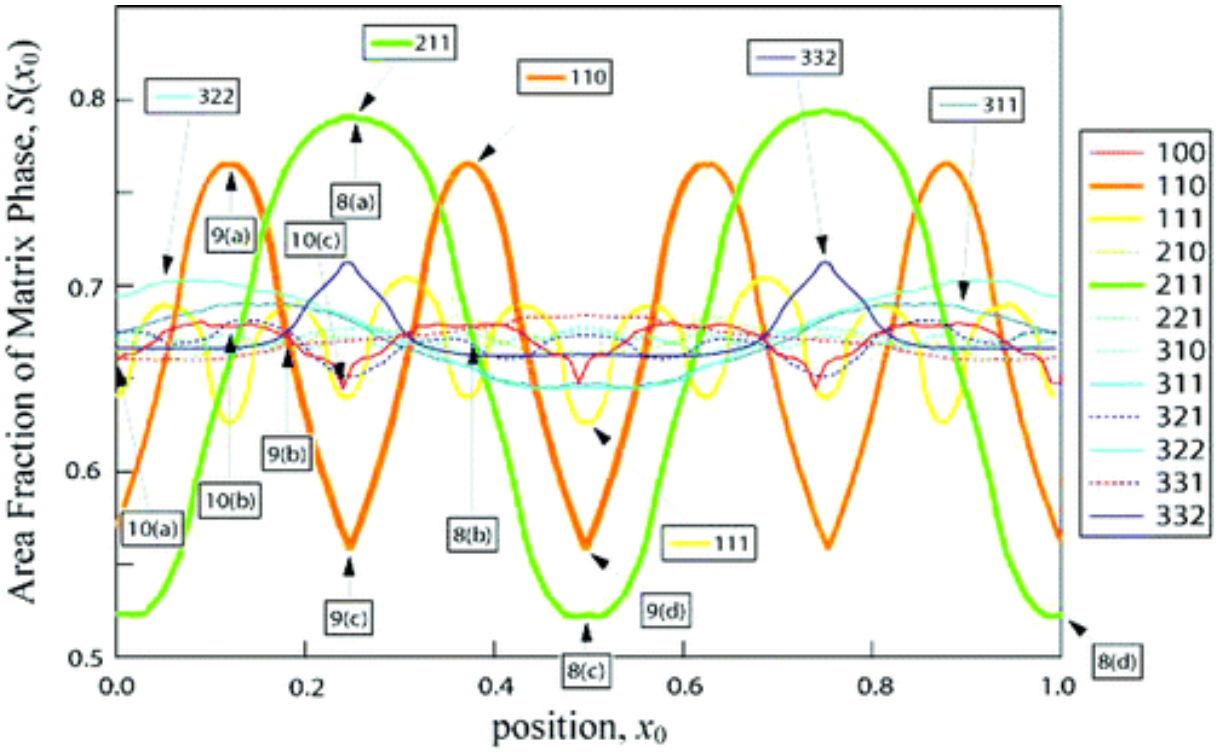

Figure 8: Calculated area fraction of the matrix phase S(x0) cut along the planes parallel to various crystallographic planes, as shown by three digits hkl in the legend, at various positions x0.

They proved that the film thickness is related to the area fraction of the matrix phase which is correlated to the area fraction of other blocks. Since the PI block has the smallest surface energy, the area fraction of PI at the air/surface interface is increased when the area fraction of the PS matrix is minimal. This is satisfied when the (211) plane is oriented parallel

to the air surface (see Fig. 8) which explains why such a plane orientation is observed for the thicker film. As the film thickness decreases, the incommensurability between the gyroid unit cell dimension and the polymeric layer thickness drives the self-assembly of the PS-*b*-P2VP-*b*-PI chains, and other planes are oriented parallel to the air/surface interface. From the Figure 9, the PI volume faction for the other planes decreases as follows at $x_0 = 0$: (110) > (111) > (100). This phenomenon is fully in accordance with order of the plane observed parallel to the air/surface interface when the film thickness is decreased (see Table 1).

Table 1: Results summary of the crystallographic planes observed for a gyroid structure depending on the area fraction of matrix phase, the PI phase, the period, and the thickness of the film.

Plane	Film thickness	Area PI fraction	Period
(211) (111) (100) (110)	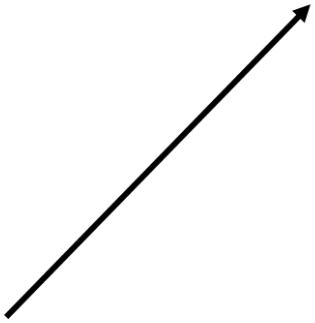	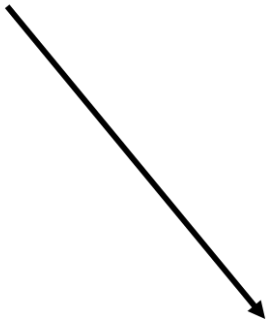	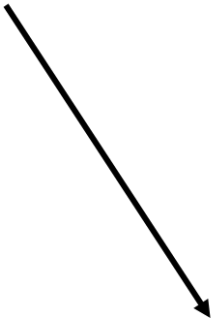

III. Conclusion

The self-assembly of a frustrated type II linear SPI terpolymer with volume fractions of 1, 1.1 and 0.5 for S, P and I, respectively, gives access to a core-shell double gyroid structure. Depending on the film thickness, different crystallographic planes of the Q^{230} structure are observed. For a film thicker than the unit cell of the gyroid network, the (211) plane is observed at the air-surface interface. Decreasing the film thickness closer to the unit cell dimension induces the stabilization of the (111) plane. If the thickness is well below the unit cell dimension, the (100) plane is observed. The different crystallographic plane formation is driven by the commensurability of the structure period with the film thickness and the preferential segregation of the PI block at the free-surface.

1. Leibler, L. Theory of Microphase Separation in Block Copolymers. *Macromolecules* **13,** 1602–1617 (1980).

2. Fridman. Plasma etching and modification of organic polymers. in *Pure and Applied Chemistry* **62,** 1699–1708 (1990).

3. Pederson, L. A. L. A. A. & Deep, U. V. L. I. T. H. O. G. R. A. P. H. Y. Structural Composition of Polymers Relative to Their Plasma Etch Characteristics. *J. Electrochem. Soc.* **I,** 205–208 (1978).

4. Ramin, M. A. *et al.* PM-IRRAS investigation of self-assembled monolayers grafted onto SiO 2/Au substrates. *Langmuir* **27,** 6076–6084 (2011).

5. Buffeteau, T., Desbat, B., Blaudez, D. & Turlet, J. M. Calibration procedure to derive IRRAS spectra from PM-IRRAS spectra. *Appl. Spectrosc.* **54,** 1646–1650 (2000).

6. Funaki, Y. *et al.* Influence of casting solvents on microphase-separated structures of poly(2-vinylpyridine)-block-polyisoprene. *Polymer (Guildf).* **40,** 7147–7156 (1999).

7. Ren, Y., Lodge, T. P. & Hillmyer, M. A. Synthesis, characterization, and interaction strengths of difluorocarbene-modified polystyrene-polyisoprene block copolymers. *Macromolecules* **33,** 866–876 (2000).

8. Hammond, M. R., Cochran, E., Fredrickson, G. H. & Kramer, E. J. Temperature dependence of order, disorder, and defects in laterally confined diblock copolymer cylinder monolayers. *Macromolecules* **38,** 6575–6585 (2005).

9. Brinkmann, S., Stadler, R. & Thomas, E. L. New structural motif in hexagonally ordered cylindrical ternary (ABC) block copolymer microdomains. *Macromolecules* **31,** 6566–6572 (1998).

10. Balsamo, V., von Gyldenfeldt, F. & Stadler, R. 'Superductile' Semicrystalline ABC Triblock Copolymers with the Polystyrene Block (A) as the Matrix. *Macromolecules* **32,** 1226–1232 (1999).

11. Guo, Z. *et al.* Discovering ordered phases of block copolymers: New results from a generic fourier-space approach. *Phys. Rev. Lett.* **101,** 28301 (2008).

12. Van Zoelen, W., Asumaa, T., Ruokolainen, J., Ikkala, O. & Ten Brinke, G. Phase behavior of solvent vapor annealed thin films of PS-b-P4VP(PDP) supramolecules.

Macromolecules **41,** 3199–3208 (2008).

13. Gu, X., Gunkel, I., Hexemer, A. & Russell, T. P. Solvent vapor annealing of block copolymer thin films: Removal of processing history. *Colloid Polym. Sci.* **292,** 1795–1802 (2014).

14. Aissou, K., Choi, H. K., Nunns, A., Manners, I. & Ross, C. A. Ordered nanoscale archimedean tilings of a templated 3-miktoarm star terpolymer. *Nano Lett.* **13,** 835–839 (2013).

15. Hashimoto, T., Nishikawa, Y. & Tsutsumi, K. Identification of the 'voided double-gyroid-channel': A new morphology in block copolymers. *Macromolecules* **40,** 1066–1072 (2007).

16. Hückstädt, H., Goldacker, T., Göpfert, A. & Abetz, V. Core-shell double gyroid morphologies in ABC triblock copolymers with different chain topologies. *Macromolecules* **33,** 3757–3761 (2000).

17. Goldacker, T. & Abetz, V. Core-shell cylinders and core-shell gyroid morphologies via blending of lamellar ABC triblock and BC diblock copolymers. *Macromolecules* **32,** 5165–5167 (1999).

18. Tyler, C. A., Qin, J., Bates, F. S. & Morse, D. C. SCFT study of nonfrustrated ABC triblock copolymer melts. *Macromolecules* **40,** 4654–4668 (2007).

19. Bailey, T. S., Pham, H. D. & Bates, F. S. Morphological behavior bridging the symmetric AB and ABC states in the poly(styrene-b-isoprene-b-ethylene oxide) triblock copolymer system. *Macromolecules* **34,** 6994–7008 (2001).

20. Wu, Y.-H., Lo, T.-Y., She, M.-S. & Ho, R.-M. Morphological Evolution of Gyroid-Forming Block Copolymer Thin Films with Varying Solvent Evaporation Rate. *ACS Appl. Mater. Interfaces* **7,** 16536–16547 (2015).

21. Dair, B. J., Avgeropoulos, A., Hadjichristidis, N. & Thomas, E. L. Mechanical properties of the double gyroid phase in oriented thermoplastic elastomers. *J. Mater. Sci.* **35,** 5207–5213 (2000).

22. Kirkensgaard, J. J. K. Kaleidoscopic tilings, networks and hierarchical structures in blends of 3-miktoarm star terpolymers. *Interface Focus* **2,** 602–607 (2012).

CHAPTER 4: SELF-ASSEMBLED PS-*arm*-P2VP-*arm*-PI THIN FILMS

I. Introduction

In this part, we will study the self-assembly of star miktoarm ABC terpolymers. In contrast to linear ABC terpolymer, star miktoarm ABC terpolymers have only one junction point. This unique junction point imposes interfaces between the three different blocks (A/B, B/C and C/A interfaces), and is located along a line.[1] This topographical requirement induces new phases not accessible from linear ABC terpolymers such as Archimedean tiling patterns.[2–6]

It is important to define the nomenclature used to distinguish the different Archimedean tiling patterns. They are identify by symbols based on the orders of the polygons meeting at a given vertex.[7] According to Kepler, only 11 tilings can fill the plane without gaps and are denoted ($m_1^{n1}.m_2^{n2}$. ...) where m_i refers to the number of sides of each polygon, and the superscript n_i denotes the number of adjacent identical polygons around a vertex. For instance, the two-dimensional honeycomb pattern consisting of regular hexagons is denoted (6.6.6) because three hexagons meet at each vertex.

Only few papers deal with the self-assembly of star miktoarm ABC terpolymer thin films. The (6.6.6) and (4.8.8) Archimedean tiling patterns have been reported in thin films by Aissou *et al.*.[3,8,9] Hierarchical morphologies consisting of lamellae separated by an alternation of cylinders have also been reported by Aissou *et al*. and Choi *et al*..[3,10]

In this chapter, the thin film morphologies obtained from the self-assembly of two star miktoarm ABC terpolymers composed of PI, PS and P2VP will be discussed. The volume ratio of PI varies whereas the volume ratios of PS and P2VP are constant. One star miktoarm ABC terpolymer has a nearly-symmetric composition, whereas the other one has a smaller PI volume ratio.

II. Thin film (4.6.12) Archimedean tiling patterns

Thin film morphologies of 3 μ-SPI (S:P:I = 1:1.2:0.6) and 3 μ-SPI (S:P:I = 1: 1.2: 1) were studied. For that purpose, a 2 wt. % polymer solution in toluene was spin-coated on smooth silicon substrates. The 3 μ-SPI self-assembly was promoted by exposing samples to a continuous stream of a $CHCl_3$ or THF vapor produced by bubbling nitrogen gas through the liquid solvent as described previously.[11,12] The morphology of the solvent-annealed 3 μ-SPI thin films was frozen by quickly removing the lid of the chamber. The solvent annealing process under a vapor of either $CHCl_3$ or even THF favors the formation of a PI top surface layer. A fluorine-rich plasma was therefore applied to remove this low surface energy layer which revealed the thin film morphology (plasma conditions are 40 W, 17 sccm CF_4 and 3 sccm O_2, 45 s).

In this chapter, we will first described the morphologies obtained from the self-assembled 3 μ-SPI (S:P:I = 1:1.2:1) thin films under a chloroform vapor. The microphase-separation of 3 μ-SPI (S:P:I = 1:1.2:0.6) thin films placed under a THF vapor will be then discussed.

1) Solvent annealed 3 μ-SPI (S:P:I = 1:1.2:1) under a $CHCl_3$ vapor

In this part, the self-assembly of the 3 μ-SIP chains having a quasi-symmetric composition (S: P:I = 1:1.2:1) will be studied. In this case, the thin film was treated by a $CHCl_3$ vapor for 2 hours. The thickness of the film was determined to be 80 nm by light reflection using a Filmetrics apparatus. The AFM topographic image of the resulting structure is presented in Figure 1. Here, PI (dark brown) occupying the inner part of the structure is surrounded by an alternation of PS (yellow) and P2VP (brown) domains. The structure exhibits an out-of-plane columnar structure ordered into a hexagonal array. The 2D-FFT presented in Figure 1 confirms the *p6mm* symmetry of the array having a single grain orientation since six first-order spots are clearly visible. PI domains have a period of 41 nm according to the 2D-FFT while PS and P2VP domains have a similar period of 24 nm. Both the array symmetry and the distribution of periodicities are in accordance with the formation of (4.6.12) Archimedean tiling pattern as illustrated by the schematic representation of the structure showed on the bottom right corner of the AFM image. From this representation, PS, PI and P2VP occupy the blue, orange and red regions, respectively, of the (4.6.12) Archimedean tiling pattern.

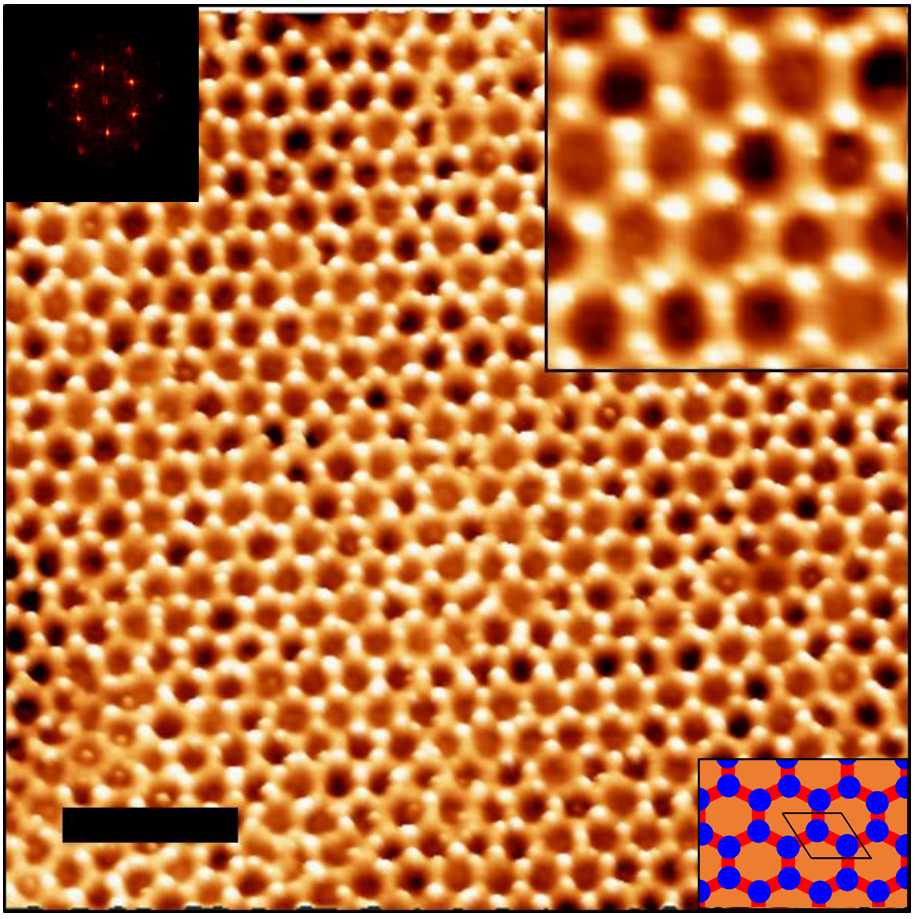

Figure 1: (1 x 1 µm², inset: 150 x 150 nm²) AFM topographic views of a solvent annealed 3 µ-SPI (S:P:I=1:1.2:1) thin film under a $CHCl_3$ vapor for 2 hours and etched with a CF_4/O_2 plasma (scale bar: 200 nm). The 2D-FFT corresponding to the low magnified AFM image and the schematic representation of the (4.6.12) tiling pattern are presented on the upper left and bottom right corners of the figure, respectively.

Importantly, the (3.4.6.4) Archimedean tiling pattern, accessible from microphase separated 3 μ-ABC chains (see chapter I), has also a *p6mm* symmetry and a similar domain distribution surrounding the main domain. However, it was not retained as a possible model for the self-assembly of 3 μ-SPI thin films since it favors a large interfacial area between the P2VP and PI domains, which have the highest incompatibility.

We can note that the PI domains are well-ordered into a hexagonal array although these domains are not all the time surrounded by exactly 12 domains made of PS and P2VP (6 PS + 6 P2VP) as expected for a well-developed (4.6.12) Archimedean tilling pattern. This phenomenon implies that the long-range ordered PI domains are formed first, and the PS and P2VP chains are then microphase-separated in a second step around the PI domains. These results indicate that the microphase-separation occurs in two-steps mechanism as already

observed by Aissou *et al.*[9] for self-assembled polyisoprene-*arm*-polystyrene-*arm*-polyferrocenylethylmethylsilane chains into a *c*2*mm* pattern symmetry.

The (4.6.12) tiling pattern has already been described in theoretical studies. In 2002 Gemma *et al.*[13] reported on this tiling pattern using Monte Carlo simulations for star miktoarm ABC terpolymers with arm-length ratio of 1:1:x and a χ-parameter equal for each pair as shown in Figure 2.

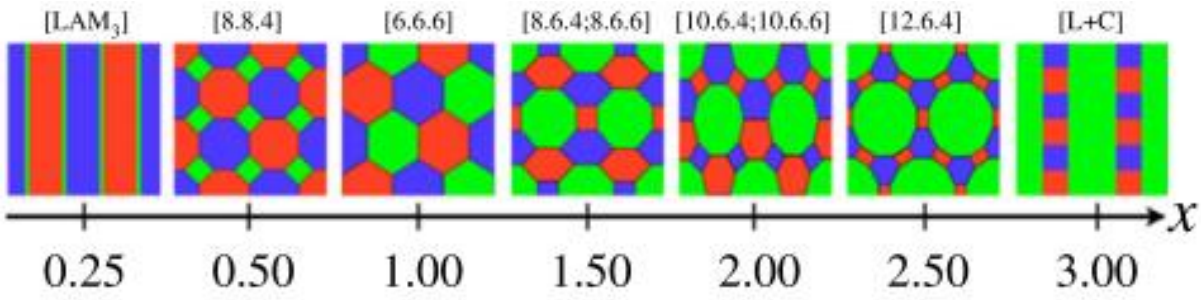

Figure 2: Schematic phase diagram for 3-miktoarm star terpolymers under the constraint of the A and B components occupying equal volume fractions and invoking symmetric interactions between all unlike components. The different phases are placed at their approximate compositional positions quantified by the parameter x, the volume ratio of the C and A components. (Adapted from Gemma et al.) [13]

The (4.6.12) tiling pattern was found for x = 2.5. Even if the volume ratio of the PI block is increased during the SVA process because of $CHCl_3$ swells more the PI domains, the result obtained from the Monte Carlo simulations does not match exactly with our experimental result. This slight difference can be explained by the fact that they considered that all the interaction parameters between blocks are equal which is not the case in our study ($\chi_{PI\text{-}P2VP} >> \chi_{PS\text{-}P2VP} = \chi_{PI\text{-}PS}$).

A different morphology was observed in the substrate corner (where the film is over 110 nm thick). A square array is observed in the thicker part of the film, as shown on the AFM topographic image presented in Figure 3. This morphology is stable only when the film thickness is over 110 nm. According to the 2D-FFT corresponding to the inset AFM topographic image, domains are ordered into a square array (four first-order spots are clearly visible) with a period of 35 nm.

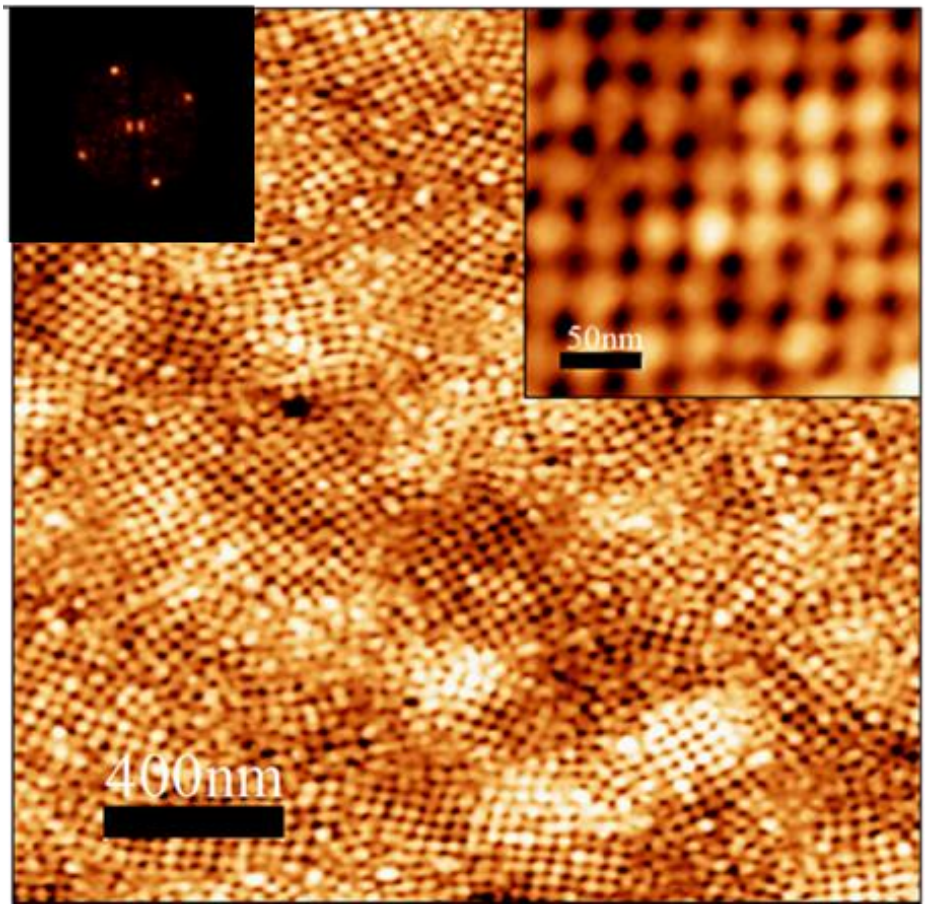

Figure 3: (2 x 2 µm², inset: 150 x 150 nm^2) AFM topographic views of the thicker part of a solvent annealed 3 µ-SPI film (S:P:I = 1:1.2:1) thin film placed under a $CHCl_3$ vapor for 2 hours and etched with a CF_4/O_2 plasma. The 2D-FFT corresponding to high magnified AFM image is presented on the upper left corner of the figure.

This *p*4*mm* symmetry structure could correspond to a (4.8.8) structure or a tetragonally perforated lamellae (TPL) morphology. According to the theoretical SCFT predictions reported by Jiang *et al.*,[14] the (4.8.8) and the TPL phases have their free energy close to that of the (4.6.12) tiling pattern (see Fig.4). Although a "three-colored" pattern cannot be clearly observed in Figure 3, the presence of discrete domains on film free-surface rather than a continuous, uniform matrix supports the formation of the (4.8.8) tiling pattern. Further experiments are required to confirm this conclusion.

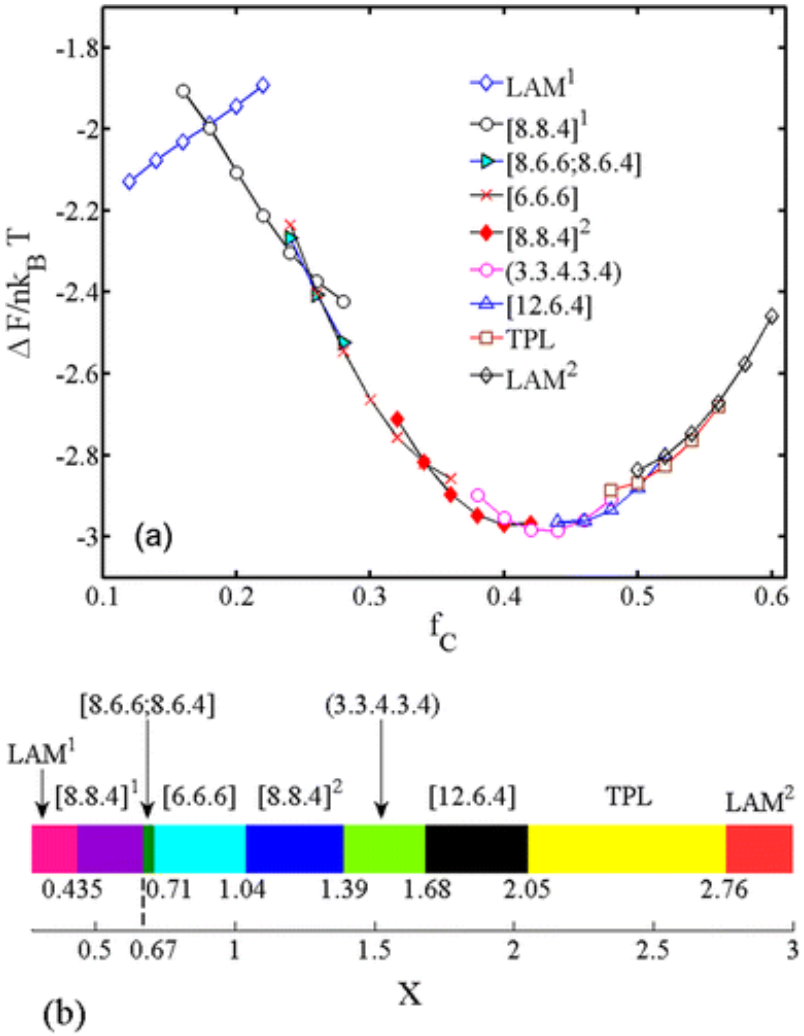

Figure 4: (a) Free energy differences from the value of the homogeneous phase as a function of the volume fraction of C composition for ABC star triblock copolymers with symmetric A and B arms. (b) Phase stability regions as a function of the arm-length ratio of $x = f_C/f_A$ ($f_A = f_B$). Note that in the $[8.8.4]^1$ phase, the minority C blocks forms the 4-coordinated domains, and blocks A and B alternatively form 8-coordinated microdomains. In the $[8.8.4]^2$ morphology, the A and C blocks form the 8-coordinated polygons, and B blocks form the domains with 4-coordinations.

2) Solvent annealed 3 μ-SPI (S:P: I = 1:1.2:0.6) under a THF vapor

We also studied the self-assembly of 3 μ-SPI thin films with volume fractions of 1, 1.2, and 0.6 for PS, P2VP and PI, respectively. The thickness of the film was determined to be 80 nm. The film was exposed to a THF vapor for 2 hours. The corresponding AFM topographic image is presented in Figure 5.

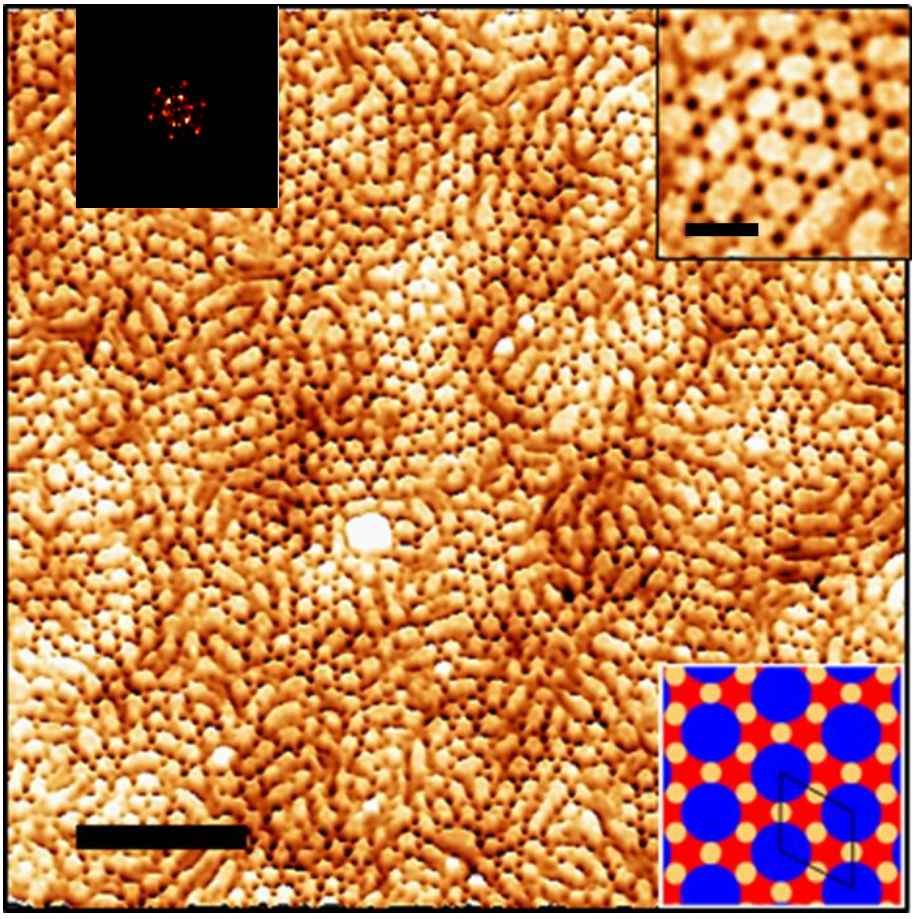

Figure 5: (2 x 2 μm^2, inset: 150 x 150 nm^2) AFM topographic views of 3 μ-SPI (S:P:I = 1:1.2:0.6) thin film treated by a THF vapor and etched with a CF_4/O_2 plasma (scale bars: 400 nm). The 2D-FFT corresponding to the high magnified AFM image and the schematic representation of the (4.6.12) tiling pattern are presented on the upper left and bottom right corners of the figure, respectively.

The thin film exhibits an out-of-plane columnar morphology arranged into a hexagonal array. As PI domains are preferentially etched under a CF_4/O_2 plasma treatment, they appear in dark brown on the AFM topographic image while the P2VP and PS domains correspond to the white brown and yellow regions, respectively. The PS domains form the inner part of the structure and are surrounded by twelve columns (6 P2VP + 6 PI). PS domains have a period of 46 nm according to the 2D-FFT associated to the Figure 5 inset while the PI and P2VP domain pitches are about 23 nm. The 2D-FFT confirms the formation of *p6mm* symmetry pattern since six first-order spots can be observed. The high contrast between all domains allows to conclude that the flower-shape morphology corresponds to the (4.6.12) Archimedean tiling pattern. A schematic representation of the morphology is depicted in the right bottom corner of the Figure 5 where the PS, P2VP and PI domains appear in the blue, red and yellow colors, respectively.

This (4.6.12) Archimedean tiling pattern is similar than the morphology achieved by a solvent-annealed ($CHCl_3$, 2h) 3 μ-SPI thin film with a nearly-symmetrical composition (S:P:I = 1:1.2:1) (see Fig. 1). The main difference resides in the fact that all the blocks do not occupy the same positions on the two (4.6.12) patterns consisting of different domain sizes. This phenomenon is due to a change in the volume fraction of each block for the different 3 μ-SPI systems under their respective swelling conditions. Indeed, the largest block under swelling condition would occupy the inner part of the morphology where column diameter is the largest.

We also studied the morphology in the substrate corner where the film thickness is increased by side effects occurring during the spin-coating process, and found that a different phase behavior happened in the region where the film thickness was about 100 nm. Indeed, a mixture of in-plane and out-of-plane cylindrical domains can be observed on the AFM topographic image presented in Figure 6.

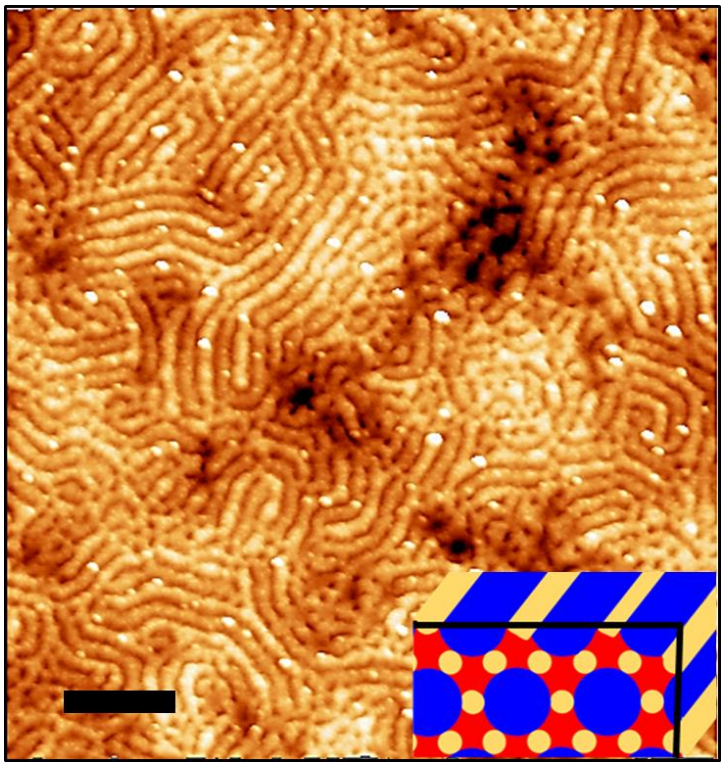

Figure 6: (1 x 1 µm²) AFM topographic view of the thicker part of 3 µ-SPI film (S:P:I = 1:1.2:0.6) thin film treated by a THF vapor and etched with a CF_4/O_2 plasma (scale bar: 200 nm). The schematic representation of the (4.6.12) tiling pattern having an in-plane orientation is presented on the bottom right corner of the figure.

The period of the structure is determined to be 50 nm, which approximatively corresponds to the pitch of out-of-plane PS columns arranged within the (4.6.12) tilling pattern presented in Figure 5. Here, PS (yellow) forms large in-plane cylinders separated by smaller in-plane PI columns (dark brown) whereas the P2VP domains do not appear on the film free surface. It is

well-known that polymers can adopt in-plane or out-of-plane morphologies depending on the film thickness.[15] In thicker films, the elastic strain energy can be more readily accommodated, which decreases the thickness dependence. For example, in the case of AB-type BCP, it was showed an in-plane orientation of the domains is promoted when the film thickness is increased.[16]

We assume that this in-plane columns corresponds to the plane that cut the (4.6.12) pattern along PS (yellow) and PI (dark brown) domains (black line on the schema) as shown in the inset of the Figure 6. This cutting axis along the PS and PI domains corresponds to the most stable plane since (*i*) it coincides with the plane incorporating cutting cylindrical domains in their middle and (*ii*) it allows the low surface energy PI block to easily form a wetting layer.

To summarize, the 3 μ-SPI chains with volume fraction of 1, 1.2, and 0.6 for PS, P2VP, and PI, respectively, treated in a THF vapor leads to the formation of a (4.6.12) Archimedean tiling pattern. Depending on the film thickness, different orientations of the columns can be observed. The in-plane structure is only observed on the corner substrate where the layer thickness is increased.

III. Conclusion

Thin film (4.6.12) Archimedean tilling patterns were produced from the self-assembly of two 3 μ-SPI systems. Depending on the solvent used for the SVA process and the composition of 3 μ-SPI chains, the largest domains of the (4.6.12) Archimedean were occupied by either the PS block or the PI one. Indeed, the PI block was located in the inner part of the morphology of a solvent-annealed ($CHCl_3$, 2h) 3 μ-SPI thin film having a nearly-symmetrical composition (S:P:I = 1:1.2:1) while it was replaced by the PS block for a solvent-annealed (THF, 2h) 3 μ-SPI thin film having an asymmetrical composition (S:P:I = 1:1.2:0.6). To the best of our knowledge, it is the first time that thin film (4.6.12) Archimedean tiling patterns formed by star miktoarm ABC terpolymers are demonstrated.

Interestingly, morphology changes were demonstrated when the film thickness was increased from 80 nm to 110 nm. A (4.8.8) Archimedean tiling pattern was observed for a solvent-annealed ($CHCl_3$, 2h) 3 μ-SPI thin film (S:P:I = 1:1.2:1) while a mixture of in-plane and out-of-plane columnar domains was achieved for a solvent-annealed (THF, 2h) 3 μ-SPI thin film having an asymmetrical composition.

1. Okamoto, S. *et al.* Morphology of model three-component three-arm star-shaped copolymers. *Polymer (Guildf).* **38,** 5275–5281 (1997).

2. Takano, A. *et al.* A mesoscopic archimedean tiling having a new complexity in an ABC star polymer. *J. Polym. Sci. Part B Polym. Phys.* **43,** 2427–2432 (2005).

3. Aissou, K. *et al.* Archimedean Tilings and Hierarchical Lamellar Morphology Formed by Semicrystalline Miktoarm Star Terpolymer Thin Films. *ACS Nano* **10,** 4055–4061 (2016).

4. Hayashida, K. *et al.* Archimedean tiling patterns of ABC star-shaped terpolymers studied by microbeam small-angle X-ray scattering. *Macromolecules* **39,** 4869–4872 (2006).

5. Ouyang, P., Zhao, W. & Huang, X. Beautiful Math, Part 5: Colorful Archimedean Tilings from Dynamical Systems. *IEEE Comput. Graph. Appl.* **35,** 90–96 (2015).

6. Matsushita, Y., Hayashida, K., Dotera, T. & Takano, A. Kaleidoscopic morphologies from ABC star-shaped terpolymers. *J. Phys. Condens. Matter* **23,** 284111 (2011).

7. Bell, S. B. M., Diaz, B. M., Holroyd, F. & Jackson, M. J. Spatially referenced methods of processing raster and vector data. *Image Vis. Comput.* **1,** 211–220 (1983).

8. Aissou, K., Choi, H. K., Nunns, A., Manners, I. & Ross, C. A. Ordered nanoscale archimedean tilings of a templated 3-miktoarm star terpolymer. *Nano Lett.* **13,** 835–839 (2013).

9. Aissou, K., Nunns, A., Manners, I. & Ross, C. A. Square and rectangular symmetry tiles from bulk and thin film 3-miktoarm star terpolymers. *Small* **9,** 4077–4084 (2013).

10. Choi, H. K., Nunns, A., Sun, X. Y., Manners, I. & Ross, C. A. Thin film knitting pattern morphology from a miktoarm star terpolymer. *Adv. Mater.* **26,** 2474–2479 (2014).

11. Li, Y., Huang, H., He, T. & Gong, Y. Solvent vapor induced morphology transition in thin film of cylinder forming diblock copolymer. *Appl. Surf. Sci.* **257,** 8093–8101 (2011).

12. Aissou, K. *et al.* Highly Ordered Nanoring Arrays Formed by Templated Si-Containing Triblock Terpolymer Thin Films. *Small* **13,** 1603184 (2017).

13. Gemma, T., Hatano, A. & Dotera, T. Monte Carlo simulations of the morphology of ABC star polymers using the diagonal bond method. *Macromolecules* **35,** 3225–3237 (2002).

14. Jiang, K., Zhang, J. & Liang, Q. Self-Assembly of Asymmetrically Interacting ABC Star Triblock Copolymer Melts. *J. Phys. Chem. B* **119,** 14551–14562 (2015).

15. Farrell, R. A., Fitzgerald, T. G., Borah, D., Holmes, J. D. & Morris, M. A. Chemical interactions and their role in the microphase separation of block copolymer thin films. *International Journal of Molecular Sciences* **10,** 3671–3712 (2009).

16. Suh, K. Y., Kim, Y. S. & Lee, H. H. Parallel and vertical morphologies in block copolymers of cylindrical domain. *J. Chem. Phys.* **108,** 1253–1256 (1998).

Conclusion

In this thesis, we developed an effective method for the synthesis of linear and star miktoarm ABC terpolymers composed of PS, P2VP and PI. A library of linear and star miktoarm ABC terpolymer was done by keeping constant the PS and P2VP molecular weights and by varying the PI block size. The synthesis method developed in this thesis revealed to be interesting since functionalization steps were facilitate by few purification steps and the coupling method did not involve metal catalyst to achieve well-defined linear and star miktoarm ABC terpolymers.

The self-assembly of linear and star miktoarm terpolymers was demonstrated in thin film configuration. For that purpose, a solvent-vapor annealing process was used to promote the mobility of polymeric chains then a plasma treatment was performed on the film free-surface to improve the contrast between the different blocks for the microscopy imaging. The effect of a fluorine-rich plasma on the etching rate of the different block was characterized by PM-IRRAS experiments, which revealed that the PI domains are removed more easily than the P2VP and PS ones.

We demonstrated that the self-assembly of type II linear ABC terpolymers enable the formation of a thin film core-shell double gyroid structure when the volume fractions of PI, PS and P2VP are 0.5, 1.1 and 1, respectively. Depending on the film thickness, four different planes were obtained. The (211), (111) and (100) planes were observed for 190 nm, 90 nm and 75 nm thick films, respectively, whereas the (111) plane was only observed between terraces.

A (4.6.12) Archimedean tiling pattern was also demonstrated from the self-assembly of two 3 μ-SPI terpolymers. Interestingly, changing the volume ratio of one block and the solvent annealing conditions allowed to obtain the same structure with a different block located in the inner part of the (4.6.12) tiling pattern. The PI block is located within the inner part domains of the morphology when 3 μ-SPI chains with a nearly symmetrical composition are placed under a chloroform vapor. In contrast, solvent-annealed asymmetric 3 μ-SPI chains under a THF vapor give access to a (4.6.12) tiling pattern where the inner part domains are occupied by the PS block.

APPENDIX

I. Thin film process

The spin coating process is one of the most commonly used techniques for the deposition of polymeric thin films on substrates. It is used in a wide variety of industries and technology sectors. The advantage of spin coating is its ability to quickly and easily produce uniform films with thicknesses of a few nanometers.[1]

First the substrate is coated with the solution containing the polymer dissolved in a solvent. The substrate starts to rotate at a constant acceleration rate until the desired rotation speed is reached (1500 – 3000 rpm), and the majority of the solvent is evaporated during this process. Varying the rotation speed or the polymer concentration in the starting solution allows to control the thickness of the film and so, different film thicknesses can be prepared.[1–3]

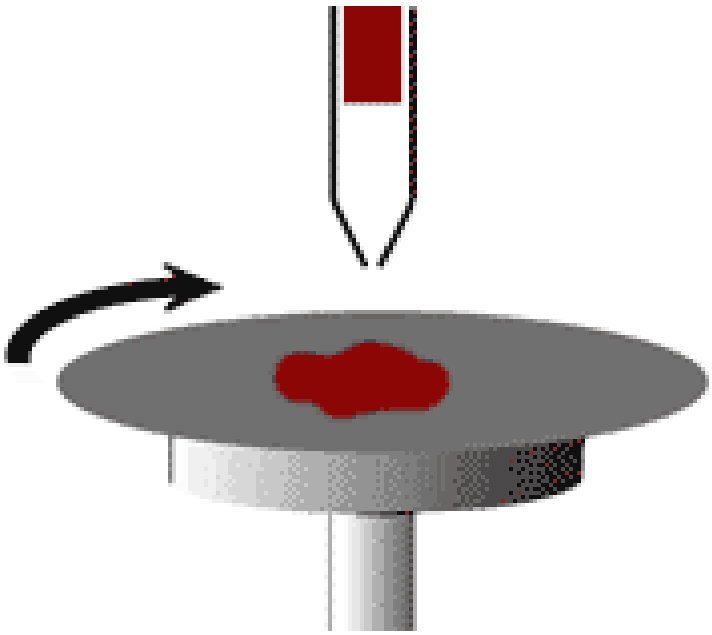

Figure 1: Schematic representation of the spin-coating process.

To produce uniform polymeric thin films, the solvent used to solubilize the PS-*b*-P2VP-*b*-PI and 3μ-SPI chains must be a good solvent for all the blocks. Therefore, we choose to work with toluene. The affinities between the different blocks and the solvent can be evaluated with the Hildebrand parameters reported in Table 1.[4] A solvent is considered as a good solvent for a given polymer when the difference between the Hildebrand solubility parameters of the solvent and the polymer is low.[5] The solubility parameter of PS, P2VP and PI are 18.5, 20.6 and 16.3

$MPa^{1/2}$, respectively.[6] As the difference between the solubility parameters of the toluene and the three different blocks is low, this solvent will be used as a non-selective good solvent.

As the boiling point of toluene is 111°C, its evaporation is not too fast and allows to obtain homogeneous thin film for a speed coating rate between 1500 and 4000 rpm. Going below 1500 rpm leads to a heterogeneous film since it involves a slower evaporation of toluene.

Table 1: Hildebrand parameters for several solvents and the polymers used in this study.

	Hildebrand solubility parameter ($MPa^{1/2}$)
Chloroform	17,8
Tetrahydrofuran	19,5
Toluene	18,1
Polystyrene	18,5
Poly(2-vinylpyridine)	20,6
Polyisoprene	16,3

II. Solvent vapor annealing process

Several methods can be used to promote the self-assembly of BCP thin films. The thermal annealing[7–9] is the most used methodology because of it is easy to set up, but also because it does no present any toxicity problems. Generally, in this process, the applied temperature is above the glass transition temperature (T_g) of the different blocks in order to increase the chain mobility and thus promote the self-assembly. Other technics have been developed, such as mechanic flow field[10,11], electronic or magnetic fields[12–14] and solvent annealing[15–20]. In this study, we will use a solvent vapor annealing (SVA) process to promote the ABC terpolymer chain mobility.

Once the polymeric films are deposited on the silicon wafer, they are treated with a SVA process. Some studies showed that it is possible to go from a disordered structure to a well-organized phase with SVA.[19–21] The SVA process is composed of two steps. The first one consists in the solvent molecules adsorption at the film surface. The wettability of the film is stable when the chemical potential of the solvent contained in the film is equal to that of the one contained in the vapor phase. The T_g of the film is therefore decreased and the chain mobility is increased. Thus, the interactions between polymer chains, the volume fraction of blocks, and the period between domains are affected by this adsorption and can lead to different structures. The second step occurs during the solvent removing. A fast evaporation of the solvent can freeze the BCP morphology. During the SVA process, it is important to control the temperature and the vapor pressure into the chamber. For this purpose, the SVA process was all the time performed at 22°C (clean room temperature), and the vapor pressure was controlled with a mass flow.[16] Samples were exposed to a continuous stream of solvent vapor produced by bubbling nitrogen gas through the liquid solvent as shown in the Figure 2.

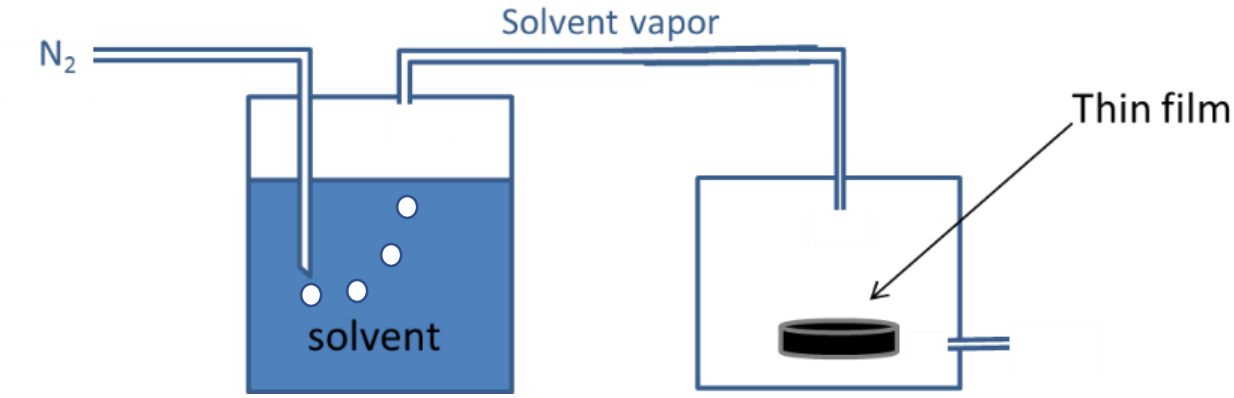

Figure 2: Schematic representation of the solvent vapor annealing set-up.

Different solvents were used to promote the self-assembly of BCPs and, we mainly worked with tetrahydrofuran (THF) and chloroform ($CHCl_3$). The affinity of each blocks with the solvent is different, therefore their swelling ratio is changed. In order to characterize this phenomenon, swelling ratio measurements of each block were done. Homopolymer thin films were deposited from a solution of 2 wt. % in toluene. First, one can notice that despite the use of the same polymer concentration in toluene, different film thicknesses were obtained.

In-situ variations of the swelling ratio was followed using a Filmetrics spectroscopic white light reflectometer apparatus. The solvent chamber lid of the SVA set-up was made of quartz, which allowed the *in-situ* measurements of the film thickness variation during the SVA process. The homopolymer film thickness was evaluated before and every 5 minutes after the beginning of the SVA process. Because of the difference of the initial film thicknesses, each layer was normalized, and the variations of the film thicknesses over the SVA time were compared. The curves are displayed in Figure 3.

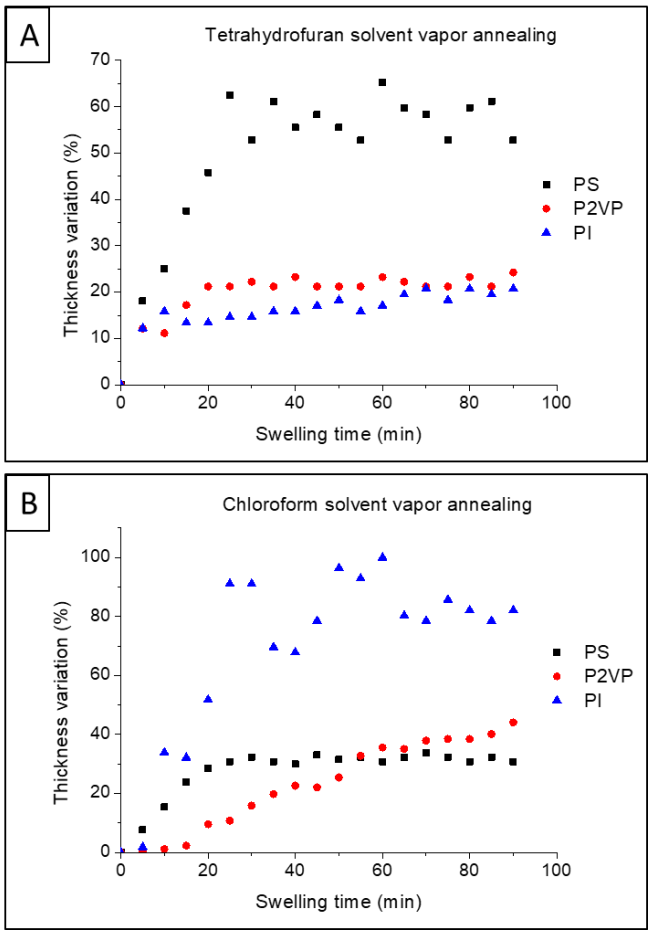

Figure 3: Film thickness variations versus the swelling time: (a) in THF and (b) in $CHCl_3$.

In the case of a chloroform vapor, hPI reaches a plateau for a thickness variation of 90%, whereas hPS and hP2VP reached a plateau for a 35% thickness variation. Therefore, hPI has a larger affinity with chloroform than hPS and hP2VP. In other words, hPI is more swollen by $CHCl_3$ than hPS and hP2VP, making the hPI chains more mobile in chloroform.

hPI and hP2VP behave similarly in THF with a slowly increase of the film thickness of about 20%. In contrast, the hPS film thickness increases strongly for low swelling times, and eventually reaches a plateau of about 65%. Therefore, hPS has a larger affinity with THF making the hPS chain mobility is more important than that of the hP2VP and hPI ones.

It is noteworthy that the layer thickness variations is more important when a $CHCl_3$ vapor is used. $CHCl_3$ has a larger saturated vapor pressure than THF, which leads to a larger swelling of polymers under a $CHCl_3$ vapor.

In this part, we have shown that the SVA process was done under controlled parameters (temperature and vapor pressure in the chamber). Moreover, chloroform and tetrahydrofuran have been shown to swell preferentially hPI and hPS, respectively.

III. Reactive ion etching plasma

After the spin-coating and solvent annealing processes, some contrast between polymers must be established in order to precisely characterize the self-assembled structure by microscopy.

Plasma etching has proven to be a great tool for surface modification of polymeric materials.[23,24] Gas plasma (glow discharge) is a partially ionized gas, which can be generated by an electrical discharge (see Figure 4a). A plasma can etch in three different manners. The material can be chemically etched by reactive species of the plasma (*e.g.* radicals or ions created in the plasma). In this case, we talk about chemical etching. The ion bombardment on a polymer surface, which causes sputtering of the surface, is referred to as physical process. UV radiation from the plasma can also lead to dissociation of chemical bonds, which leads to the formation of low molecular weight materials. Generally, those three mechanisms simultaneously occur during a plasma treatment and induce the formation of volatiles products in the plasma chamber. The main advantage of this technique is its selectivity regarding the chemical structure of the polymers. The plasma etcher used in this study is the PE-100 Benchtop Plasma System (Figure 4b).

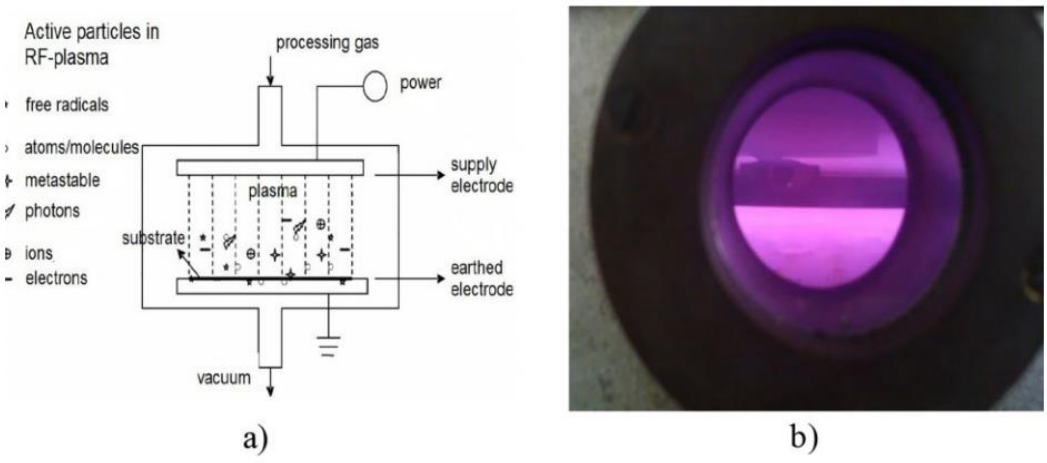

Figure 4: (a) Schematic representation of the plasma etching process and (b) plasma reactor chamber used in this work.

In this study a CF_4/O_2 plasma (40W, 17sccn CF4 and 3sccm O2, 45s) was currently used to reveal the BCP self-assembled structure as different etching behaviors were observed between PS, PI and P2VP. In order to gain more insights into the etching behaviors of the various materials, phase modulation infrared reflection absorption spectroscopy (PM-IRRAS) experiments were performed.

IV. Phase Modulation Infrared Reflection Absorption Spectroscopy (PM-IRRAS) experiments

The Phase Modulation Infrared Reflection Absorption Spectroscopy (PM-IRRAS) method benefits from the IRRAS advantages of electric field enhancement and surface selection, but also presents the tremendous advantage of having high sensitivity in surface absorption detection (see Figure 5).

Herein, the PM-IRRAS experiment was used to characterize the effect of the plasma etching on polymers. The polymers were spin-coated on a gold coated substrates. The thin films were treated with a solvent annealing process and etched as described previously. Their absolute reflectance was over 98% in the 1.2-12 µm spectral range.

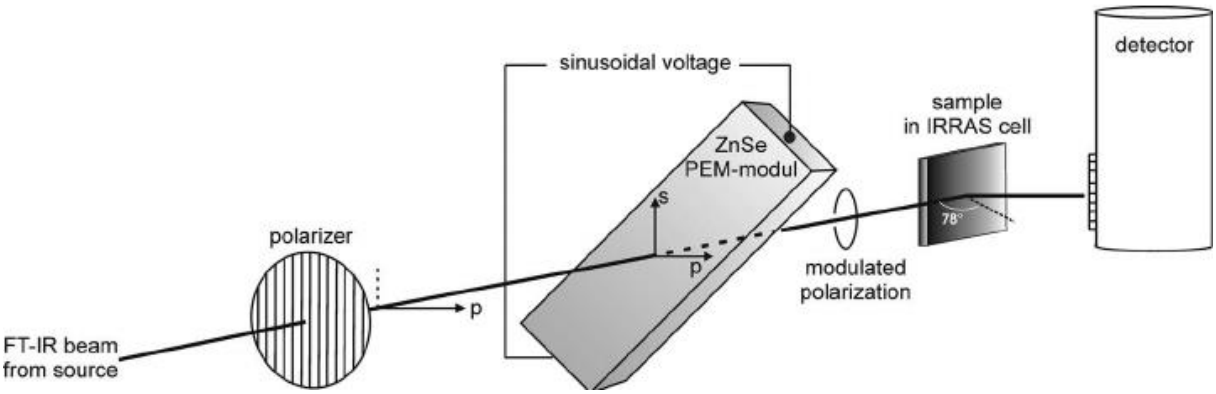

Figure 5: Scheme of the optical PM-IRRAS set-up. The first polarizer creates a p-polarized incident beam on the sample that is polarization-modulated by the PEM.

The PM-IRRAS spectra were recorded on a ThermoNicolet Nexus 670 FTIR spectrometer at a resolution of 4 cm^{-1}, by coadding several blocks of 1500 scans (30 minutes acquisition time). Generally, eight blocks (4 hours acquisition time) were necessary to obtain PM-IRRAS spectra of ultra-thin films with good signal-to-noise ratios. All spectra were collected in a dry-air atmosphere after a 30-min- incubation in the chamber. Experiments were performed at an incidence angle of 75° using an external homemade goniometer reflection attachment.[25] The infrared parallel beam (modulated in intensity at frequency ω_i lower than 5 KHz) was directed out of the spectrometer with an optional flipper mirror and made slightly convergent with a first BaF_2 lens (191 mm focal length). The IR beam passed through a BaF_2 wire grid polarizer (Specac) to select the p-polarized radiation and a ZnSe photoelastic modulator (PEM, Hinds Instruments, type III). The PEM modulated the polarization of the beam at a high fixed frequency, ω_m =74 KHz, between the parallel and perpendicular linear

states. After reflection on the sample, the double modulated (in intensity and in polarization) infrared beam was focused with a second ZnSe lens (38.1 mm focal length) onto a photovoltaic MCT detector (Kolmar Technologies, Model KV104) cooled at 77 K. The polarization modulated signal I_{AC} was separated from the low frequency signal I_{DC} (ω_i between 500 and 5000 Hz) with a 40 KHz high pass filter and then demodulated with a lock-in amplifier (Stanford Model SR 830). The output time constant was set to 1 ms. The two interferograms were high-pass and low-pass filtered (Stanford Model SR 650) and simultaneously sampled in the dual channel electronics of the spectrometer. In all the experiments, the PEM was adjusted for a maximum efficiency at 2500 cm^{-1} to cover the mid-IR range in only one spectrum. For calibration measurements, a second linear polarizer (oriented parallel or perpendicular to the first preceding the PEM) was inserted between the sample and the second ZnSe lens. This procedure was used to calibrate and convert the PM-IRRAS signal in terms of the IRRAS signal (i.e. $1-\frac{R_p(d)}{R_p(0)}$, where $R_p(d)$ and $R_p(0)$ stand for the p-polarized reflectance of the film/substrate and bare substrate systems, respectively).[26,27]

Homopolymers of PS, P2VP, and PI as well as a star ABC terpolymer with volume ratios of PS:P2VP:PI = 1:1.2:1 were spin-coated on gold coated substrates. They were exposed to a $CHCl_3$ solvent vapor annealing for two hours. Then, PM-IRRAS spectra were recorded before and after the plasma treatment (plasma conditions: 40 W, 17 sccm CF_4 and 3 sccm O_2, 45 s). The PM-IRRAS spectra are presented in Figure 6.

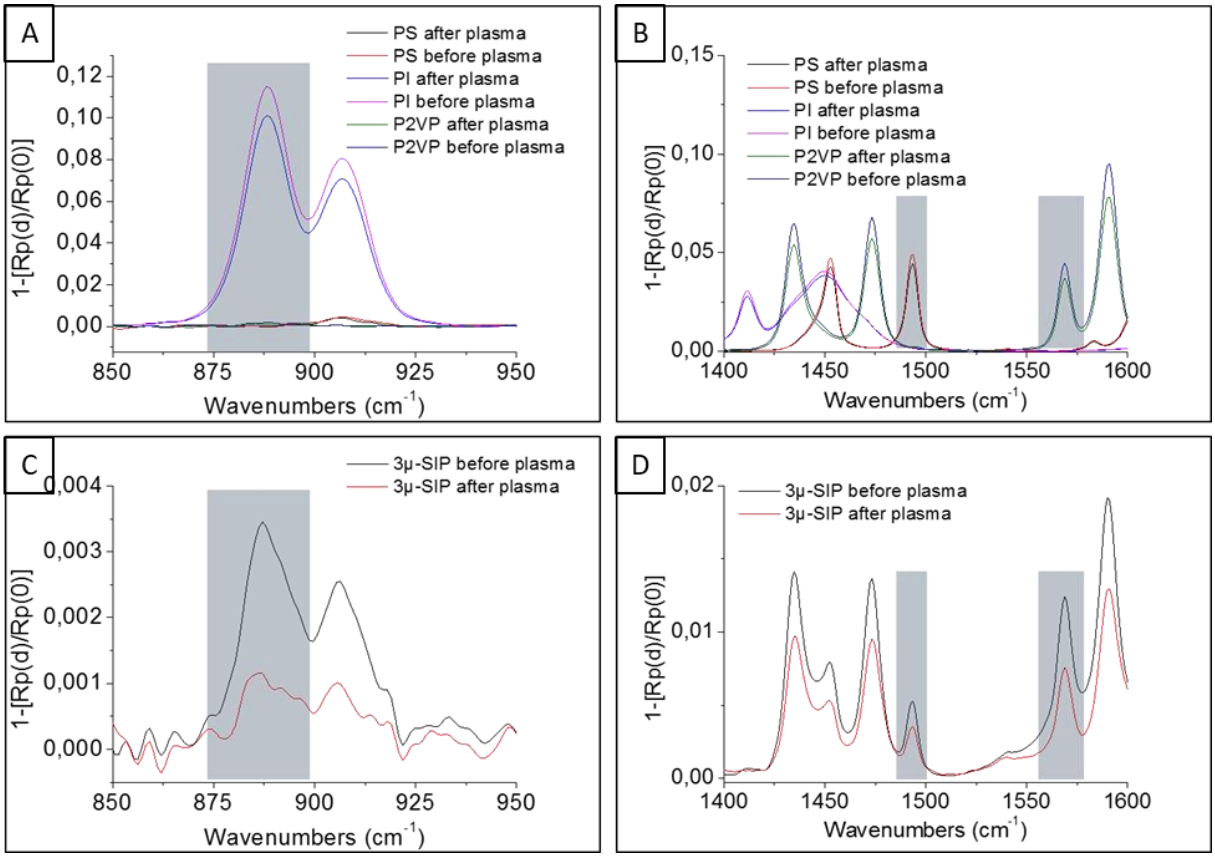

Figure 6: PM-IRRAS spectra of PS, PI and P2VP homopolymer thin films (A) before and (B) after the plasma treatment. PM-IRRAS spectra of 3 µ-ISP thin film (C) before and (D) after the plasma treatment.

To investigate the effect of the plasma, the characteristic peak at a given wavenumber for a given homopolymer was chosen to not overlap with the signal of the other homopolymers. We choose the peak located at 1493 cm^{-1}, at 887 cm^{-1}, and at 1567 cm^{-1}, for hPS, hPI and hP2VP, respectively. After the plasma etching treatment, the area under all the peaks decreased. The peak integrals were calculated from the spectrum of the self-assembled star ABC terpolymer before and after the plasma etching. The polymer loss percentage was calculated for each block. After RIE treatment, 65% of the PI domains were etched while 41% and 26% of the P2VP and PS domains were also removed. These results confirm that the CF_4/O_2 plasma used in this study preferentially etches the PI block than the PS and P2VP ones.

V. AFM Characterization

To characterize the structure of the self-assembled polymeric thin films, the atomic force microscopy (AFM) was mainly used. The AFM is a high-resolution type of scanning probe microscopy (SPM), with demonstrated resolution in the nanometer scale. Until now, TM AFM (Tappingmode or intermittent contact mode atomic force microscopy) has been the most often applied direct imaging technique to characterize the thin film morphology. In Tappingmode, the cantilever is oscillated up and down at or near its resonance frequency, in a direction normal to the sample surface. The frequency and amplitude of the driving signal are kept constant, leading to a constant amplitude of the cantilever oscillation as long as there is no drift or interaction with the surface. Typical amplitudes of oscillation are in the range of tens of nanometers. The Tappingmode does not measure a direct force, but short range repulsive and long range repulsive forces. The general operation is shown in Figure 7a.

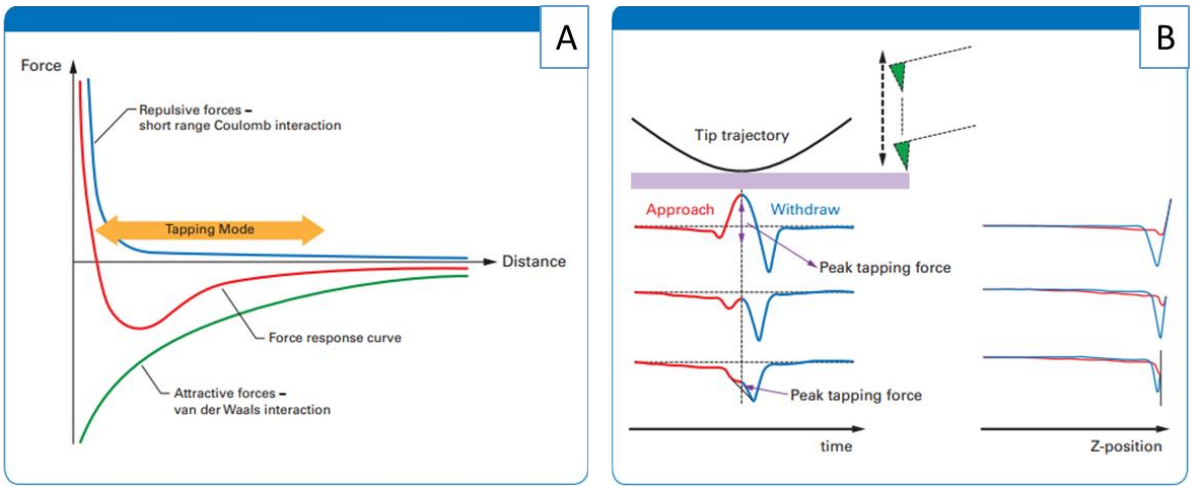

Figure 7: (a) Force curves highlighting the motion of an oscillating cantilever in Tappingmode; (b) Force curves for a cantilever operated in PeakForce Tapping.

In our case, the TM allows for a good contrast between PI and other blocks, but does not allow enough contrast between the PS and P2VP blocks to determine their relative position in the structure. To overcome this lack of contrast, we tried another mode called PeakForce Tapping (PFT). Similar to TM, in PFT, the AFM tip is brought intermittently into contact with the sample surface. In contrast with Tappingmode, the PFT operates in a non-resonant mode. The PFT oscillations are performed at frequencies well below the cantilever resonance. Moreover, the z-position is modulated (by a sine wave or triangular one) to avoid unwanted

resonances. The general operation is illustrated in Figure 7b. It also allows to work with softer cantilever than in the TM mode leading to an improved measurement sensitivity.

To prove the efficiency and the requirement to use the PFT instead of the TM AFM, the same sample was imaged using both modes. The AFM topographic views are presented in Figure 8. The AFM image produced with the TM exhibits only two colors, the PI is in black, but it is not possible to distinguish the PS from the P2VP (see Fig. 8a). On the other hand, the AFM topographic view obtained with PFT shows a three colored pattern where PI, PS and P2VP appear in dark brown, yellow, and brown, respectively (see Fig. 8b). The PI, PS and P2VP domains are well resolved under these imaging conditions.

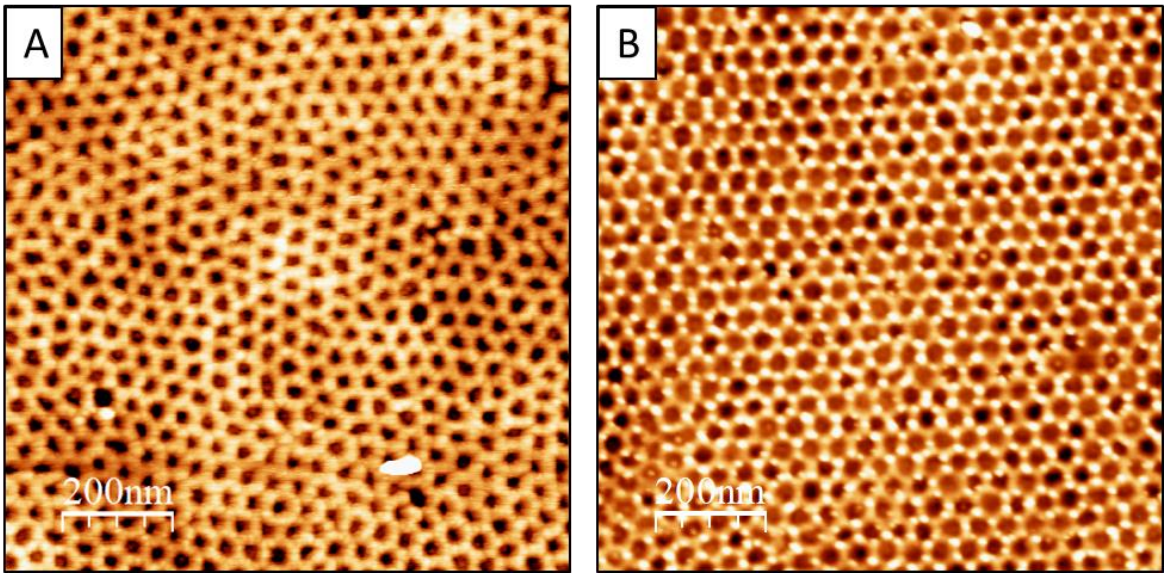

Figure 8: (1 x 1 µm²) AFM topographic view of a star ABC terpolymer composed of PS, PI and P2VP self-assembled in thin film (a) recorded using TappingMode (TM); (b) recorded using PeakForce Tapping (PFT).

1. Lee, D. H., Park, S., Gu, W. & Russell, T. P. Highly ordered nanoporous template from triblock copolymer. *ACS Nano* **5,** 1207–1214 (2011).
2. Wadley, M. L., Hsieh, I. F., Cavicchi, K. A. & Cheng, S. Z. D. Solvent dependence of the morphology of spin-coated thin films of polydimethylsiloxane-rich polystyrene-block-polydimethylsiloxane copolymers. *Macromolecules* **45,** 5538–5545 (2012).
3. Park, S., Wang, J. Y., Kim, B., Chen, W. & Russell, T. P. Solvent-induced transition from micelles in solution to cylindrical microdomains in diblock copolymer thin films. *Macromolecules* **40,** 9059–9063 (2007).
4. Hansen, C. *Hansen Solubility Parameters*. (CRC Press, 2007). doi:10.1201/9781420006834
5. Scott, R. L. The Thermodynamics of High Polymer Solutions. V. Phase Equilibria in the Ternary System: Polymer 1—Polymer 2—Solvent. *J. Chem. Phys.* **17,** 279–284 (1949).
6. Koenhen, D. M. & Smolders, C. A. The determination of solubility parameters of solvents and polymers by means of correlations with other physical quantities. *J. Appl. Polym. Sci.* **19,** 1163–1179 (1975).
7. Berry, B. C., Bosse, A. W., Douglas, J. F., Jones, R. L. & Karim, A. Orientational order in block copolymer films zone annealed below the order-disorder transition temperature. *Nano Lett.* **7,** 2789–2794 (2007).
8. Singh, G. *et al.* Tuning molecular relaxation for vertical orientation in cylindrical block copolymer films via sharp dynamic zone annealing. *Macromolecules* **45,** 7107–7117 (2012).
9. Park, W. I. *et al.* Directed self-assembly with sub-100 degrees celsius processing temperature, sub-10 nanometer resolution, and sub-1 minute assembly time. *Small* **8,** 3762–3768 (2012).
10. Wang, J. *et al.* Biaxial alignment of block copolymer-complex lamellae. *Soft Matter* **9,** 1337–1343 (2013).
11. Yu, H., Li, J., Ikeda, T. & Iyoda, T. Macroscopic parallel nanocylinder array fabrication using a simple rubbing technique. *Adv. Mater.* **18,** 2213–2215 (2006).
12. Thurn-Albrecht, T., DeRouchey, J., Russell, T. P. & Kolb, R. Pathways toward electric field induced alignment of block copolymers. *Macromolecules* **35,** 8106–8110 (2002).
13. Majewski, P. W., Gopinadhan, M. & Osuji, C. O. Magnetic field alignment of block copolymers and polymer nanocomposites: Scalable microstructure control in functional soft materials. *Journal of Polymer Science, Part B: Polymer Physics* **50,** 2–8 (2012).
14. Thurn-Albrecht, T. *et al.* Ultrahigh-Density Nanowire Arrays Grown in Self-Assembled

Diblock Copolymer Templates. *Science (80-.).* **290,** 2126–2129 (2000).

15. Darling, S. B. Directing the self-assembly of block copolymers. *Prog. Polym. Sci.* **32,** 1152–1204 (2007).
16. Gotrik, K. W. *et al.* Morphology control in block copolymer films using mixed solvent vapors. *ACS Nano* **6,** 8052–8059 (2012).
17. O'Driscoll, S. *et al.* The morphology and structure of PS-b-P4VP block copolymer films by solvent annealing: Effect of the solvent parameter. *Polym. Adv. Technol.* **22,** 915–923 (2011).
18. Li, X., Peng, J., Wen, Y., Kim, D. H. & Knoll, W. Morphology change of asymmetric diblock copolymer micellar films during solvent annealing. *Polymer (Guildf).* **48,** 2434–2443 (2007).
19. Gu, X., Gunkel, I., Hexemer, A. & Russell, T. P. Solvent vapor annealing of block copolymer thin films: Removal of processing history. *Colloid Polym. Sci.* **292,** 1795–1802 (2014).
20. Li, Y., Huang, H., He, T. & Gong, Y. Solvent vapor induced morphology transition in thin film of cylinder forming diblock copolymer. *Appl. Surf. Sci.* **257,** 8093–8101 (2011).
21. Aissou, K. *et al.* Highly Ordered Nanoring Arrays Formed by Templated Si-Containing Triblock Terpolymer Thin Films. *Small* **13,** 1603184 (2017).
22. Owens, D. K. & Wendt, R. C. Estimation of the surface free energy of polymers. *J. Appl. Polym. Sci.* **13,** 1741–1747 (1969).
23. Pederson, L. A. L. A. A. & Deep, U. V. L. I. T. H. O. G. R. A. P. H. Y. Structural Composition of Polymers Relative to Their Plasma Etch Characteristics. *J. Electrochem. Soc.* **I,** 205–208 (1978).
24. Fridman. Plasma etching and modification of organic polymers. in *Pure and Applied Chemistry* **62,** 1699–1708 (1990).
25. Buffeteau, T., Desbat, B. & Turlet, J. M. Polarization Modulation FT-IR Spectroscopy of Surfaces and Ultra-Thin Films: Experimental Procedure and Quantitative Analysis. *Appl. Spectrosc.* **45,** 380–389 (1991).
26. Ramin, M. A. *et al.* PM-IRRAS investigation of self-assembled monolayers grafted onto SiO 2/Au substrates. *Langmuir* **27,** 6076–6084 (2011).
27. Buffeteau, T., Desbat, B., Blaudez, D. & Turlet, J. M. Calibration procedure to derive IRRAS spectra from PM-IRRAS spectra. *Appl. Spectrosc.* **54,** 1646–1650 (2000).

Synthesis of linear and star miktoarm ABC terpolymers and their self-assembly in thin films

The first objective of this work was to develop a synthesis method enabling the preparation of linear and star ABC terpolymers. The molecular weights of the A and B (PS and P2VP) blocks were kept constant while the size of the C (PI) block was varied to achieve different morphologies. The second objective of this work was devoted to the study of the self-assembly of linear and star ABC terpolymer thin films. A synthesis route combining the anionic polymerization with a coupling method was developed. The PS and P2VP blocks were synthesized by a sequential anionic polymerization. The PI block separately synthesized by anionic polymerization was then coupled to the PS-*b*-P2VP diblock *via* a Steglich esterification. This method revealed to be efficient since it is a catalyst metal-free reaction enabling to achieve well-defined terpolymers with a dispersity below 1.1

The study of star and linear ABC terpolymer self-assembly led to new morphologies in thin film. A solvent vapor annealing treatment was used to promote the mobility of the polymeric chains. A core-shell double gyroid structure was produced from the self-assembly of linear PS-*b*-P2VP-*b*-PI thin films. Four different crystallographic planes were observed depending on the film thickness. Moreover, the self-assembly of star ABC terpolymer chains into a thin film (4.6.12) Archimedean tilling pattern was demonstrated for the first time. Here, the PS and PI blocks occupied different places within the (4.6.12) tiling pattern depending on the PI volume ratio and the solvent selected to swell the film.

Synthèse de terpolymères ABC linéaires et en étoile et étude de leur auto-organisation en films minces

L'objectif premier de ce travail a été de trouver une méthode de synthèse permettant de préparer des terpolymères ABC linéaires et en étoile en gardant la masse molaire des blocs A et B (PS et P2VP) constantes, tout en faisant varier la masse molaire du bloc C (PI) de sorte à avoir accès à différentes morphologies. Le deuxième objectif consistait en l'auto-assemblage des terpolymères synthétisés sous forme de films minces.

Afin de répondre au premier objectif de cette thèse, une voie de synthèse, combinant la polymérisation anionique avec une méthode de couplage, a été mise au point. La polymérisation anionique séquentielle des blocs PS et P2VP a donné lieu à des chaînes PS-*b*-P2VP fonctionnalisées qui ont été ensuite couplées à différents blocs PI *via* une estérification de Steglich. Cette méthode de synthèse s'est révélée pertinente car des terpolymères ABC linéaires et en étoile très bien définis (*c-à-d* ayant une dispersité inférieure à 1.1) ont pu être synthétisés. De plus, la méthode de couplage, ayant un rendement proche de 100%, ne met pas en jeu l'utilisation de métal en tant que catalyseur.

Dans un deuxième temps, l'auto-organisation des terpolymères a permis d'obtenir de nouvelles morphologies sous forme de films minces. Un recuit par vapeur de solvant a été utilisé pour apporter de la mobilité aux chaînes terpolymères. Ainsi, nous avons montré que l'auto-organisation de chaînes terpolymères linéaires (PS-*b*-P2VP-*b*-PI) permettait la formation d'une phase double gyroid cœur-écorce en film mince. De plus, l'auto-organisation des terpolymères en étoile (3 μ-ISP) a permis d'obtenir un pavage d'Archimède de type (4.6.12) pour la première fois en film mince. Dans ce cas, nous avons aussi montré que varier la masse molaire du bloc PI ainsi que la nature du solvant de recuit permettait une rotation des domaines au sein la structure. Typiquement le cœur de la structure peut être occupé soit par le PI ou bien le PS.